Nanoscale Biomolecular Mapping in Cells and Tissues with Expansion Microscopy

By

Asmamaw T. Wassie
B.S. Biological Engineering (2013)
Massachusetts Institute of Technology

Submitted to the Department of Biological Engineering
in Partial Fulfillment of the Requirements for the Degree of

Doctor of Philosophy

at the

MASSACHUSETTS INSTITUTE OF TECHNOLOGY

June 2019

Signature redacted

Author..... .....

Department of Biological Engineering
April 01, 2019

Signature redacted

Certified By..... .....

Edward S. Boyden
Y. Eva Tan Professor in Neurotechnology
Associate Professor of Biological Engineering and Brain and Cognitive Sciences,
MIT Media Lab and McGovern Institute
Thesis Supervisor

Signature redacted

Accepted By..... .....

Forest White
Professor of Biological Engineering
Chair of Graduate Program, Department of Biological Engineering

This thesis has been examined and approved by a committee of the Department of Biological Engineering:

Forest White
Professor of Biological Engineering
Thesis Committee Chair

Paul Blainey
Associate Professor of Biological Engineering
Thesis Committee Member

Edward S. Boyden
Y. Eva Tan Professor in Neurotechnology
Associate Professor of Biological Engineering and Brain and Cognitive Sciences,
MIT Media Lab and McGovern Institute
Thesis Supervisor

Nanoscale Biomolecular Mapping in Cells and Tissues with Expansion Microscopy

By

Asmamaw T. Wassie

Submitted to the Department of Biological Engineering on
April 01, 2019 in Partial Fulfillment of the Requirements
for the Degree of Doctor of Philosophy in Biological Engineering

Abstract:

The ability to map the molecular organization of cells and tissues with nanoscale precision would open the door to understanding their biological functions as well as the mechanisms that lead to pathologies. Though recent technological advances have expanded the repertoire of biological tools, this crucial ability remains an unmet need. Expansion Microscopy (ExM) enables the 3D, nanoscale imaging of biological structures by physically magnifying cells and tissues. Specimens, embedded in a swellable hydrogel, undergo uniform expansion as covalently anchored labels and tags are isotropically separated. ExM thereby allows for the inexpensive nanoscale imaging of biological samples on conventional light microscopes. In this thesis, I describe the development of a method called Expansion FISH (ExFISH) that uses ExM to enable the nanoscale imaging of RNA throughout cells and tissues. A novel chemical approach covalently retains endogenous RNA molecules in the ExM hydrogel. After expansion, RNA molecules can be interrogated with *in situ* hybridization. ExFISH opens the door for the investigation of the nanoscale organization of RNA molecules in various contexts. Applied to the brain, ExFISH allows for the precise localization of RNA in nanoscale neuronal compartments such as dendrites and spines. Furthermore, the optical homogeneity of expanded samples enables the imaging of RNA in thick tissue-sections. ExFISH also supports multiplexed imaging of RNA as well as signal amplification techniques. Finally, this thesis describes strategies for the multiplexed characterization of biological specimens. Taken together, these approaches will find applications in developing an integrative understanding of cellular and tissue biology.

Thesis Supervisor: Edward S. Boyden
Title: Y. Eva Tan Professor in Neurotechnology
Associate Professor of Biological Engineering and Brain and Cognitive Sciences,
MIT Media Lab and McGovern Institute

Acknowledgments

My research and my growth as a scientist would not have been possible without the contributions of many individuals that I would like to acknowledge here.

Firstly, I am extremely grateful to my advisor, Ed Boyden, for showing me how to think critically about problems in science. His commitment to science and dedication to his students is inspiring. I feel lucky to have spent the past six years in his vibrant lab where innovative ideas, however radical they may seem, are always welcome. In addition, I would especially like to thank my committee members, Forest White and Paul Blainey, for their invaluable input to my research over the years; I am grateful for their constructive feedback and deep expertise. I also would like to express my gratitude to the Hertz Foundation Fellowship for their generous support of my graduate research.

I would also like to thank many members of the Boyden lab. First, I am very grateful to Fei Chen, Anu Sinha, Shahar Alon, Dan Goodwin, and Deblina Sarkar. They have been amazing colleagues and friends in working with me to bring to fruition so many exciting research ideas. I have learned so much from each of them, and they have made my PhD experience memorable. In particular, I would like to thank Kiryl Piatkevich for his generosity, wisdom, and friendship over the years. I am also grateful to both Or Shemesh and Kiryl for teaching me much about molecular biology as I was beginning my PhD journey. I would further more like to acknowledge Nikita Pak, Paul Tillberg, Changyang Linghu, Jenna Aronson, Alexander Clifton, Shoh Asano, Rui Gao, Manos Karagiannis, Eghbal Hosseini, Kate Adamala, and Jay Yu for their input and contributions to many aspects of my research. In addition, I want to thank Dan Estandian, Eghbal Hosseini, and Nikita Pak for stimulating discussions on science and other matters. Finally, I am grateful to the lab admins I have worked with over the years namely, Lisa Lieberson, Holly Birns, Macey Lavoie, and Cynthia Smith.

Additionally, I want to express my gratitude to Shuguang Zhang and Andreas Mershin. When I came to MIT as a freshman, with very little idea of what research meant, they were kind enough to invite me into their lab as a UROP student. I am deeply indebted to both of them for teaching me about science and research. My desire to pursue graduate studies in science sprung from my experience working with them. I am fortunate to have spent my undergrad years in their lab, which truly felt like a second home.

Going to the same school as my brother, Brook Wassie, made my time at MIT that much more fun. I am so grateful to have had his companionship and support. I feel fortunate to have been able to see each of us grow and mature in his own way over the years. I also want to thank Linda Chen, one of my closest friends during my time at MIT. I have learned so much from our friendship. I am truly lucky to call my friend someone like her who constantly inspires me with her values and courage.

Most importantly, I dedicate this thesis to my parents Thomas Wassie and Yalem Tikue. Growing up, as far back as I can remember, my parents always encouraged me to appreciate the value of education. When I became interested in science as a kid, they nurtured my desire to be a scientist however improbable that path seemed. Words cannot express my appreciation for their love and support.

Table of Contents

List of Figures

Published Content

Chen, F.*, Wassie, A.T.*, Cote, A.J., Sinha, A., Alon, S., Asano, S., Daugharthy, E.R., Chang, J.-B., Marblestone, A., Church, G.M., Raj, A., Boyden, E.S. (2016) Nanoscale Imaging of RNA with Expansion Microscopy, Nature Methods, doi:10.1038/nmeth.3899. (*, co-first author)

- *Portions of Chapters 2,3,4, and the appendix were adapted from this manuscript*

Wassie, A.T.*, Zhao, Y.*, Boyden, E.S. (2019) Expansion Microscopy: Principles and Applications in Biological Research. Nature Methods, 16(1):33-41. (*, co-first author)

- *Portions of Chapters 1, 5 and the appendix were adapted from this manuscript.*

Asano, S.*, Gao, R.*, Wassie, A.T.*, Chen, F., Tillberg, P.W., Boyden E.S. (2018) Expansion Microscopy: Protocols for Imaging Proteins and RNA in Cells and Tissues. Current Protocols in Cell Biology. doi:10.1002/cpcb.56 (*, co-first author)

Chang, J.-B., Chen, F., Yoon, Y.-G., Jung, E. E., Babcock H., Kang J.-S., Asano S., Suk H.-J., Pak N., Tillberg P.W., Wassie A,T., Cai D., Boyden E.S. (2017) Iterative expansion microscopy, Nature Methods, doi:10.1038/nmeth.4261.

To my parents,

Thomas Wassie and Yalem Tikue

Chapter 1: Introduction

Background and Significance

Nanoscale organization of molecules is a ubiquitous feature of cellular and tissue biology. Almost every known biological system ranging from viruses to multi-cellular organisms shows evidence of intricate arrangement at the level of the nanoscale[1]. At the sub-cellular level, life is highly organized in both time and space, and especially at the nanoscale. Different cellular processes are compartmentalized into membrane bound organelles that carry out specific functions[2]. While many of these organelles are large, such as the Endoplasmic Reticulum, covering substantial portions of the cell body, nanoscale and dynamic contacts between organelles are involved in the transfer of biomolecules, organelle remodeling, and organelle biogenesis[2–4]. Within organelles themselves, there exists immense nanoscale organization. For example, the eukaryotic genome is organized at the nanoscale in a hierarchical fashion[5–8]. Not only is the architecture of the genome dynamic, there is evidence for the presence of small compartments involved in specific functions such as transcription[9,10]. Beyond organelles, the cellular cytoskeleton is another example of nanoscale arrangement. Microtubules, which are hollow-rod like structures about 25 nm in diameter and formed from tubulin monomers, represent an important structural component of cells[1]. In addition, the centrosome, which plays a key role in cell division, is another example of a nano-sized structure[11]. Indeed, nanoscale arrangement is a vital and characteristic aspect of cellular biology.

At the tissue level, biology is spatially organized over many length scales. The functions and properties of tissues arise from their intricate cellular and molecular architectures. This principle is most evident with the organization of the brain. In the case of the human brain, 100 billion neurons form 10^{15} synaptic connections between them giving rise to cognition and behavior[12]. While many subtypes of neurons exist, they also intimately interact with glia cells such as astrocytes and oligodendrocytes, among others, which play various roles ranging from providing electrical insulation to supporting synaptic signaling[13,14]. At the subcellular level, neurons exhibit nanoscale organization of biomolecules which endows these cells with their particular functions. For instance, neurons can possess hundreds of processes emerging from the cell body. While only one process, the axon, communicates electrical signal downstream,

dendrites, the remaining processes, receive and integrate inputs from upstream neurons. Indeed, the distribution of proteins and other biomolecules in these processes is reflective of their specific function. The most striking examples of nanoscale sub-cellular organization in neurons are chemical synapses. In these intimate contacts between neurons, which are as close as 20 nm, a panoply of proteins consisting of scaffolding proteins, cytoskeletal proteins, receptors, and many others are organized in 3D to give rise to the structure and functions of synapses. In addition, synapses contain ribosomes, transcripts, mitochondria, and vesicles[13–15]. Therefore, understanding communication between neurons spanning many regions of the brain requires understanding the nanoscale organization of the synaptic contacts between them. While most prominent in the structure of the brain, nanoscale organization is a hallmark of many tissues, as well as pathologies.

Given that the biological processes that give rise to the functions of tissues span wide spatial scales, from cellular level interactions to nanoscale molecular arrangements, a bottom-up understanding of biology requires tools with capabilities to observe biological structures across these length scales. Even more, technologies are required with the ability to observe a wide-array of molecules and their interactions. In part, the goal of this thesis is to point a way towards the development of such tools. While existing tools offer either high-resolution imaging, *in situ* multiplexed molecular imaging, or *in vitro* high throughput molecular profiling, there remains a need for methods that combine these abilities towards a reductive understanding of biology. In the following two sections, I will discuss some of these current technologies.

Tools for High Resolution Imaging

Until the arrival of light microscopy-based Super Resolution methods, the tool of choice for high-resolution imaging has been (and in many cases continues to be) electron microscopy (EM)[16]. In the context of neuroscience, EM has been used to map the connections of the nervous system (i.e. connectomics), such as the connectome of C.elegans[17], owing to its nanometer-level resolution, which is needed to accurately trace and map the minute processes of neurons. Recent advances in automation and Scanning Electron Microscopy (SEM) have enabled connectomic reconstruction of biologically significant volumes of the mammalian brain[18,19]. Beyond neuroscience, cryo-electron microscopy and electron tomography have enabled the molecular-level reconstruction of protein complexes, even in an *in situ* context[20–22]. While EM has been

invaluable for structural biology, some of its limitations include the need for expensive and specialized equipment, thin biological sections, demanding sample preparation, and its restricted output of monochromatic images. That being said, recent advances have combined light microscopy imaging with EM to enable multi-color imaging of biological structures[23].

The advent of Super-resolution Microscopy has opened the door to nanoscale imaging with light microscopy. Classical super-resolution microscopy (SRM) techniques achieve high levels of resolution by overcoming Abbe's diffraction limit (on the order of half the wavelength of light) via two general classes of strategy. The first class of strategy uses patterned illumination to manipulate the fluorescence behavior of molecules in a region smaller than the diffraction limit. This way, nearby fluorophores within a diffraction-limited distance can be uniquely identified, thereby achieving subdiffraction-limit resolution. For example, stimulated emission depletion (STED) microscopy[24,25], REversible Saturable Optical Linear Fluorescence Transitions (RESOLFT) technology[26], and super-resolution structured illumination microscopy (SIM)[27,28] belong to this group. The second class of strategy utilizes the photoswitching properties of genetically encoded or small-molecule fluorophores to stochastically enable individual molecules to be visualized at different times, so that each frame contains sparsely distributed, rarely overlapping bright spots representing individual fluorophores, for which the localization can be determined with nanoscale precision by calculation of the centroid of each spot. Assembling these points over time enables reconstruction of the entire image, but now with nanoscale resolution. This second group includes photoactivated localization microscopy (PALM)[29], fluorescence photoactivation localization microscopy (FPALM)[30], stochastic optical reconstruction microscopy (STORM)[31], and DNA points accumulation for imaging in nanoscale topography (DNA PAINT) [32,33]. The first class of strategy presents specialized hardware requirements (e.g., special laser or optical configurations), and while the second class of strategy can take advantage of conventional widefield or TIRF microscopes, one challenge is in achieving high efficacy contrast and switching of single molecules. In addition, these tools can be complex to use, and exhibit shallow depth of imaging capability, and/or slow imaging speed in comparison to standard microscopes.

Tools for Molecular Mapping of Biological Systems

Techniques for investigating the spatial molecular profiles of cells and tissues are invaluable in the types of biological insights they provide. While the past two decades have witnessed remarkable progress in high throughput *in vitro* techniques that involve isolating cells and tissue content[6,34–37], methods for in situ molecular profiling have also undergone dramatic improvements.

Recent advances have opened the door for the multiplexed imaging of proteins *in situ*. One technique that relies on antibodies for mapping proteins is array tomography[38]. In this approach, tissues are physically sectioned into 200 nm thick slices, which can then be stained and imaged via immunofluorescence over multiple rounds. While this technique increases the multiplexing capability of immunofluorescence, the volumetric reconstruction required can be cumbersome and prone to errors. Another technique that relies on immunostaining for mapping proteins is imaging mass cytometry[39]. This method represents a recent advance towards multiplexed *in situ* proteomics by combining mass spectrometry with immunohistochemistry. In this approach, fixed tissue samples are stained with antibodies labeled with heavy-metal tags. Thin tissue sections are then analyzed via line-scanning laser-ablation system coupled to a mass spectrometer. Despite its limited resolution and sensitivity, imaging mass spectrometry, such as MALDI imaging, has the potential to be a high-throughput tool for mapping proteins *in situ*[40]. Finally, recent advancement in multiplexed stimulated Raman scattering has yielded sets of dyes that can be imaged a dozen or more at a time and thus could also be adapted for multiplexed imaging of a large number of biomolecules simultaneously in a sample[41,42].

Mapping RNA *in situ* has traditionally relied on *in situ* hybridization (ISH), such as the use of digoxigenin-tagged ISH probes[43]. While the use of colorimetric ISH probes has provided many insights in mapping gene expression in tissues, it is limited by its lack of sub-cellular resolution as well as limited multiplexing capability. The development of single molecule Fluorescent In Situ Hybridization (smFISH) over a decade ago has enabled the imaging of RNA with single molecule precision[44,45]. In this approach, RNA targets are labeled with multiple probes bearing individual fluorophores, such that the binding of these probes to an individual RNA molecule produces a bright punctate signal. Recent developments in RNA-FISH have expanded the multiplexing capability of single molecule FISH (smFISH) for mapping RNA.

Pioneering strategies have exploited the ability to repeatedly interrogate RNA molecules with smFISH to devise approaches where RNA targets can be assigned a unique identifiable barcode. In two of the most successful approaches, transcripts are sequentially labeled with probes bearing different fluorophores[46,47]. As the color of a particular transcript changes over several sequential hybridization rounds, the sequence of colors provides a temporal barcode. In another temporal multiplexing approach, transcripts are combinatorically labeled over several hybridization rounds, where in a given hybridization round only a subset of transcripts are labeled. This combinatorial labeling provides each transcript a unique temporal barcode based on the detection of that transcripts in a given hybridization round. Furthermore, the past few years have witnessed success in implementing Next Generation Sequencing (NGS) sequencing chemistries in an *in situ* context to either sequence transcripts in an untargeted or targeted fashion using FISH probes[48,49]. While these techniques have opened the door for the multiplexed imaging of RNA, there exist limitations to their performance. Primarily, the resolution of optical microscopy impedes high levels of multiplexing because imaging a large fraction of the transcriptome requires the ability to resolve individual RNA molecules with in a small volume. Therefore, scaling up multiplexing levels demands a higher resolution than can be afforded by ordinary light microscopy. In addition, extending these approaches to thick tissue specimens can be challenging due to low smFISH signals, high levels of background, scattering, as well as low yields for reactions.

Molecular profiling in thick specimens was recently enabled with the development of clearing techniques. These methods use chemical approaches to minimize tissue scattering, allowing imaging through thick tissue sections. Biological specimens appear opaque due to an inhomogeneous refractive index (RI) arising from the distribution of the various molecular components of tissues. This inhomogeneity results in non-uniform scattering, which renders the specimen opaque. Furthermore, absorption of light by molecules reduces imaging depth. Tissue clearing techniques work by homogenizing the RI within a specimen so that non-uniform light scattering is minimized[50]. Various techniques clear tissues using various chemical approaches to homogenize RI within specimens. Some of these approaches include solvent-based dehydration and RI matching (3DISCO, BABB, iDISCO) [51–53], hyper-hydration based clearing (Scale, CUBIC) [54,55], RI matching in aqueous solutions (SeeDB)[56], and hydrogel-supported lipid-removal and RI matching (CLARITY, PACT/PARS)[57,58]. The last set of protocols also use

hydrogel embedding chemistries related to the Hausen and Dreyer protocol[59], but follow the embedding with removal of the lipids and immersion in compounds that even out refractive index.

Expansion Microscopy

Optical microscopy techniques make up one of the most important toolsets in the history of biology and medicine. Until recently, the diffraction limit posed by physics limited the resolution of optical microscopes to values of a few hundred nanometers—far greater than the size of biological molecules. The development of near-field imaging[60,61] and a suite of far-field super-resolution microscopy techniques[62,63] have enabled researchers to optically image single molecules and nanoscale structures in biology. Although powerful, such technologies typically require expensive equipment and/or have slow imaging speeds; 3D super-resolution imaging, especially of specimens of tissues and organs, remains a challenge. Recently it was discovered that preserved biological specimens can be physically magnified in an even fashion by synthesizing a dense, cross-linked network of swellable polyelectrolyte hydrogel throughout such a specimen[64]. This new method, termed Expansion Microscopy (ExM), can smoothly and isotropically expand biomolecules or labels away from each other after chemical processing (**Figure 1.1**). After such physical magnification, molecules in a diffraction-limited region are separated in space to greater distances, and therefore can be resolved even by conventional diffraction-limited microscopes.

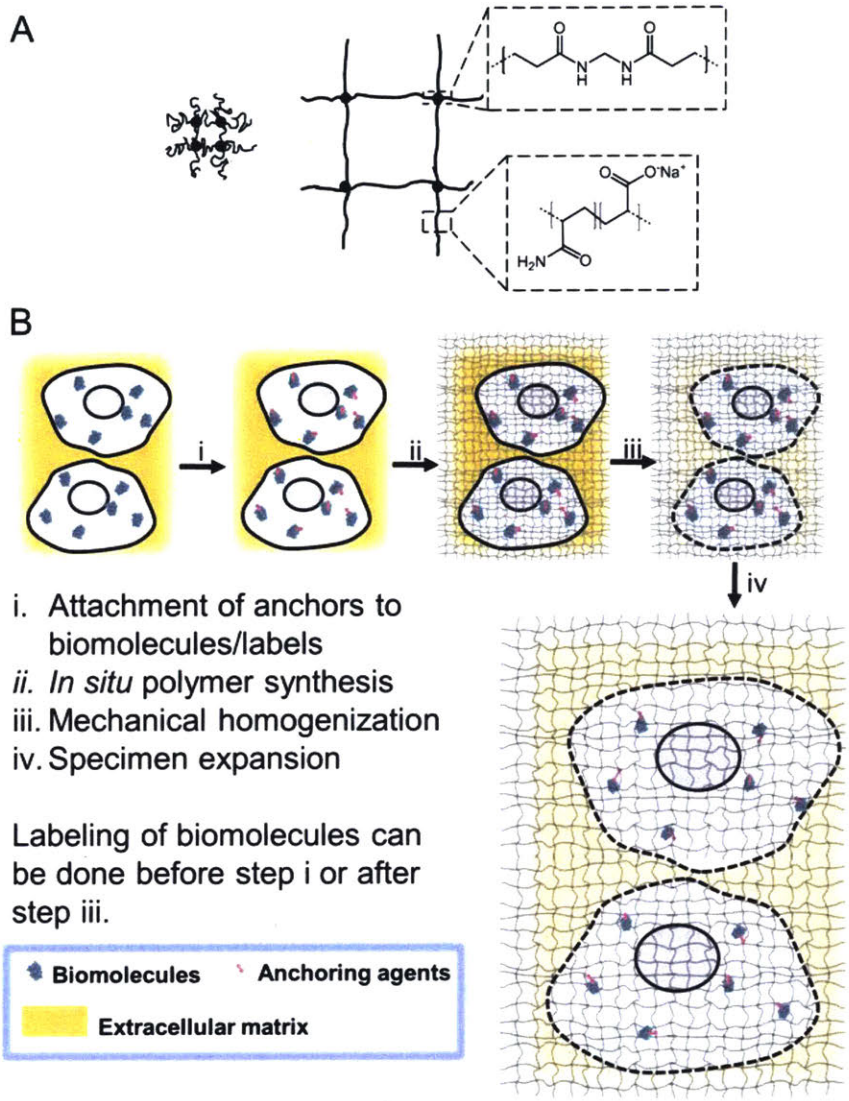

Figure 1.1: Expansion Microscopy. A, Schematic of the ExM polyelectrolyte hydrogel, cross-linked sodium polyacrylate, showing the cross-linker (dots) and polymer chain (lines) in the collapsed state before expansion (left) and in the expanded state (right). Chemical structures of cross-linker and monomer components, in the synthesized polymer context, are shown on the right. B, Diagram showing the generalized workflow for ExM. Not to scale. Adapted from refs.[64,65]

The ExM approach brings together two different fields: the physics of swellable polyelectrolyte hydrogels, which vastly increase in size when immersed in a solvent such as water and which were explored in depth by groups such as that of Toyoichi Tanaka in the late 1970s[66], and the embedding of preserved biological specimens in polymer hydrogels for imaging purposes, pioneered by teams such as that of Peter Hausen and Christine Dreyer, who used

uncharged polyacrylamide hydrogels to facilitate tissue staining and imaging in the early 1980s[59]. Such gels have polymer spacings (or mesh sizes) that are quite small—approximately 1–2 nm[67]—suggesting that the errors introduced by *in situ* polymerization and expansion could in principle also be quite small, perhaps on the order of the size of a biomolecule.

Expansion microscopy provides a set of distinct advantages that make it desirable for the multiplexed *in situ* mapping of biomolecules such as RNA and proteins. Primarily, ExM offers an easy route for the nanoscale imaging of tissues in 3D. Given the nanoscale organization of tissues, the resolution provided by ExM is critical to enable meaningful mapping of biomolecules. Even more, the resolution afforded by ExM enables high levels of multiplexing. The main challenge for highly multiplexed detection is that the single molecule resolution demanded cannot be achieved in many contexts where the high abundance of biomolecules, such as RNA, results in many targets residing within a diffraction limited volume. ExM can significantly alleviate this challenge as the physical expansion of the tissues separates targets that lie within close proximity, thereby opening the door for the implementation of highly multiplexed detection. Second, ExM enables fast reagent exchanges. After expansion, ~99% of the volume of the gel is water. As a result, reagents, such as FISH probes, can diffuse in unhindered compared to an intact tissue. Rapid diffusion of reagents is crucial for multiplexing approaches that require exchanging reagents and buffers. Finally, ExM offers a quasi *in-vitro* environment where only molecules of interest can be interrogated at a given time. Harsh reagents used for multiplexed staining and imaging may irreversibly affect tissue specimens over time. Since ExM involves anchoring only tags and biomolecules of interest, it provides a controlled and homogeneous chemical environment.

Objectives and Summary of Thesis

In this thesis, I describe how ExM can be leveraged towards mapping biomolecules with nanoscale precision in cells and tissues. In Chapter 2, I discuss the development of an approach called ExFISH, which enables the nanoscale imaging of RNA using Expansion Microscopy. I also discuss our work in validating and deploying ExFISH to visualize the nanoscale organization of RNA. In Chapter 3, I discuss our work in extending ExFISH to enable the mapping of RNA in thick tissue specimens. In Chapter 4, I describe a strategy towards the highly multiplexed imaging of transcripts. I also show how ExFISH can enable the multiplexed

detection of RNA along with proteins. Finally, in Chapter 5, I discuss the future directions and the scientific applications of the approaches developed in this thesis.

References:

1. Lodish, H. *et al. Molecular Cell Biology*. (Freeman-Macmillan Learning, 2016).
2. Cohen, S., Valm, A. M. & Lippincott-Schwartz, J. Interacting organelles. *Curr. Opin. Cell Biol.* **53,** 84–91 (2018).
3. Valm, A. M. *et al.* Applying systems-level spectral imaging and analysis to reveal the organelle interactome. *Nature* **546,** 162–167 (2017).
4. Guo, Y. *et al.* Visualizing Intracellular Organelle and Cytoskeletal Interactions at Nanoscale Resolution on Millisecond Timescales. *Cell* **175,** 1430–1442.e17 (2018).
5. Cremer, M. & Cremer, T. Nuclear compartmentalization, dynamics, and function of regulatory DNA sequences. *Genes, Chromosom. Cancer* (2019). doi:10.1002/gcc.22714
6. Lieberman-Aiden, E. *et al.* Comprehensive mapping of long-range interactions reveals folding principles of the human genome. *Science* **326,** 289–93 (2009).
7. Bickmore, W. A. The Spatial Organization of the Human Genome. *Annu. Rev. Genomics Hum. Genet.* **14,** 67–84 (2013).
8. Yu, M. & Ren, B. The Three-Dimensional Organization of Mammalian Genomes. *Annu. Rev. Cell Dev. Biol. Annu. Rev. Cell Dev. Biol* **33,** 265–89 (2017).
9. Hnisz, D., Shrinivas, K., Young, R. A., Chakraborty, A. K. & Sharp, P. A. A Phase Separation Model for Transcriptional Control. *Cell* **169,** 13–23 (2017).
10. Cisse, I. I. *et al.* Real-time dynamics of RNA polymerase II clustering in live human cells. *Science* **341,** 664–7 (2013).
11. Bornens, M. The centrosome in cells and organisms. *Science* **335,** 422–6 (2012).
12. Sporns, O., Tononi, G. & Kötter, R. The Human Connectome: A Structural Description of the Human Brain. *PLoS Comput. Biol.* **1,** e42 (2005).
13. Kandel, E. R., Schwartz, J. H. & Jessell, T. M. *Principles of Neural Science*. (McGraw-

Hill, Health Professions Division, 2012).

14. Shepherd, G. *Synaptic Organization of The Brain*. (Oxford University Press, 2004).

15. Wilhelm, B. G. *et al.* Composition of isolated synaptic boutons reveals the amounts of vesicle trafficking proteins. *Science* **344,** 1023–8 (2014).

16. Kourkoutis, L. F., Plitzko, J. M. & Baumeister, W. Electron Microscopy of Biological Materials at the Nanometer Scale. *Annu. Rev. Mater. Res.* **42,** 33–58 (2012).

17. White, J., Southgate, E., Thomson, J. N. & Brenner, S. The structure of the nervous system of the nematode Caenorhabditis elegans. *Philos. Trans. R. Soc. London* **314,** 1–340 (1986).

18. Helmstaedter, M. *et al.* Connectomic reconstruction of the inner plexiform layer in the mouse retina. *Nature* **500,** 168–174 (2013).

19. Kasthuri, N. *et al.* Saturated Reconstruction of a Volume of Neocortex. *Cell* **162,** 648–661 (2015).

20. Koning, R. I., Koster, A. J. & Sharp, T. H. Advances in cryo-electron tomography for biology and medicine. *Ann. Anat. - Anat. Anzeiger* **217,** 82–96 (2018).

21. Asano, S., Engel, B. D. & Baumeister, W. In Situ Cryo-Electron Tomography: A Post-Reductionist Approach to Structural Biology. *J. Mol. Biol.* **428,** 332–343 (2016).

22. Asano, S. *et al.* Proteasomes. A molecular census of 26S proteasomes in intact neurons. *Science* **347,** 439–42 (2015).

23. de Boer, P., Hoogenboom, J. P. & Giepmans, B. N. G. Correlated light and electron microscopy: ultrastructure lights up! *Nat. Methods* **12,** 503–513 (2015).

24. Hell, S. W. & Wichmann, J. Breaking the diffraction resolution limit by stimulated emission: stimulated-emission-depletion fluorescence microscopy. *Opt. Lett.* **19,** 780–2 (1994).

25. Klar, T. A., Jakobs, S., Dyba, M., Egner, A. & Hell, S. W. Fluorescence microscopy with diffraction resolution barrier broken by stimulated emission. *Proc. Natl. Acad. Sci. U. S. A.* **97,** 8206–10 (2000).

26. Hofmann, M., Eggeling, C., Jakobs, S. & Hell, S. W. Breaking the diffraction barrier in fluorescence microscopy at low light intensities by using reversibly photoswitchable proteins. *Proc. Natl. Acad. Sci.* **102,** 17565–17569 (2005).

27. Gustafsson, M. G. Surpassing the lateral resolution limit by a factor of two using structured illumination microscopy. *J. Microsc.* **198,** 82–7 (2000).

28. Heintzmann, R. & Cremer, C. G. Laterally modulated excitation microscopy: improvement of resolution by using a diffraction grating. in *Proc. SPIE* (eds. Bigio, I. J., Schneckenburger, H., Slavik, J., Svanberg, K. & Viallet, P. M.) **3568,** 185–196 (International Society for Optics and Photonics, 1999).

29. Betzig, E. *et al.* Imaging Intracellular Fluorescent Proteins at Nanometer Resolution. *Science (80-.).* **313,** 1642–1645 (2006).

30. Hess, S. T., Girirajan, T. P. K. & Mason, M. D. Ultra-high resolution imaging by fluorescence photoactivation localization microscopy. *Biophys. J.* **91,** 4258–72 (2006).

31. Rust, M. J., Bates, M. & Zhuang, X. Sub-diffraction-limit imaging by stochastic optical reconstruction microscopy (STORM). *Nat. Methods* **3,** 793–796 (2006).

32. Jungmann, R. *et al.* Single-molecule kinetics and super-resolution microscopy by fluorescence imaging of transient binding on DNA origami. *Nano Lett.* **10,** 4756–61 (2010).

33. Jungmann, R. *et al.* Multiplexed 3D cellular super-resolution imaging with DNA-PAINT and Exchange-PAINT. *Nat. Methods* **11,** 313–8 (2014).

34. Mortazavi, A., Williams, B. A., McCue, K., Schaeffer, L. & Wold, B. Mapping and quantifying mammalian transcriptomes by RNA-Seq. *Nat. Methods* **5,** 621–628 (2008).

35. Macosko, E. Z. *et al.* Highly parallel genome-wide expression profiling of individual cells using nanoliter droplets. *Cell* **161,** 1202–1214 (2015).

36. Buenrostro, J. D. *et al.* Single-cell chromatin accessibility reveals principles of regulatory variation. *Nature* **523,** 486–490 (2015).

37. Aebersold, R. & Mann, M. Mass spectrometry-based proteomics. *Nature* **422,** 198–207

(2003).

38. Micheva, K. D. & Smith, S. J. Array Tomography: A New Tool for Imaging the Molecular Architecture and Ultrastructure of Neural Circuits. *Neuron* **55,** 25–36 (2007).

39. Giesen, C. *et al.* Highly multiplexed imaging of tumor tissues with subcellular resolution by mass cytometry. *Nat. Methods* **11,** 417–22 (2014).

40. Cornett, D. S., Reyzer, M. L., Chaurand, P. & Caprioli, R. M. MALDI imaging mass spectrometry: molecular snapshots of biochemical systems. *Nat. Methods* **4,** 828–833 (2007).

41. Hu, F. *et al.* Supermultiplexed optical imaging and barcoding with engineered polyynes. *Nat. Methods* **15,** 194–200 (2018).

42. Wei, L. *et al.* Super-multiplex vibrational imaging. *Nature* **544,** 465–470 (2017).

43. Lein, E. S. *et al.* Genome-wide atlas of gene expression in the adult mouse brain. *Nature* **445,** 168–176 (2007).

44. Femino, A. M., Fay, F. S., Fogarty, K. & Singer, R. H. Visualization of single RNA transcripts in situ. *Science* **280,** 585–90 (1998).

45. Raj, A., van den Bogaard, P., Rifkin, S. A., van Oudenaarden, A. & Tyagi, S. Imaging individual mRNA molecules using multiple singly labeled probes. *Nat. Methods* **5,** 877–9 (2008).

46. Lubeck, E., Coskun, A. F., Zhiyentayev, T., Ahmad, M. & Cai, L. Single-cell in situ RNA profiling by sequential hybridization. *Nat. Methods* **11,** 360–1 (2014).

47. Chen, K. H., Boettiger, A. N., Moffitt, J. R., Wang, S. & Zhuang, X. Spatially resolved, highly multiplexed RNA profiling in single cells. *Sci.* **348,** (2015).

48. Lee, J. H. *et al.* Highly Multiplexed Subcellular RNA Sequencing in Situ. *Science (80-.).* **343,** 1360–1363 (2014).

49. Ke, R. *et al.* In situ sequencing for RNA analysis in preserved tissue and cells. *Nat. Methods* **10,** 857–60 (2013).

50. Richardson, D. S. & Lichtman, J. W. Clarifying Tissue Clearing. *Cell* **162,** 246–257 (2015).

51. Dodt, H.-U. *et al.* Ultramicroscopy: three-dimensional visualization of neuronal networks in the whole mouse brain. *Nat. Methods* **4,** 331–336 (2007).

52. Ertürk, A. *et al.* Three-dimensional imaging of solvent-cleared organs using 3DISCO. *Nat Protoc* **7,** 1983–1995 (2012).

53. Renier, N. *et al.* iDISCO: A Simple, Rapid Method to Immunolabel Large Tissue Samples for Volume Imaging - suppl original. *Cell* **159,** (2014).

54. Hama, H. *et al.* Scale: a chemical approach for fluorescence imaging and reconstruction of transparent mouse brain. *Nat. Neurosci.* **14,** 1481–8 (2011).

55. Susaki, E. A. *et al.* Whole-brain imaging with single-cell resolution using chemical cocktails and computational analysis. *Cell* **157,** 726–739 (2014).

56. Ke, M.-T., Fujimoto, S. & Imai, T. SeeDB : a simple and morphology-preserving optical clearing agent for neuronal circuit reconstruction. *Nat. Publ. Gr.* **16,** 1154–1161 (2013).

57. Yang, B. *et al.* Single-cell phenotyping within transparent intact tissue through whole-body clearing. *Cell* **158,** 945–958 (2014).

58. Chung, K. *et al.* Structural and molecular interrogation of intact biological systems. *Nature* **497,** 332–7 (2013).

59. Hausen, P. & Dreyer, C. The Use of Polyacrylamide as an Embedding Medium for Immunohistochemical Studies of Embryonic Tissues. *Stain Technol.* **56,** 287–293 (1981).

60. Dunn, R. C. Near-field scanning optical microscopy. *Chem. Rev.* **99,** 2891–928 (1999).

61. Dürig, U., Pohl, D. W. & Rohner, F. Near-field optical-scanning microscopy. *J. Appl. Phys.* **59,** 3318–3327 (1986).

62. Hell, S. W. Far-field optical nanoscopy. in *2010 23rd Annual Meeting of the IEEE Photonics Society, PHOTINICS 2010* 3–4 (2010). doi:10.1109/PHOTONICS.2010.5698725

63. Huang, B., Bates, M. & Zhuang, X. Super-Resolution Fluorescence Microscopy. *Annu. Rev. Biochem.* **78,** 993–1016 (2009).

64. Chen, F., Tillberg, P. W. & Boyden, E. S. Expansion Microscopy. *Science* **347,** 543–548 (2015).

65. Wassie, A. T., Zhao, Y. & Boyden, E. S. Expansion microscopy: principles and uses in biological research. *Nat. Methods* **16,** 33–41 (2019).

66. Tanaka, T. *et al.* Phase Transitions in Ionic Gels. *Phys. Rev. Lett.* **45,** 1636–1639 (1980).

67. Cohen, Y., Ramon, O., Kopelman, I. J. & Mizrahi, S. Characterization of inhomogeneous polyacrylamide hydrogels. *J. Polym. Sci. Part B Polym. Phys.* **30,** 1055–1067 (1992).

Chapter 2: Development and Validation of ExFISH

Introduction:

Nanoscale-resolution imaging of RNA throughout cells, tissues, and organs is key for an understanding of local RNA processing, mapping structural roles of RNA, and defining cell types and states. However, it has remained difficult to image RNA in intact tissues with the nanoscale precision required to pinpoint associations with cellular compartments or proteins important for RNA function. Recently an approach was developed to physically magnify tissues, expansion microscopy (ExM)[1]. ExM isotropically magnifies tissues, enabling super-resolution imaging on conventional diffraction-limited microscopes. For example, ~4× linear expansion yields ~70 nm resolution using a ~300 nm diffraction-limited objective lens. In the original protocol, fluorophore tags were first targeted to proteins of interest via antibodies, and then anchored to a swellable polyelectrolyte gel synthesized *in situ*. Isotropic expansion was subsequently enabled by proteolytic treatment to homogenize specimen mechanical properties followed by osmotic swelling of the specimen-gel composite.

Here, we have developed a small molecule linker that enables RNA to be covalently attached to the ExM gel. We show that this procedure, which we call ExFISH, enables RNA fluorescent *in situ* hybridization (FISH), which enables identification of transcripts *in situ* with single molecule precision. In RNA FISH, a set of fluorescent probes complementary to a target strand of mRNA are delivered[2,3]. Single molecule FISH (smFISH) can be performed with multiple fluorophores delivered to a single mRNA via oligonucleotide probes[4]. In intact tissues, amplification strategies, such as hybridization chain reaction (HCR)[5,6], and branched DNA amplification[7,8], can enable a large number of fluorophores to be targeted to a single mRNA. We show that ExFISH can support smFISH in cell culture (Chapter 2), and HCR-amplified FISH in intact mouse brain tissues (Chapter 3). We demonstrate the power of ExFISH for revealing nanoscale structures of long non-coding RNAs (lncRNAs), as well as for localizing neural mRNAs to individual dendritic spines (Chapter 3). ExFISH will be useful for a diversity of questions relating the structure and location of RNA to biological functions.

ExFISH: Design and RNA Anchoring Chemistry

We first determined a strategy for covalently linking RNAs directly to the ExM gel. Although transcripts are crosslinked to proteins during fixation, the strong proteolysis of ExM precludes a reliance on proteins for RNA retention (**Figure 2.1**). We thus reasoned that covalently securing RNA molecules directly to the ExM gel via a small molecule linker would enable the interrogation of these molecules post-expansion. To achieve this aim, we synthesized a reagent from two building blocks: a molecule containing both an amine as well as an alkylating group that primarily reacts to the N7 of guanine, and a molecule that contains an amine-reactive succinamide ester and a polymerizable acrylamide moiety. Commercially available reagents exist that satisfy each of these two profiles, such as Label-IT Amine (MirusBio) and 6-((Acryloyl)amino)hexanoic acid (Acryloyl-X SE, here abbreviated AcX, Life Technologies; all reagents are listed in **Supplementary Table 1**).

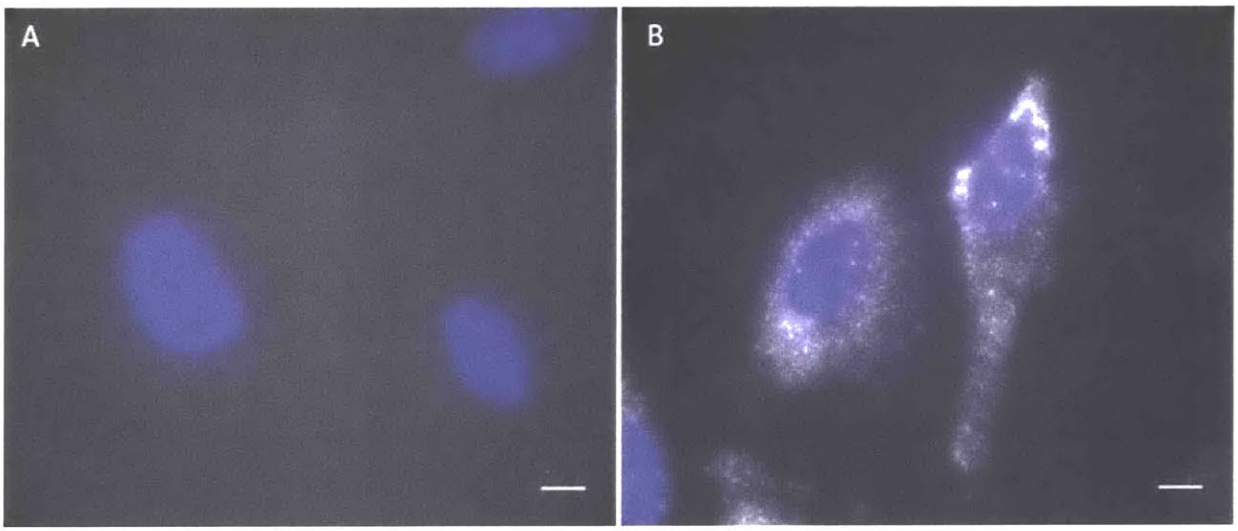

Figure 2.1: Retention of RNA with LabelX. (a) Epi-fluorescence image of single molecule FISH (smFISH) against GAPDH on HeLa cells expanded without LabelX treatment. (b) Epi-fluorescence image of smFISH performed against GAPDH on expanded HeLa cells treated with LabelX. Images are maximum intensity projections of 3-D stacks. Nuclei stained with DAPI (shown in blue). Scale bars: 20 μm (post-expanded units).

We named this molecule, which enables RNA to be covalently functionalized with a free radical polymerizable group, LabelX (**Figure 2.2a**). We verified that LabelX does not impede smFISH readout (**Figure 2.3**). We then designed a procedure where a sample could be treated with LabelX to make its RNAs gel-anchorable, followed by gel formation, proteolysis, and osmotic

swelling as performed in the original ExM protocol. Once a sample was thus expanded, the RNAs could then be interrogated through FISH (**Figure 2.2b**).

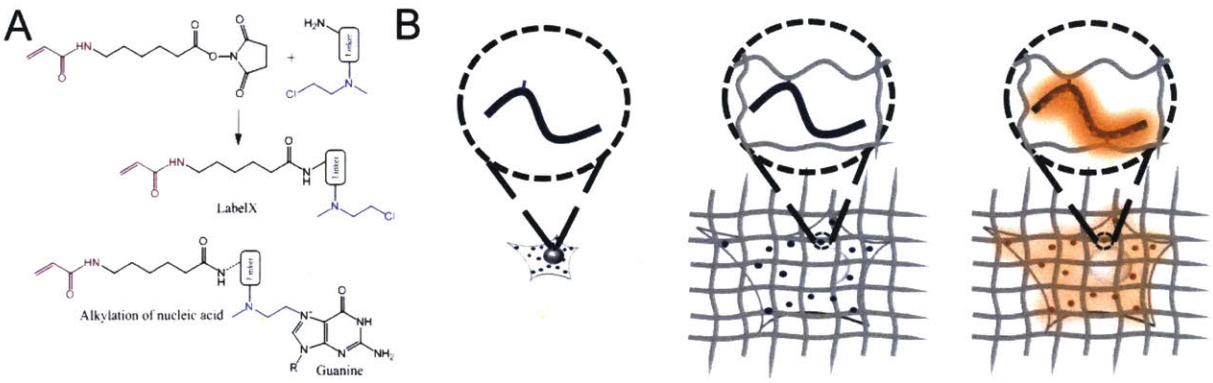

Figure 2.2. Design of ExFISH chemistry. (a) Acryloyl-X SE (top left) is reacted to Label-IT® amine (top right) via NHS-ester chemistry to form LabelX (middle), which serves to make RNA gel-anchorable by alkylating its bases (e.g., the N7 position of guanines) (bottom). (b) Workflow for ExFISH: biological specimens are treated with LabelX (left), which enables RNA to be anchored to the ExM gel (middle). Anchored RNA can be probed via hybridization (right), after gelation, digestion, and expansion.

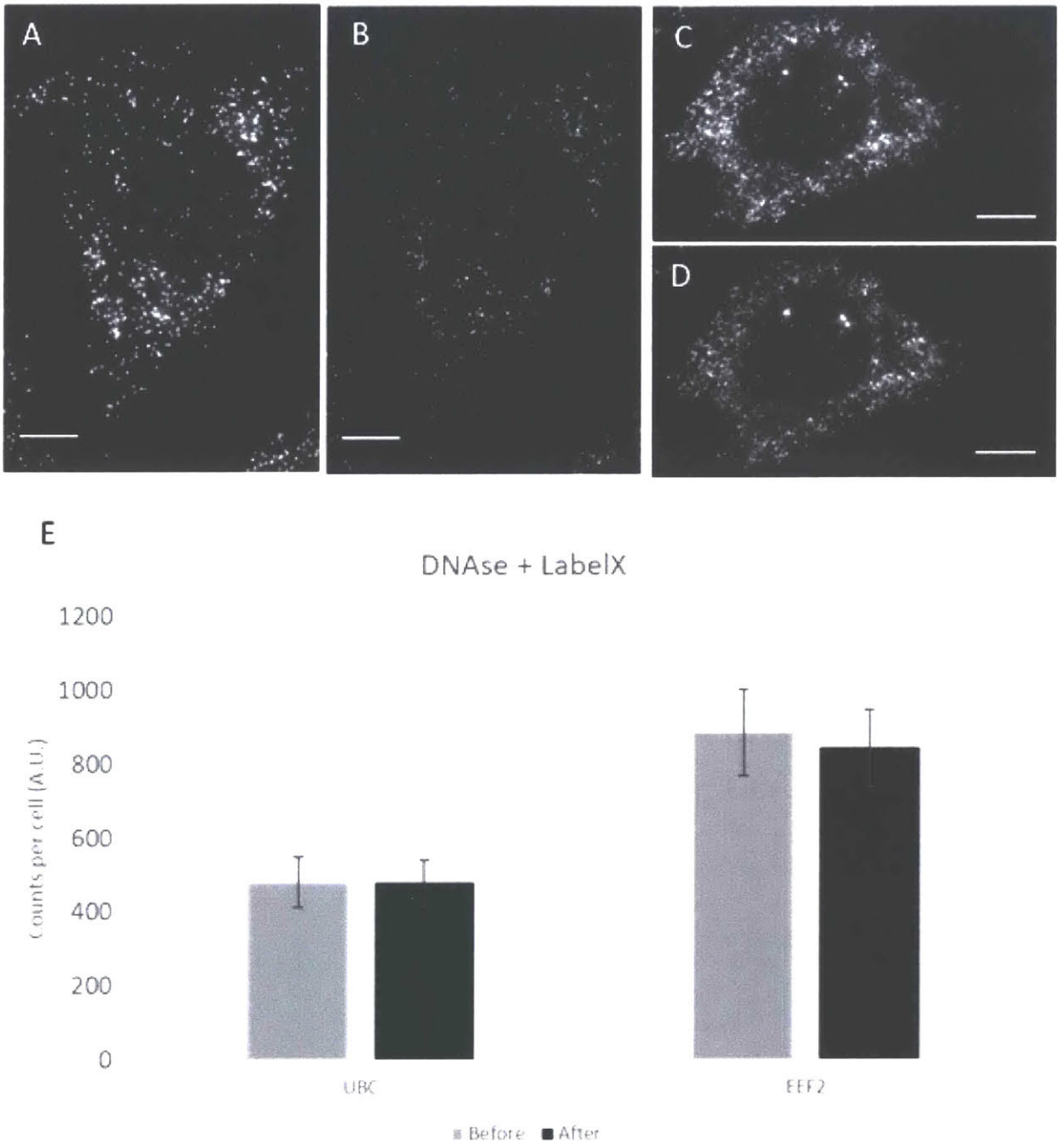

Figure 2.3. Effect of LabelX on fluorescent *in situ* hybridization. To access the effect of LabelX on fluorescent *in situ* hybridization, fixed HeLa cells were stained with smFISH probe-sets, followed by DNAse I treatment to remove the staining. The cells were then treated with LabelX and stained again with the same smFISH probe-sets. (a) UBC staining before LabelX treatment and (b) UBC staining after probe removal and LabelX treatment. (c) EEF2 staining before LabelX treatment. (d) EEF2 staining after probe removal and LabelX treatment. (e) Comparison of smFISH spots counted for individual cells before LabelX, and after probe removal and application of LabelX. The number of RNA molecules detected in a given cell was quantified using an automated spot counting algorithm (n=7 cells for each bar).

Plotted are mean + standard error; no significant difference in spot counts before vs after LabelX ($p > 0.5$ for before vs. after for UBC, $p > 0.5$ for before vs. after for EEF2; t-test, unpaired, two-tailed). Images in a-d are maximum intensity projections of 3-D stacks; scale bars: 10 μm (pre-expanded units).

Validation of Yield and Isotropy of ExFISH

To quantify RNA transcript anchoring yield after expansion, we used smFISH probes targeting mRNAs of varying copy number (7 targets, with copy number ranging from ~10 to ~10,000 per cell, $n = 59$ cells across all 7 targets). smFISH images, taken with probes delivered before (**Figure 2.4a**) and after (**Figure 2.4b**) expansion, to the same cells, showed no loss of transcript detectability with expansion for both low- and high-copy number transcripts (**Figure 2.4c**). The ratio of transcripts detected was near unity at low transcript counts (e.g., in the 10's), however, more transcripts were detected after expansion for highly expressed mRNAs (e.g., in the 1,000's) (**Figure 2.5, Supplementary Table 2**). This difference arises from the high density of smFISH spots for these targets in the un-expanded state, with the expansion process de-crowding spots that previously were indistinguishable. For example, for smFISH against *ACTB*, we were able to resolve individual *ACTB* mRNA puncta post-expansion even within transcriptional foci in the nucleus (**Figure 2.4a**, versus **2.4b**), which can be dense with mRNA due to transcriptional bursting. Thus, ExFISH is capable of supporting single molecule RNA readout in the expanded state.

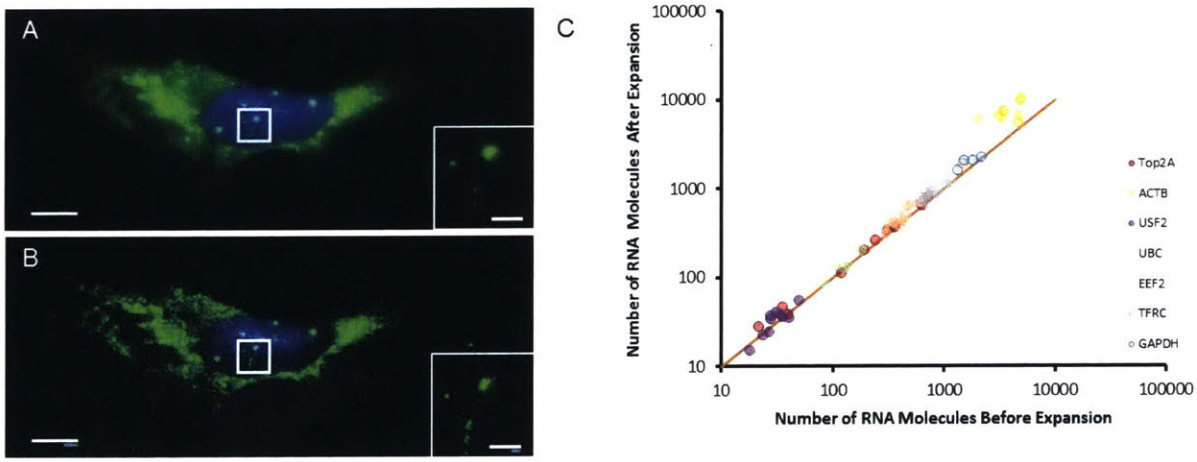

Figure 2.4. LabelX Retains RNA with High Efficiency (a) smFISH image of ACTB before expansion. Inset shows zoomed-in region, highlighting transcription sites in nucleus. (b) As in (a), using ExFISH. (c) smFISH counts before versus after expansion for seven different transcripts (n = 59 cells; each symbol represents one

cell).). Scale bars (white, in pre-expansion units; blue scale bars are divided by the expansion factor noted))): (a, b) 10 μm (expansion factor, 3.3×), inset 2 μm.

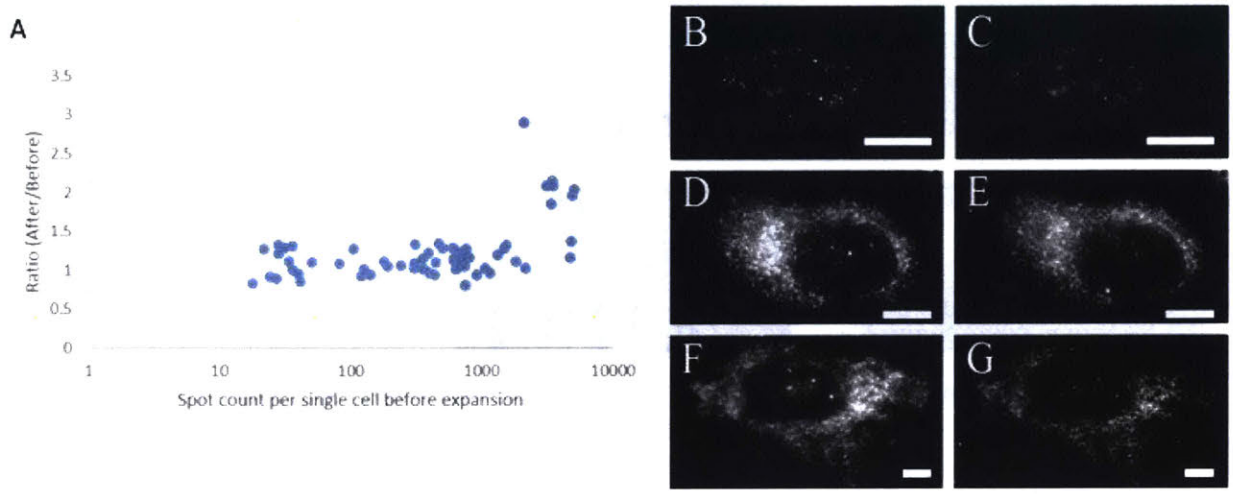

Figure 2.5. High efficiency covalent anchoring of RNA to the ExM polymer gel. Different RNA species spanning 3 orders of magnitude in abundance were detected via single molecule RNA fluorescent in situ hybridization (FISH) in HeLa cells before and after ExM with LabelX treatment (shown in Fig. 1e). (a) Ratio of FISH spots detected after expansion to spots detected before expansion for single cells. Representative before vs. after ExFISH images shown: (b,c) TFRC; (d,e) GAPDH; (f,g) ACTB. Scale bars, 10 μm (pre-expanded units) in b, d, f; c, e, g, expanded physical size 21 μm (imaged in PBS).

Since Label-IT also reacts to DNA, the ExFISH process enables uniform expansion of the nucleus (**Figure 2.6**). The isotropy of ExFISH (**Figure 2.7**) was numerically similar to that observed when protein targets were labeled and expanded in the original ExM protocol[1]. In recent ExM protocols in which proteins are anchored to the same hydrogel as used in ExFISH, with a similar linker[9,10], the distortion is small (a few percent distortion, in cells and tissues). These earlier results, since they were obtained with similar polymer chemistry, serve to bound the ExFISH distortion. The expansion factor is slightly lower than in the original ExM paper (i.e., ~3.3× versus ~4×, expansion factors can be found in Figure Legends) due to the salt required to support hybridization of probes.

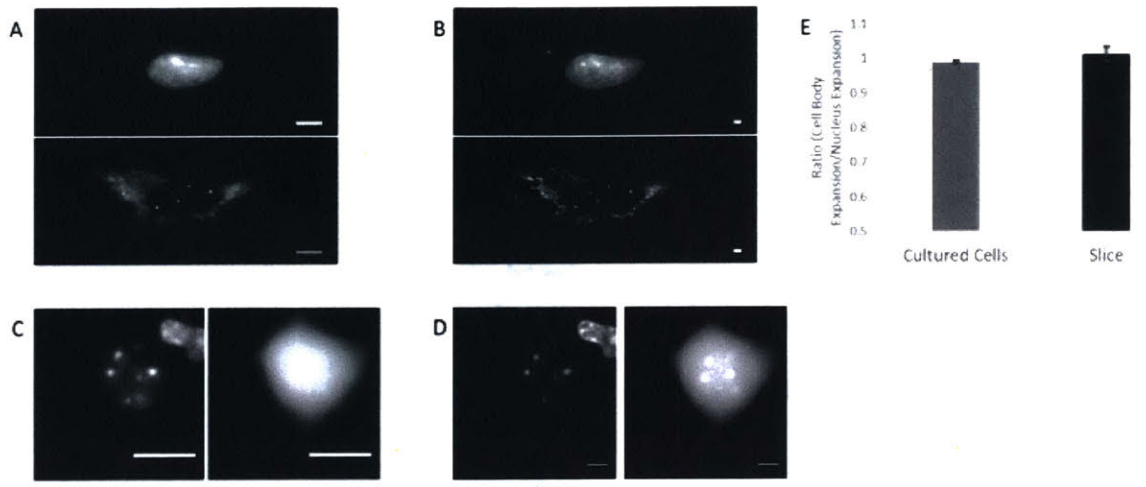

Figure 2.6. Label-X does not impede nuclear expansion. (a) Pre-expansion widefield image of a cultured HeLa cell stained with DAPI to visualize the nucleus (top panel) and smFISH probes against ACTB (bottom panel). (b) Post-expansion widefield image of the same cell as in (a). (c) Pre-expansion widefield image of Label-X treated Thy1-YFP brain slice (left panel, YFP protein) stained with DAPI (right panel) (MIP, 4 μm z-depth). (d) Post-expansion image of the same region as in (c) (MIP, 12 μm). (e) Ratio of the expansion factor of cell bodies for individual cells to the expansion factor of their respective nuclei. smFISH stain is used to outline the boundaries of the cell bodies of cultured cells while the endogenous YFP protein is used to demarcate the cell bodies of neurons in Thy1-YFP brain slices. Plotted are mean ± standard error. The ratio for both cultured cells and brain slices did not significantly deviate from one ($p > 0.05$ for both, 1-sample t-test; $n = 6$, cultured HeLa cells; $n = 7$, cells in 1 brain slice). Scale bars, 10 μm.

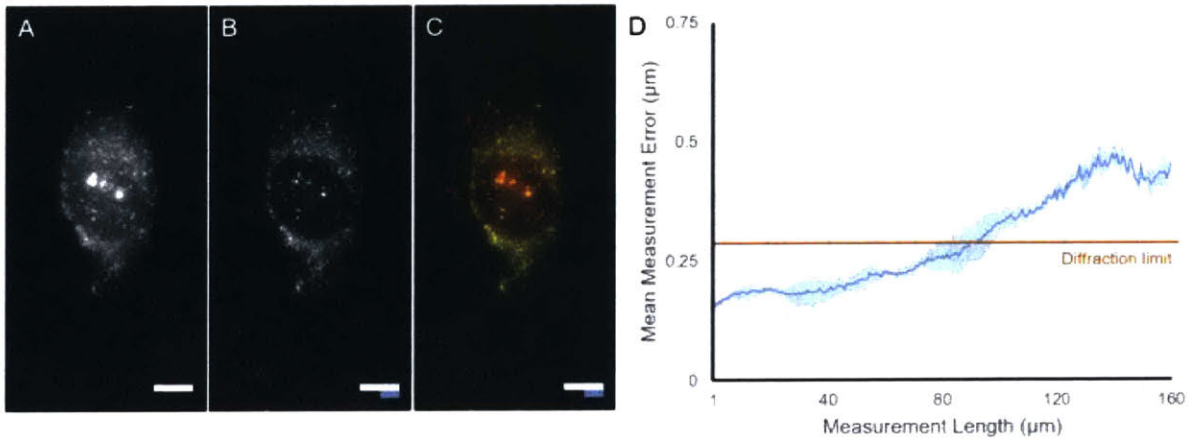

Figure 2.7. Isotropy of ExFISH. (**a**) Representative FISH image of *TOP2A* in a single HeLa cell before expansion (MIP of cell thickness). (**b**) ExFISH image of cell in (**a**) taken with the same optical parameters. (**c**) Merged image of (**a**) and (**b**) (red and green for before and after expansion respectively); distance measurements between pairs of mRNA spots before (L, red line) and after (L', green line; note

that these lines overlap nearly completely) expansion were used to quantify expansion isotropy. (**d**) Mean of the absolute value of the measurement error (i.e., |L-L'|) plotted against measurement length (L) for all pairs of mRNA spots (mean ± standard deviation, $N = 4$ samples, 6.8 x 10^5 measurements). Scale bars: white, 10 μm pre-expansion units; blue, white scale bar divided by expansion factor. Orange line indicates diffraction limit of the microscope used (see Methods for details).

Nanoscale Imaging of lncRNA with ExFISH

We imaged long non-coding RNAs (lncRNAs) known to serve structural roles in cell biology. We imaged the lncRNA *XIST*, whose role in inactivating the X chromosome may depend on initial association with specific chromatin subregions through a process which is still being revealed[11]. The pre-expansion image (**Figure 2.8a**) shows two bright globular fluorescent regions, presumably corresponding to the X chromosomes of HEK cells undergoing inactivation[11–13], but post-expansion, individual puncta were apparent both within the globular regions as well as nearby (**Figure 2.8b**). We additionally used ExFISH to examine the previously described[14] ring-shaped morphology of ensembles of *NEAT1* lncRNAs (**Figure 2.8c**), which has been hypothesized to play an important role in gene expression regulation and nuclear mRNA retention[15]. Before expansion, *NEAT1* presents in the form of bright, diffraction-limited puncta (**Figure 2.8c, Figure 2.8d**), but after expansion, the ring-shaped morphology becomes clear (**Figure 2.8c, Figure 2.8d**). Given the complex 3-D structure of the genome[16], mapping lncRNAs may be useful in defining key chromatin regulatory complexes and their spatial configurations.

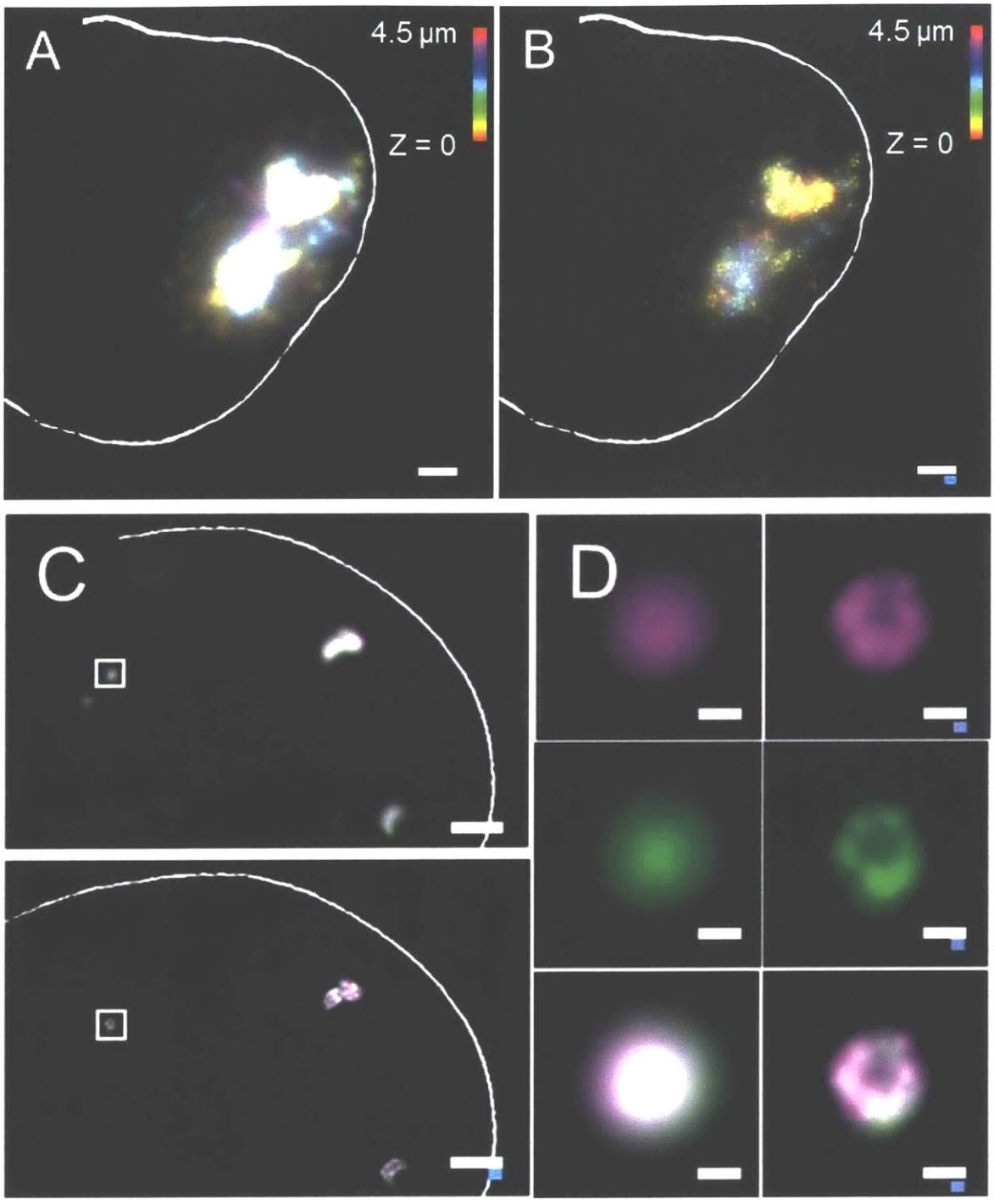

Figure 2.8. Nanoscale Imaging of lncRNA Organization with ExFISH. (**a**) smFISH image of *XIST* long non-coding RNA (lncRNA) in the nucleus of a HEK293 cell before expansion (white line denotes nuclear envelope in **a-c**). (**b**) As in (**a**), using ExFISH. (**c**) smFISH image before expansion (top), and using ExFISH (bottom), of *NEAT1* lncRNA in the nucleus of a HeLa cell. Magenta and green indicate probesets binding to different parts of the 5' (1-3756 nts) of *NEAT1* (see Methods). (**d**) Insets showing a *NEAT1* cluster (boxed region of (**c**)) with smFISH (left) and ExFISH (right). Scale bars (white, in pre-expansion units; blue scale bars are

divided by the expansion factor noted))): (**a, b**) 2 μm (3.3×), Z scale represented by color coding in pre-expansion units; (**c**) 2 μm (3.3×); (**d**) 200 nm (3.3×).

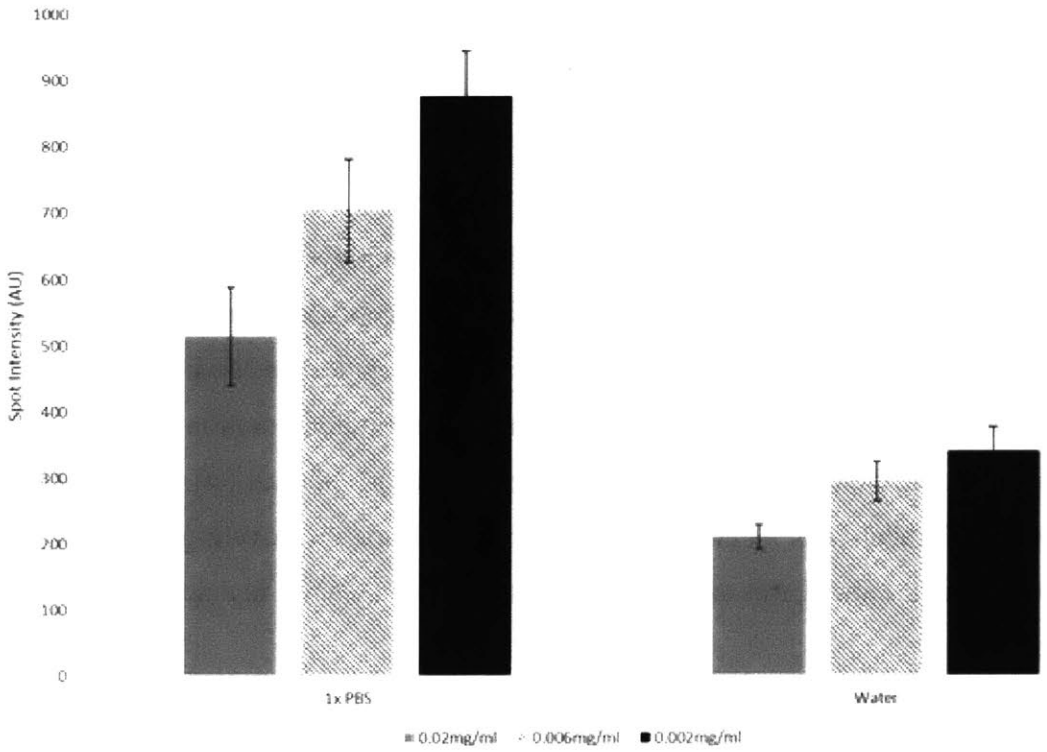

Figure 2.9. Dependence of RNA FISH spot intensity on degree of expansion and concentration of LabelX. HeLa cells, treated with LabelX diluted to different final concentrations of Label-IT Amine concentration, were expanded and stained with a probe-set against *GAPDH*. After staining, the gelled samples were expanded in 1× PBS (~2× expansion ratio) and water (~4× expansion ratio) and the spot intensity for the different samples was quantified. Plotted are mean ± standard error; $N = 6$ cells.

Materials and Methods

A table of all reagents and chemicals with part numbers and suppliers can be found in **Supplementary Table 1**.

Cell Culture and Fixation:

HeLa (ATCC CCL-2) cells and HEK293-FT cells (Invitrogen) were cultured on Nunc Lab-Tek II Chambered Coverglass (Thermo Scientific) in D10 medium (Cellgro) supplemented with 10% FBS (Invitrogen), 1% penicillin/streptomycin (Cellgro), and 1% sodium pyruvate

(BioWhittaker). Cells were authenticated by the manufacturer and tested for mycoplasma contamination to their standard levels of stringency, and were here used because they are common cell lines for testing new tools. Cultured cells were washed once with DPBS (Cellgro), fixed with 10% formalin for 10 mins, and washed twice with 1× PBS. Fixed cells were then stored in 70% Ethanol at 4°C until use.

Preparation of LabelX:

Acryloyl-X, SE (6-((acryloyl)amino)hexanoic acid, succinimidyl ester, here abbreviated AcX; Thermo-Fisher) was resuspended in anhydrous DMSO at a concentration of 10 mg/mL, aliquoted and stored frozen in a desiccated environment. Label-IT ® Amine Modifying Reagent (Mirus Bio, LLC) was resuspended in the provided Mirus Reconstitution Solution at 1mg/ml and stored frozen in a desiccated environment. To prepare LabelX, 10 μL of AcX (10 mg/mL) was reacted with 100 μL of Label-IT ® Amine Modifying Reagent (1 mg/mL) overnight at room temperature with shaking. LabelX was subsequently stored frozen (-20 °C) in a desiccated environment until use.

LabelX Treatment of Cultured Cells:

Fixed cells were washed twice with 1× PBS, once with 20 mM MOPS pH 7.7, and incubated with LabelX diluted to a desired final concentration in MOPS buffer (20 mM MOPS pH 7.7) at 37 °C overnight followed by two washes with 1× PBS. For cells, ranges of LabelX were used that resulted in a Label-IT ® Amine concentration of 0.006-0.02 mg/mL; higher concentrations resulted in somewhat dimmer smFISH staining (**Figure 2.9**), but otherwise no difference in staining quality was observed with Label-IT ® Amine concentrations in this range. For Figure 2.1, Figure 2.2, Figure 2.4c, and Figure 2.5 fixed cells were incubated with LabelX diluted to a final Label-IT ® Amine concentration of 0.02 mg/mL. For all other experiments in cells, fixed cells were treated with LabelX diluted to a final Label-IT ® Amine concentration of 0.006 mg/mL.

smFISH in Fixed Cultured Cells Before Expansion:

Fixed cells were briefly washed once with wash buffer (10% formamide, 2× SSC) and hybridized with RNA FISH probes in hybridization buffer (10% formamide, 10% dextran sulfate, 2× SSC) overnight at 37 °C. Following hybridization, samples were washed twice with wash buffer, 30mins per wash, and washed once with 1× PBS. Imaging was performed in 1× PBS.

smFISH probe sets targeting the human transcripts for *TFRC*, *ACTB*, *GAPDH*, *XIST*, and 5' portion of *NEAT1* were ordered from Stellaris with Quasar 570 dye. Probe sets against *UBC*, *EEF2*, *USF2*, *TOP2A* and full length *NEAT1* were synthesized, conjugated to fluorophores, and subsequently purified by HPLC as described previously[17]. Oligonucleotide sequences for probe sets and accession numbers can be found in **Supplementary Table 4**.

Gelation, Digestion and Expansion:

Monomer solution (1× PBS, 2 M NaCl, 8.625% (w/w) sodium acrylate, 2.5% (w/w) acrylamide, 0.15% (w/w) N,N'-methylenebisacrylamide) was mixed, frozen in aliquots, and thawed before use. Monomer solution was cooled to 4°C before use. For gelling cultured cells treated with LabelX, a concentrated stock of VA-044 (25% w/w, chosen instead of the Ammonium persulfate (APS)/Tetramethylethylenediamine (TEMED) of the original ExM protocol[1] because APS/TEMED resulted in autofluorescence that was small in magnitude but appreciable in the context of smFISH) was added to the monomer solution to a final concentration of 0.5% (w/w) and degassed in 200 µl aliquots for 15 mins. Cells were briefly incubated with the monomer solution plus VA-044 and transferred to a humidified chamber. Subsequently, the humidified chamber was purged with nitrogen gas. To initiate gelation, the humidified chamber was transferred to a 60 °C incubator for two hours. Gelled cultured cells and were digested with Proteinase K (New England Biolabs) diluted 1:100 to 8 units/mL in digestion buffer (50 mM Tris (pH 8), 1 mM EDTA, 0.5% Triton X-100, 500 mM NaCl) and digestion was carried out overnight at 37 °C. The gels expand slightly in the high osmolarity digestion buffer (~1.5×). After digestion, gels were stored in 1× PBS until use and expansion was carried out as previously described.

smFISH Staining After Expansion:

Expanded gels were incubated with wash buffer (10% formamide, 2× SSC) for 30 mins at room temperature and hybridized with RNA FISH probes in hybridization buffer (10% formamide, 10% dextran sulfate, 2× SSC) overnight at 37 °C. Following hybridization, samples were washed twice with wash buffer, 30 minutes per wash, and washed once with 1× PBS for another 30 mins. Imaging was performed in 1× PBS.

Image Processing and Analysis of smFISH performed on Cultured Cells:

Widefield images of smFISH staining performed before or after expansion were first processed using a rolling-ball background subtraction algorithm (FIJI)[18] with a 200 pixel radius. Subsequently, maximum intensity Z-projections of these images were generated. Spots were

then localized and counted using a code developed by the Raj lab and available online (http://rajlab.seas.upenn.edu/StarSearch/launch.html).

Analysis of Expansion Isotropy:

smFISH images before and after expansion of *TOP2A* was rigidly aligned via two control points using the FIJI plugin Turboreg[19]. Spots were localized and counted via a custom spot counting Matlab code developed by the Raj lab (complete source code and instructions can be found at https://bitbucket.org/arjunrajlaboratory/rajlabimagetools/wiki/Home). Length measurements were performed among all pairs of points before expansion and the corresponding pairs of points after expansion via a custom Matlab script. Measurement error was defined as the absolute difference between the before and after expansion length measurements (Figure 2.7d).

Imaging of Cultured Cells using ExFISH:

Both cultured cells as well as LabelX treated and expanded cultured cells were imaged on a Nikon Ti-E epifluorescence microscope with a SPECTRA X light engine (Lumencor), and a 5.5 Zyla sCMOS camera (Andor), controlled by NIS-Elements AR software. For Figure 2.4-2.7 a 40× 1.15 NA water immersion objective was used. For all other experiments with cultured cells, a 60× 1.4 NA oil immersion objective was used.

For imaging smFISH probes labeled with fluorophores, the following filter cubes (Semrock, Rochester, NY) were used: Alexa 488, GFP-1828A-NTE-ZERO; Quasar 570, LF561-B-000; Alexa 594, FITC/TXRED-2X-B-NTE; Atto 647N, Cy5-4040C-000.

References:

1. Chen, F., Tillberg, P. W. & Boyden, E. S. Expansion microscopy. *Science (80-.).* **347,** 543–548 (2015).
2. Femino, A. M., Fay, F., Fogarty, K. & Singer, R. Visualization of Single RNA Transcripts in Situ. *Science (80-.).* **280,** 585–590 (1998).
3. Levsky, J. M. & Singer, R. H. Fluorescence in situ hybridization: past, present and future. *J. Cell Sci.* **116,** 2833–2838 (2003).
4. Raj, A., van den Bogaard, P., Rifkin, S. A., van Oudenaarden, A. & Tyagi, S. Imaging individual mRNA molecules using multiple singly labeled probes. *Nat. Methods* **5,** 877–9 (2008).
5. Choi, H. M. T. *et al.* Programmable in situ amplification for multiplexed imaging of

mRNA expression. *Nat. Biotechnol.* **28,** 1208–12 (2010).

6. Choi, H. M. T., Beck, V. A. & Pierce, N. A. Next-Generation *in Situ* Hybridization Chain Reaction: Higher Gain, Lower Cost, Greater Durability. *ACS Nano* **8,** 4284–4294 (2014).
7. Cajigas, I. J. *et al.* The local transcriptome in the synaptic neuropil revealed by deep sequencing and high-resolution imaging. *Neuron* **74,** 453–66 (2012).
8. Wang, F. *et al.* RNAscope: A novel in situ RNA analysis platform for formalin-fixed, paraffin-embedded tissues. *J. Mol. Diagnostics* **14,** 22–29 (2012).
9. Tillberg, P. W. *et al.* Expansion Microscopy of Biological Specimens with Protein Retention. *Nat. Biotechnol.*
10. Chozinski, T. J. *et al.* Expansion microscopy with conventional antibodies and fluorescent proteins. *Nat. Methods* (2016). doi:10.1038/nmeth.3833
11. Engreitz, J. M. *et al.* The Xist lncRNA exploits three-dimensional genome architecture to spread across the X chromosome. *Science* **341,** 1237973 (2013).
12. Panning, B., Dausman, J. & Jaenisch, R. X chromosome inactivation is mediated by Xist RNA stabilization. *Cell* **90,** 907–16 (1997).
13. Plath, K., Mlynarczyk-Evans, S., Nusinow, D. A. & Panning, B. Xist RNA and the mechanism of X chromosome inactivation. *Annu. Rev. Genet.* **36,** 233–78 (2002).
14. Mito, M., Kawaguchi, T., Hirose, T. & Nakagawa, S. Simultaneous multicolor detection of RNA and proteins using super-resolution microscopy. *Methods* (2015). doi:10.1016/j.ymeth.2015.11.007
15. Clemson, C. M. *et al.* An architectural role for a nuclear noncoding RNA: NEAT1 RNA is essential for the structure of paraspeckles. *Mol. Cell* **33,** 717–26 (2009).
16. Lieberman-Aiden, E. *et al.* Comprehensive mapping of long-range interactions reveals folding principles of the human genome. *Science* **326,** 289–93 (2009).
17. Raj, A. & Tyagi, S. *Detection of individual endogenous RNA transcripts in situ using multiple singly labeled probes. Methods in enzymology* **472,** (Elsevier Inc., 2010).
18. Schindelin, J. *et al.* Fiji: an open-source platform for biological-image analysis. *Nat. Methods* **9,** 676–82 (2012).
19. Thévenaz, P., Ruttimann, U. E. & Unser, M. A pyramid approach to subpixel registration based on intensity. *IEEE Trans. Image Process.* **7,** 27–41 (1998).

Chapter 3: Nanoscale Imaging of RNA in Tissues

3D Nanoscale Imaging of RNA in Mouse Brain Tissue

ExM allows for facile super-resolution imaging of thick 3-D specimens such as brain tissue on conventional microscopy hardware[1]. We applied ExFISH to samples of Thy1-YFP mouse brain tissue[2], using the YFP protein to delineate neural morphology (**Figure 3.1a, 3.1b**). Endogenous YFP protein was anchored to the polyacrylate gel via AcX using the proExM protocol[3], and RNA anchored via LabelX. Since smFISH yields signals too dim to visualize in intact tissues using confocal imaging, we applied the previously described technique of hybridization chain reaction (HCR)[4], in particular the next-generation DNA HCR amplifier architecture[5] (schematic in **Figure 3.2**). In samples containing mouse cortical and hippocampal regions, mRNAs for YFP (**Figure 3.1c**) and glutamic acid decarboxylase 1 *Gad1* (**Figure 3.1d**) were easily visualized using a widefield microscope, with YFP mRNA well localized to YFP-fluorescing cells (**Figure 3.1e**), and *Gad1* mRNA localized to a population of cells with characteristic arrangement throughout specific layers of the cortex and hippocampus[6]. Examining brain specimens at high magnification using a confocal spinning disk microscope revealed that individual transcripts could be distinguished due to the physical magnification of ExM (**Figure 3.1f,** with YFP and *Gad1* mRNA highlighted), with even highly overexpressed transcripts (e.g., YFP) cleanly resolved into individual puncta (**Figure 3.1f**). When FISH probes were omitted, minimal background HCR amplification was observed (**Figure 3.3**). Given that ExM enables super-resolution imaging on diffraction limited microscopes, which can be scaled to very fast imaging speeds[7], we used a commercially available lightsheet microscope on a Thy1-YFP brain slice to enable visualization of multiple transcripts, with single molecule precision, throughout a volume of ~575 μm × 575 μm × 160 μm thick in just 3 hours (~6×10^{10} voxels in 3 colors; **Figure 3.4**).

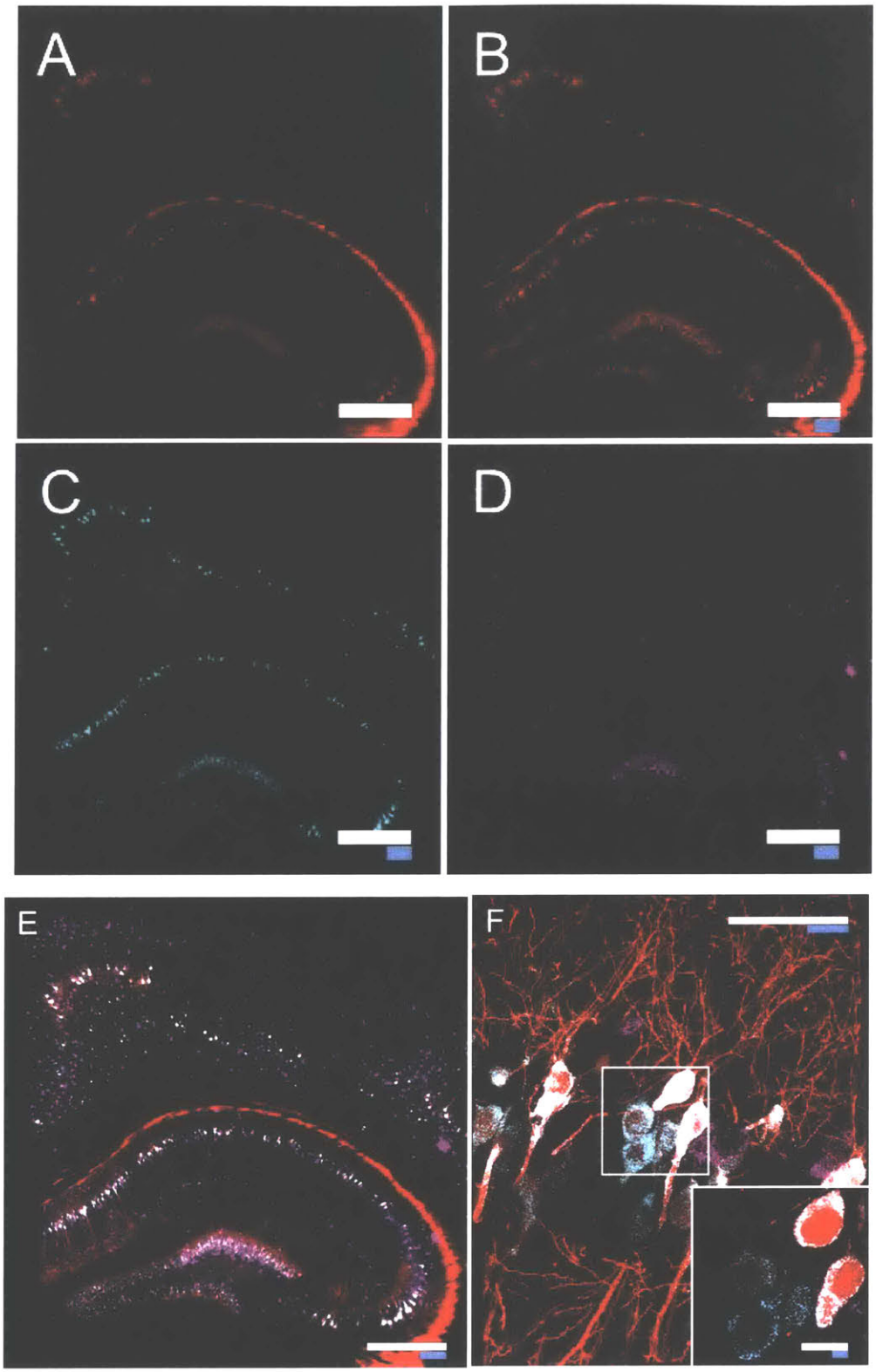

Figure 3.1. Nanoscale imaging of RNA in mammalian brain. (**a**) Widefield fluorescence image of Thy1-YFP mouse brain. (**b**) Post-expansion widefield image of (**a**). (**c**) Widefield fluorescence showing HCR-ExFISH of YFP mRNA in the sample of (**b**). (**d**) As in (**c**), but for *Gad1* mRNA. (**e**) Composite of (**b-d**),

highlighting distribution of *Gad1* versus Thy1-YFP mRNAs. (**f**) Confocal image of mouse hippocampal tissue from (**e**) showing single RNA puncta. Inset, one plane of the boxed region (red, YFP protein; cyan, YFP mRNA; magenta, *Gad1* mRNA). Scale bars (white, in pre-expansion units; blue scale bars are divided by the expansion factor noted): (**a**) 500 μm; (**b-e**) 500 μm (expansion factor 2.9×); (**f**) 50 μm (2.9×), inset 10 μm. (**e**) maximum-intensity projection (MIP) 27 μm thick (pre-expanded units).

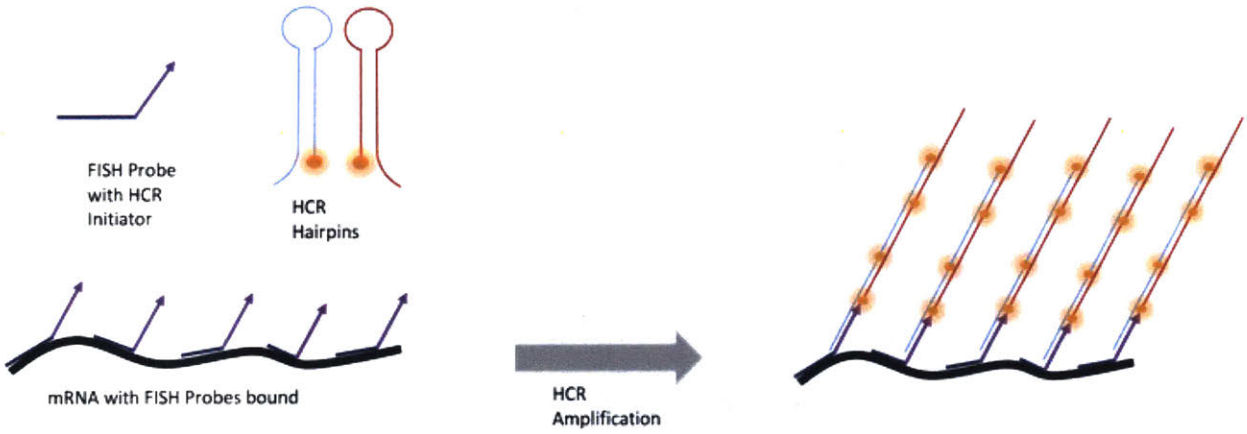

Figure 3.2. Schematic for HCR-mediated signal amplification. FISH probes bearing HCR initiators are hybridized to a target mRNA. During amplification, metastable DNA hairpins bearing fluorophores assemble into a polymer chains onto the initiators, thus amplifying signal downstream of the FISH probe hybridization event.

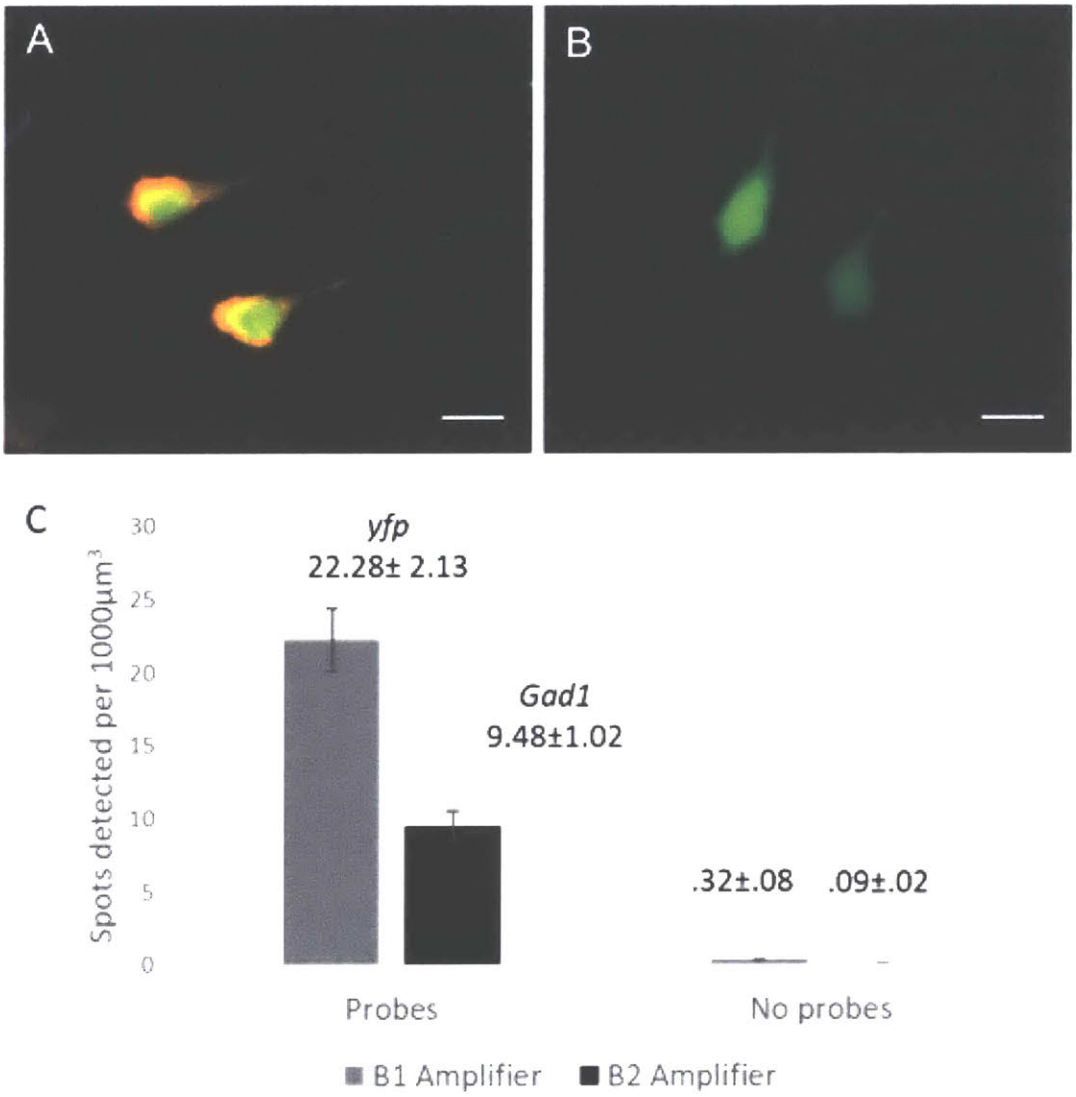

Figure 3.3. HCR Amplification False Positives. **a**) Widefield image of a LabelX treated Thy1-YFP brain slice (YFP protein, green) stained with probes against *YFP* (red) and *Gad1* (magenta) followed by HCR amplification. Probes against *YFP* transcripts were amplified with the B1 amplifier set (see Methods) while probes against *Gad1* transcripts were amplified with the B2 amplifier set (MIP, 59 µm). (**b**) Widefield image of LabelX treated Thy1-YFP brain slice (YFP protein, green) treated with the same HCR amplifiers as in (a) (namely B1 (red) and B2 (magenta)) without the addition of probes (MIP, 50 µm). (**c**) HCR spots detected per volume of expanded sample. Analysis was performed on samples which were either treated or not treated with FISH probes followed by HCR amplification. An automated spot counting algorithm (as used in Figure 2.4) was used to count HCR spots. The endogenous YFP protein was used to delineate regions used for the analysis. Plotted are mean ± standard error. HCR spot counts are significantly different in the presence of probes than without probes (p <0.05 for both B1 and B2 amplifier sets, Welch's t-test; n=4 fields of view each). Scale bars: 50 µm

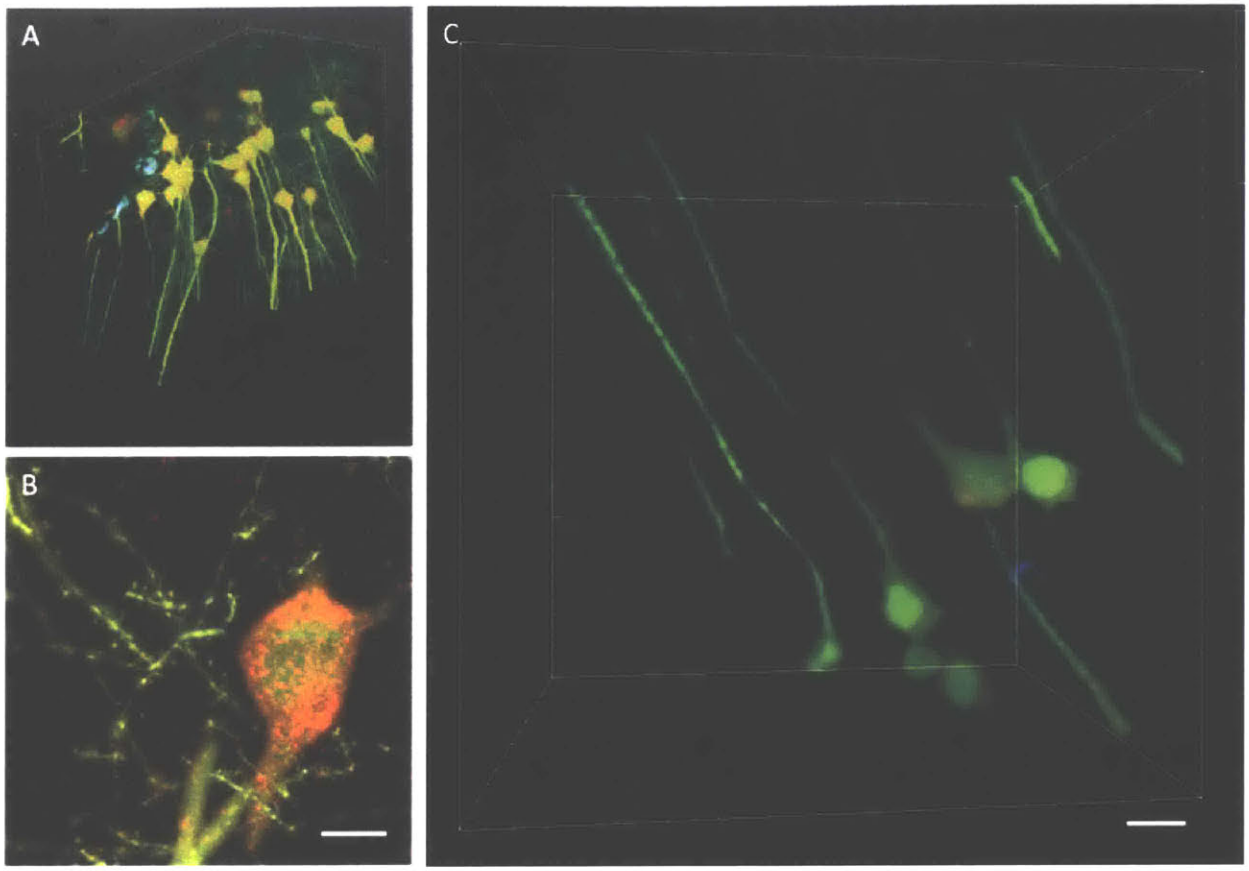

Figure 3.4: Light Sheet Microscopy of ExFISH. (**a**) Volume rendering of Thy1-YFP (green) brain tissue acquired by lightsheet microscopy with HCR-ExFISH targeting *YFP* (red) and *Gad1* (blue) mRNA. (**b**) A maximum intensity projection (~8 μm in Z) of a small subsection of the volume, showing the high resolution of imaging and single molecule localization of imaging expanded specimens with lightsheet imaging (scale bar: 10 μm, in pre-expansion units, expansion factor, 3×). (**c**) Zoom in of the volume rendering in (**a**) (scale bar: 20 μm, in pre-expansion units, 3×).

Error-Correction for Accurate Identification of RNA

HCR amplifies a target binding event into a bright fluorescent signal (**Figure 3.2**). A stringent method for assessing detection accuracy is to label individual RNAs with different probe sets bearing different colors[8,9], which shows that 50-80% of mRNAs thus targeted will be doubly labeled, when assessed in cell culture; a 50% co-localization is interpreted as $\sqrt{0.5} \sim 70\%$ detection efficiency (assuming probe independence); this is a lower bound as it excludes false positives. In order to assess the false positive and negative rates for single molecule visualization in expanded tissues, we delivered pairs of probe sets targeting the same transcript with different initiators. This scheme results in amplified fluorescent signals of two different colors from the same target (**Figure 3.5**), giving a measure of the hybridization efficiency. Delivering probe sets against a nonexistent transcript also gives a measure of false positive rate. We delivered a probe set against a missense probe (*Dlg4* reversed, **Figure 3.6a**) as well as a nonexistent transcript (mCherry, **Supplementary Table 3**), using Thy1-YFP mouse brain samples, and found a low but nonzero spatial density of dim, yet amplified, puncta (1 per 61 μm^3 in unexpanded coordinates, *Dlg4* reversed; 1 per 48 μm^3, mCherry). Essentially zero of these puncta exhibited co-localization (0/1,209 spots, *Dlg4* reversed; 4/1,540 spots mCherry). In contrast, when a transcript was present (*Actb*), a large fraction of the puncta exhibited co-localization (an average of 58% of probes in one color co-localized with other color, 15,866/27,504 spots, **Figure 3.6b, Supplementary Table 3**), indicative of a 75% detection efficiency, comparable to the non-amplified single molecule studies described above.

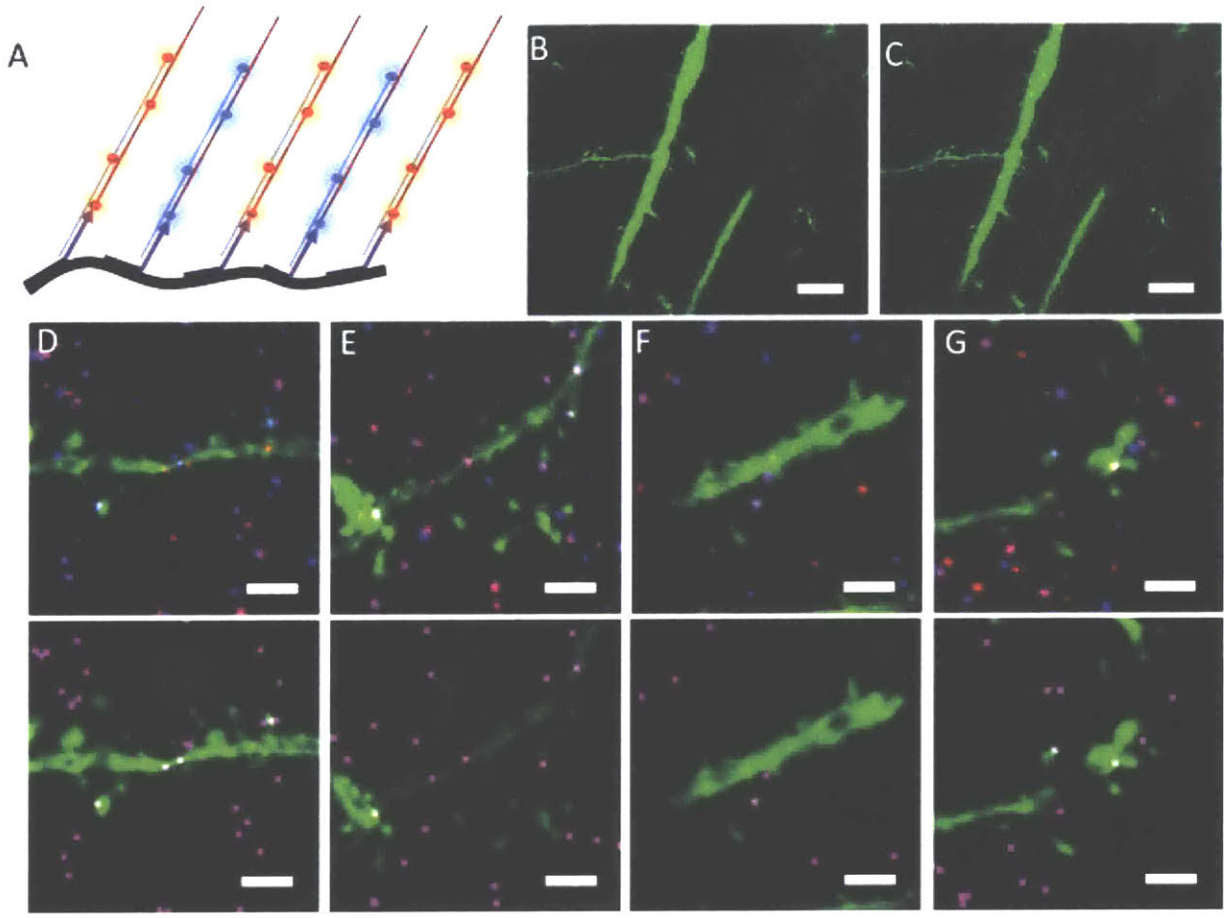

Figure 3.5. Two-color co-localization of FISH probes with HCR amplification in expanded Thy1-YFP brain slices. (**a**) Schematic showing two color amplification of the same target. A transcript of interest is targeted by probes against alternating parts of the sequence, and bearing two different HCR initiators, allowing for amplification in two colors. (**b**) Confocal image showing FISH staining with HCR amplification against the *Camk2a* transcript in two colors (red and blue; YFP fluorescence shown in green). (**c**) The result of an automated two-color spot co-localization analysis performed on the data set shown in (**b**). Each purple spot represents a positive co-localization identified by the algorithm and overlaid on the confocal image of YFP. Zoom in of dendrites showing two color FISH staining with HCR amplification against *Camk2a* (**d**,**e**) and *Dlg4* (**f**,**g**) transcripts. Top row shows the raw two color staining data corresponding to the bottom row showing co-localized spots identified by the automated algorithm. Scale bars: (**b**,**c**) 10 μm (3×); (**d-g**) 2 μm (3×). (**b-g**) are MIP of ~1.6 μm thickness in unexpanded coordinates.

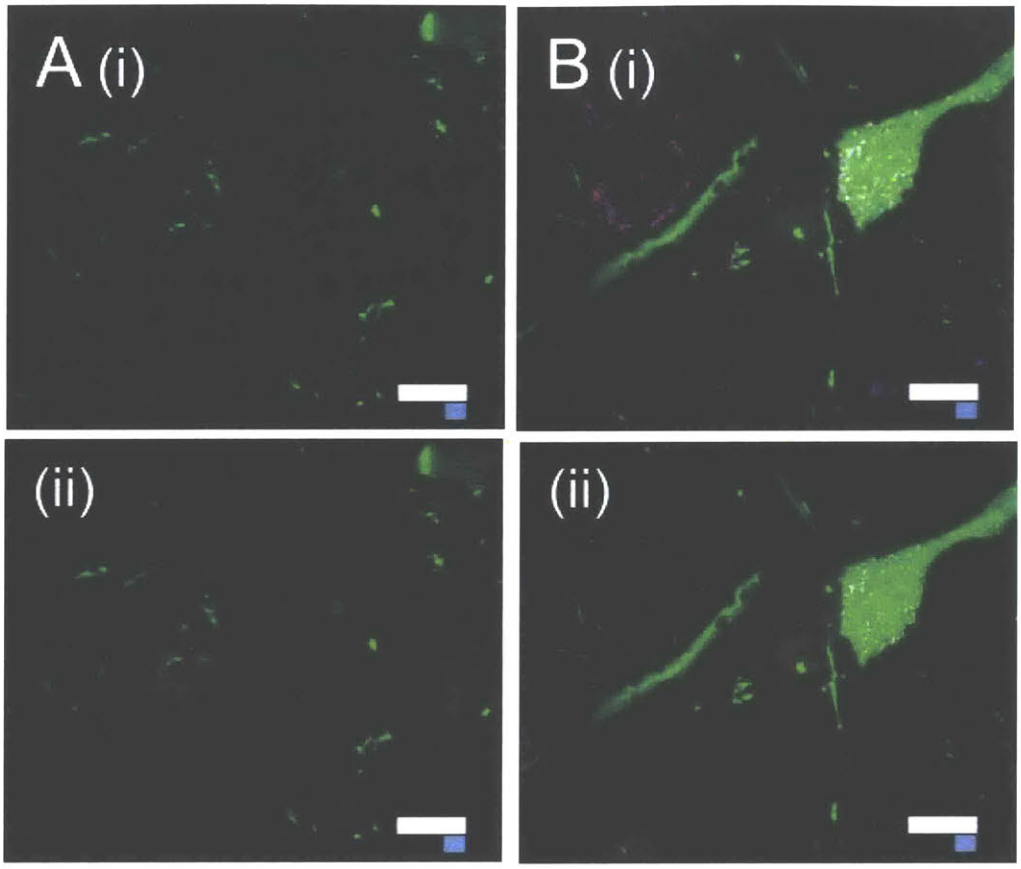

Figure 3.6: Two-Color Error Correction for Accurate Identification of RNA (**a**) Confocal image (i) and processed image (ii) of HCR-ExFISH using a missense *Dlg4* probe, in Thy1-YFP mouse tissue (green, YFP protein). The raw image (i) uses alternating probes in two colors (red, *Dlg4* missense even; blue, *Dlg4* missense odd). The processed image (ii) shows zero co-localized spots (magenta). (**b**) As in (**a**), but for HCR-ExFISH targeting *Actb* in Thy1-YFP mouse brain (green, YFP protein; red, *Actb* even, and blue, *Actb* odd in (i); co-localized spots in magenta (ii)). Scale bars (white, in pre-expansion units; blue scale bars are divided by the expansion factor noted): (**a,b**) 10 μm (3×); (**a,b**) MIPs ~1.6 μm thick.

Imaging RNA in Dendrites and Spines with ExFISH

We used two-color HCR ExFISH against mRNAs to image their position within cellular compartments such as dendritic spines, which require nanoscale resolution for accurate identification or segmentation. We probed the *Dlg4* mRNA, which encodes the prominent postsynaptic scaffolding protein PSD-95, and which is known to be dendritically enriched[10]. We obtained a degree of co-localization (53%, 5,174/9,795 spots) suggesting a high detection efficiency, 73% (**Figure 3.7a**). We also probed the mRNA for *Camk2a*, finding a detection efficiency of 78% (co-localization, 61%, 8,799/14,440 spots, **Figure 3.5**). We focused on puncta

which were co-localized, thus suppressing false positive errors, and giving a lower-bound on transcript detection (**Figure 3.5**). Focusing on individual dendrites in these expanded samples revealed that individual *Dlg4* (**Figure 3.7b**) and *Camk2a* (**Figure 3.7c**) mRNAs could indeed be detected in a sparse subset of dendritic spines as well as fine dendritic processes. Given that neurons can have tens of thousands of synapses, and mRNAs can be low copy number, the ability to map mRNAs at synapses throughout neuronal arbors may be useful for a diversity of questions in neuroscience ranging from plasticity to development to degeneration.

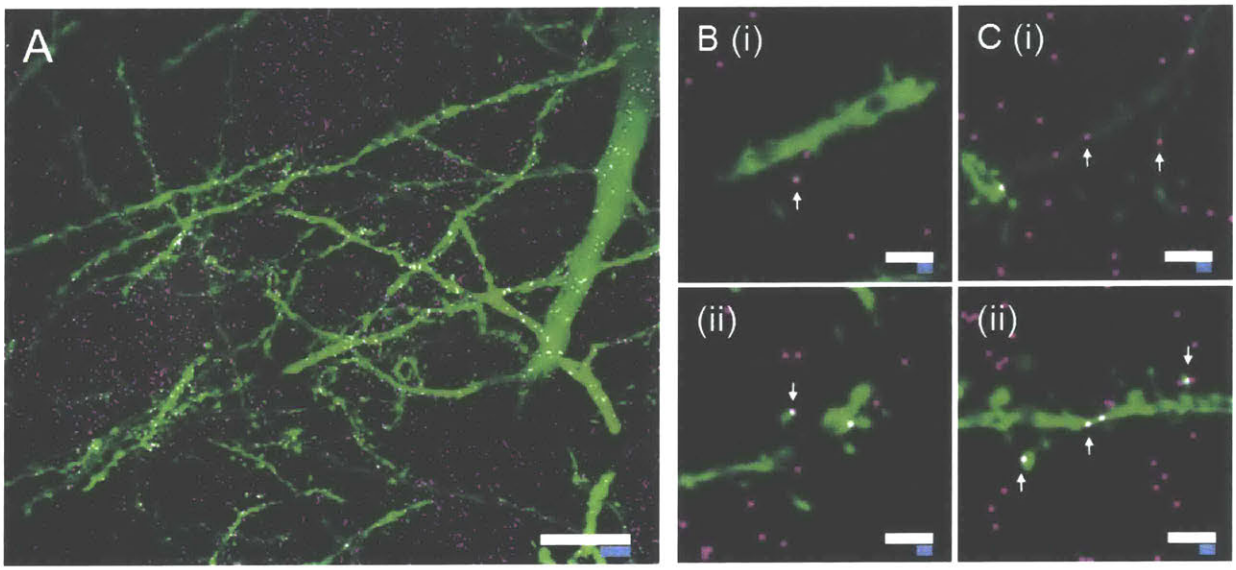

Figure 3.7 Imaging RNA in Dendrites and Spines of a Thy1-YFP Mouse Brain Section: (**a**) Confocal image of hippocampal tissue showing co-localized *Dlg4* puncta (magenta) overlaid on YFP (green). (**b**) Dendrites with *Dlg4* mRNA localized to spines (arrows). (i), (ii), two representative examples. (**c**) As in (**b**), but with HCR-ExFISH of *Camk2a* mRNA showing transcripts in dendritic spines and processes. Scale bars (white, in pre-expansion units; blue scale bars are divided by the expansion factor noted): (**a**) 10 μm (3×); (**b,c**) 2 μm (3×). (**a**) maximum-intensity projection (MIP) 27 μm thick (pre-expanded units); (**b,c**) MIPs ~1.6 μm thick.

Discussion on ExFISH Performance

We present a novel reagent, easily synthesized from commercial precursors, that enables RNA to be covalently anchored for expansion microscopy. The resulting procedure, ExFISH, enables RNAs to be probed through single-molecule FISH labeling as well as hybridization chain reaction (HCR) amplification. We validated RNA retention before versus after expansion, finding excellent yield, and de-crowding of RNAs for more accurate RNA counts and localization. This

enabled us to visualize, with nanoscale precision and single molecule resolution, RNA structures such as XIST and NEAT1, long non-coding RNAs whose emergent structure has direct implications for their biological roles. The anchoring was robust enough to support serial smFISH, including repeated washing and probe hybridization steps, and multiplexed readout of RNA identity and location, implying that using probes designed according to specific coding strategies[11–13] would support combinatorial multiplexing, in which each additional cycle yields exponentially more transcript information (Described further in Chapter 4). The covalent anchoring of RNA to the ExM gel may also support enzymatic reactions to be performed in expanded samples – such as reverse transcription, rolling circle amplification (RCA), fluorescent *in situ* sequencing (FISSEQ)[14], and other strategies for transcriptomic readout or SNP detection[15], within intact samples.

ExM, being a physical form of magnification, enables nanoscale resolution even on conventional diffraction limited microscopes. Expanding samples makes them transparent and homogeneous in index of refraction, in part because of the volumetric dilution, and in part because of washout of non-anchored components[1]. Thus, strategies combining ExM with fast diffraction limited methods like lightsheet microscopy[7] may result in "best of both worlds" performance metrics: the voxel sizes of classical super-resolution methods, but the voxel acquisition rates of increasingly fast diffraction limited microscopes[1]. The de-crowding of RNAs enables another key advantage: reducing the effective size of the self-assembled amplification product of HCR, which we here applied, following the protocols of refs. [4,5], to enable nanoscale resolution visualization of RNA in intact tissues (a paper conducted in parallel has also recently performed single molecule HCR FISH[16]). An HCR amplicon of size 500 nm in the post-expanded sample would, because of the greater distance between RNAs, have an effective size of 500 / 3.5 = ~150 nm. The lower packing density of amplicons facilitates the imaging of more transcripts per experiment[13] with nanoscale precision. Other methods of achieving brighter signals may be possible. For example, brighter fluorophores such as quantum dots[17] or bottlebrush fluorophores[18] could obviate the need for signal amplification, in principle. The expanded state may enable better delivery of these and other bulky fluorophores into samples. Other amplification strategies may be possible as well, including enzymatic (e.g., RCA[15], tyramide amplification[6], HRP amplification) as well as nonenzymatic (e.g., branched DNA) methods, although reaction efficiency and diffusion of reagents into the sample must be considered.

ExFISH may find many uses in neuroscience and other biological fields. In the brain, for example, RNA is known to be trafficked to specific synapses as a function of local synaptic activity[19] and intron content[20], and locally translated[10,21,22], and the presence and translation of axonal RNAs remains under investigation[23]. We anticipate that, coupled to straightforward multiplexed coding schemes, this method can be used for transcriptomic profiling of neuronal cell-types *in situ*, as well as for the super-resolved characterization of neuronal connectivity and synaptic organization in intact brain circuits, key for an integrative understanding of the mechanisms underlying neural circuit function and dysfunction. More broadly, visualizing RNAs within cells, and their relationship with RNA processing and trafficking machinery, may reveal new insights throughout biology and medicine.

Materials and Methods:

Mouse perfusion:

All methods for animal care and use were approved by the Massachusetts Institute of Technology Committee on Animal Care and were in accordance with the National Institutes of Health Guide for the Care and Use of Laboratory Animals. All solutions below were made up in 1× phosphate buffered saline (PBS) prepared from nuclease free reagents. Mice were anesthetized with isoflurane and perfused transcardially with ice cold 4% paraformaldehyde. Brains were dissected out, left in 4% paraformaldehyde at 4°C for one day, before moving to PBS containing 100 mM glycine. Slices (50 μm and 200 μm) were sliced on a vibratome (Leica VT1000S) and stored at 4 °C in PBS until use. The mouse used in **Figure 3.1** and related analyses was a Thy1-YFP (Tg(Thy1-YFP)16Jrs) male mouse in the age range 6-8 weeks. No sample size estimate was performed, since the goal was to demonstrate a technology. No exclusion, randomization or blinding of samples was performed.

LabelX Treatment of Brain Slices:

Brain slices, as prepared above, were incubated with 20mM MOPS pH 7.7 for 30 mins and subsequently incubated with LabelX diluted to a final Label-IT ® Amine concentration of 0.1 mg/mL (due to their increased thickness and increased fragmentation from formaldehyde post-

fixation) in MOPS buffer (20 mM MOPS pH 7.7) at 37°C overnight. For YFP retention, slices were treated with 0.05 mg/mL AcX in PBS for >6 hours @ RT.

Gelation, Digestion and Expansion:

Monomer solution (1× PBS, 2 M NaCl, 8.625% (w/w) sodium acrylate, 2.5% (w/w) acrylamide, 0.15% (w/w) N,N'-methylenebisacrylamide) was mixed, frozen in aliquots, and thawed before use. Monomer solution was cooled to 4°C before use. For gelling brain slices treated with LabelX, gelation was performed as in the original ExM protocol[1] (since, with HCR amplification, the slight autofluorescence of APS/TEMED was negligible). Gelled brain slices were digested with Proteinase K (New England Biolabs) diluted 1:100 to 8 units/mL in digestion buffer (50 mM Tris (pH 8), 1 mM EDTA, 0.5% Triton X-100, 500 mM NaCl) and digestion was carried out overnight at 37 °C. The gels expand slightly in the high osmolarity digestion buffer (~1.5×). After digestion, gels were stored in 1× PBS until use and expansion was carried out as previously described.

Probe Design for HCR-FISH:

Probe sequences and accession numbers for mRNA targets can be found in **Supplementary Table 4.** Probes were designed for HCR-FISH by tiling the CDS of mRNA targets with 22-mer oligos spaced by 3-7 bases. HCR initiators were appended to tiled sequences via a 2 base spacer (AA). For 2 color probe-sets, even and odd tiled probes were assigned different HCR-initiators to allow for amplification in different color channel.

RNA FISH with Hybridization Chain Reaction (HCR) Amplification:

Gelled samples were incubated with wash buffer (20% formamide, 2× SSC) for 30mins at room temperature and hybridized with HCR initiator tagged FISH probes in hybridization buffer (20% formamide, 10% dextran sulfate, 2× SSC) overnight at 37 °C. Following hybridization, samples were washed twice with wash buffer, 30mins per wash, and incubated with 1× PBS for 2hrs at 37°C. Subsequently, samples were incubated with 1× PBS for at least 6hrs at room temperature. Before HCR amplification, hybridized samples were pre-incubated with amplification buffer (10% dextran sulfate, 5× SSC, 0.1% Tween 20) for 30 mins. To initiate amplification, HCR hairpin stocks (Alexa 456 and Alexa 647 fluorophores) at 3 μM were snap-

cooled by heating to 95°C for 90 seconds, and leaving to cool at room temperature for 30 mins. Gelled samples were then incubated with HCR hairpins diluted to 60 nM in amplification buffer for 3hrs at room temperature. After amplification, gels were washed with 5× SSCT (5× SSC, 0.1% Tween 20) twice with one hour per wash.

Imaging of Expanded Brain Slices:

For epifluorescence imaging of brain sections before and after expansion and to quantify expansion factors of tissue slices specimens were imaged on a Nikon Ti-E epifluorescence microscope with a 4× 0.2 NA air objective, a SPECTRA X light engine (Lumencor), and a 5.5 Zyla sCMOS camera (Andor), controlled by NIS-Elements AR software.

Post-expansion confocal imaging of expanded brain tissue was performed on an Andor spinning disk (CSU-X1 Yokogawa) confocal system with a 40× 1.15 NA water objective on a Nikon TI-E microscope body. GFP was excited with a 488 nm laser, with 525/40 emission filter. Alexa 546 HCR amplicons were excited with a 561 nm laser with 607/36 emission filter. Alexa 647 amplicons were excited with a 640 nm laser with 685/40 emission filter.

Gels were expanded in with 3 washes, 15 minutes each of 0.05× SSC. The expansion factor can be controlled with the salt concentration, we found that 0.05× SSC gives 3× expansion, while still giving enough salt for hybridization stability. To stabilize the gels against drift during imaging following expansion, gels were placed in glass bottom 6 well plates with all excess liquid removed. If needed, liquid low melt agarose (2% w/w) was pipetted around the gel and allowed to solidify, to encase the gels before imaging.

Lightsheet imaging was performed on a Zeiss Z.1 lightsheet microscope. Briefly, the sample was fixed on a custom-made plastic holder using super glue and mounted on the freely rotating stage of the Z.1 lightsheet. Lightsheets were generated by two illumination objectives (5×, NA 0.1), and the fluorescence signal detected by a 20× water immersion objective (NA 1.0). Both lightsheets were used for data collection. The image volume dimensions of a single tile were 1400×1400×1057 pixels, with a voxel size of 227 nm laterally and 469 nm axially. The laserlines used for excitation were 488 nm, 561 nm and 638 nm. The individual laser transmissions were set to 5%, with the maximum output of 50 mW (488 nm and 561 nm) and 75 mW (638 nm). Optical filters used to separate and clean the fluorescence response included a Chroma T560lpxr as a dichroic, and a Chroma 59001m for GFP and 59007m for Alexa 546 and Alexa 647. Two

PCO.Edge 5.5m sCMOS cameras were used to capture two fluorescence channels simultaneously. Tiled datasets were taken with the Zeiss ZEN Software, and subsequently merged and processed with FIJI, Arivis Vision4D and Bitplane Imaris.

Two Color Analysis in Slices:

A sliding window averaging (or minimization) scheme in Z (3 optical sections) was used to suppress movement artifacts before spot detection processing. RNA puncta were detected via a custom 3D spot counting Matlab code developed by the Raj lab; complete source code and instructions can be found at https://bitbucket.org/arjunrajlaboratory/rajlabimagetools/wiki/Home.

Spot centroids were extracted from both color channels, and spots were determined to be co-localized if their centroids were within a 3 pixel radius in the x,y dimensions and a 2 pixel radius in the z dimension.

References:

1. Chen, F., Tillberg, P. W. & Boyden, E. S. Expansion microscopy. *Science (80-.).* **347,** 543–548 (2015).
2. Feng, G. *et al.* Imaging neuronal subsets in transgenic mice expressing multiple spectral variants of GFP. *Neuron* **28,** 41–51 (2000).
3. Tillberg, P. W. *et al.* Protein-retention expansion microscopy of cells and tissues labeled using standard fluorescent proteins and antibodies. *Nat. Biotechnol.*(2016)
4. Choi, H. M. T. *et al.* Programmable in situ amplification for multiplexed imaging of mRNA expression. *Nat. Biotechnol.* **28,** 1208–12 (2010).
5. Choi, H. M. T., Beck, V. A. & Pierce, N. A. Next-Generation *in Situ* Hybridization Chain Reaction: Higher Gain, Lower Cost, Greater Durability. *ACS Nano* **8,** 4284–4294 (2014).
6. Lein, E. S. *et al.* Genome-wide atlas of gene expression in the adult mouse brain. *Nature* **445,** 168–76 (2007).
7. Huisken, J., Swoger, J., Bene, F. Del, Wittbrodt, J. & Stelzer, E. H. K. Optical Sectioning Deep Inside Live Embryos by Selective Plane Illumination Microscopy. *Science* **305,** 1007–1009 (2004).
8. Batish, M., van den Bogaard, P., Kramer, F. R. & Tyagi, S. Neuronal mRNAs travel singly into dendrites. *Proc. Natl. Acad. Sci.* **109,** 4645–4650 (2012).

9. Cabili, M. N. *et al.* Localization and abundance analysis of human lncRNAs at single-cell and single-molecule resolution. *Genome Biol.* **16,** 20 (2015).
10. Cajigas, I. J. *et al.* The local transcriptome in the synaptic neuropil revealed by deep sequencing and high-resolution imaging. *Neuron* **74,** 453–66 (2012).
11. Lubeck, E. & Cai, L. Single-cell systems biology by super-resolution imaging and combinatorial labeling. *Nat. Methods* **9,** 743–8 (2012).
12. Lubeck, E., Coskun, A. F., Zhiyentayev, T., Ahmad, M. & Cai, L. Single-cell in situ RNA profiling by sequential hybridization. *Nat. Methods* **11,** 360–1 (2014).
13. Chen, K. H., Boettiger, A. N., Moffitt, J. R., Wang, S. & Zhuang, X. Spatially resolved, highly multiplexed RNA profiling in single cells. *Science (80-.).* **348,** aaa6090-aaa6090 (2015).
14. Lee, J. H. *et al.* Highly Multiplexed Subcellular RNA Sequencing in Situ. *Science (80-.).* **343,** 1360–1363 (2014).
15. Ke, R. *et al.* In situ sequencing for RNA analysis in preserved tissue and cells. *Nat. Methods* **10,** 857–60 (2013).
16. Shah, S. *et al.* Single-molecule RNA detection at depth via hybridization chain reaction and tissue hydrogel embedding and clearing. *Development*(2016).
17. Bruchez, M. *et al.* Semiconductor nanocrystals as fluorescent biological labels. *Science* **281,** 2013–6 (1998).
18. Fouz, M. F. *et al.* Bright Fluorescent Nanotags from Bottlebrush Polymers with DNA-Tipped Bristles. *ACS Cent. Sci.* **1,** 431–438 (2015).
19. Steward, O., Wallace, C. S., Lyford, G. L. & Worley, P. F. Synaptic activation causes the mRNA for the leg Arc to localize selectively near activated postsynaptic sites on dendrites. *Neuron* **21,** 741–751 (1998).
20. Buckley, P. T. *et al.* Cytoplasmic Intron Sequence-Retaining Transcripts Can Be Dendritically Targeted via ID Element Retrotransposons. *Neuron* **69,** 877–884 (2011).
21. Steward, O. & Schuman, E. M. Compartmentalized synthesis and degradation of proteins in neurons. *Neuron* **40,** 347–359 (2003).
22. Buxbaum, A. R., Wu, B. & Singer, R. H. Single -Actin mRNA Detection in Neurons Reveals a Mechanism for Regulating Its Translatability. *Science (80-.).* **343,** 419–422 (2014).

23. Jung, H., Yoon, B. C. & Holt, C. E. Axonal mRNA localization and local protein synthesis in nervous system assembly, maintenance and repair. *Nat. Rev. Neurosci.* **13,** 308–24 (2012).

Chapter 4: Towards Multiplexed, Nanoscale Imaging of Biomolecules

Super-resolved, Multiplexed Imaging of RNA with ExFISH

The combination of covalent RNA anchoring to the ExM gel, and the de-crowding of the local environment that results from expansion, could facilitate strategies that have been proposed for multiplexed RNA readout[1–3] based upon sequential hybridization with multiple probe sets. In order to facilitate multiple cycles of FISH, we re-embedded expanded specimens in charge-neutral polyacrylamide. This process allowed expanded gels to be immobilized for multi-round imaging, and additionally stabilized the expanded specimen throughout salt concentration changes in the protocol. Such re-embedded samples exhibited similar expansion factors as non-re-embedded samples (i.e., ~3×), and were robust to multiple wash-stain cycles as assessed by repeated application of the same probe set (**Figure 4.1a, b, Figure 4.2a**, showing 5 rounds of smFISH staining against *GAPDH* on cultured cells). This stability was observed even under stringent wash conditions designed to minimize cycle-to-cycle crosstalk (e.g., 100% formamide). Across the 5 rounds, there was no distortion of the locations of individual RNA spots from round to round (**Figure 4.1b**), nor variance in detection efficiency or signal-to-noise ratio (**Figure 4.1c, d**). Having validated the cycle-to-cycle consistency, we next demonstrated the capability of multiplexed ExFISH by applying probes for *GAPDH*, *UBC*, *NEAT1*, *USF2*, *ACTB*, and *EEF2* in series, enabling 6 individual RNAs to be identified and localized in the same cell (**Figure 4.1e, Figure 4.2b**). Thus, serial FISH is applicable to samples expanded after securing RNA to the swellable polymer as here described, making it straightforward to apply probe sets computationally designed to yield more information per FISH cycle, e.g. MERFISH[2–4].

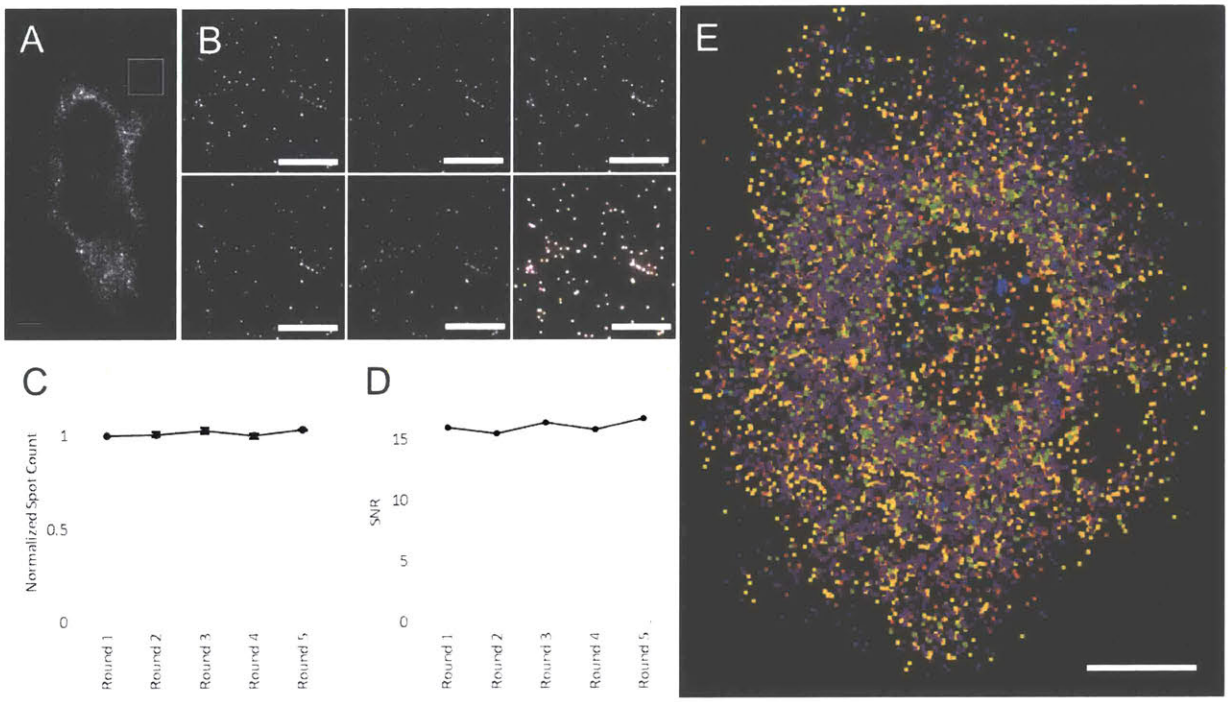

Figure 4.1. Serially hybridized and multiplexed ExFISH. (**a**) Widefield fluorescence image of ExFISH targeting *GAPDH*. (**b**) Boxed region of (**a**), showing 5 repeated re-stainings following probe removal (see Methods); lower right panel, overlay of the 5 images (with each a different color, red, green, blue, magenta, yellow), showing co-localization. (**c**) ExFISH RNA counts for each round, normalized to the round 1 count; plotted is mean $\pm$ standard error; $n = 3$ regions of (**a**). (**d**) Signal-to-noise ratio (SNR) of ExFISH across the five rounds of staining of (**a**), computed as the mean puncta brightness divided by the standard deviation of the background. (**e**) Composite image showing ExFISH with serially delivered probes against six RNA targets in a cultured HeLa cell (raw images in **Figure 4.2**); colors are as follows: *NEAT1*, blue; *EEF2*, orange; *GAPDH*, yellow; *ACTB*, purple; *UBC*, green; *USF2*, light blue. Scale bars (expanded coordinates): (**a**) 20 μm; (**b**) 10 μm; (**e**) 20 μm.

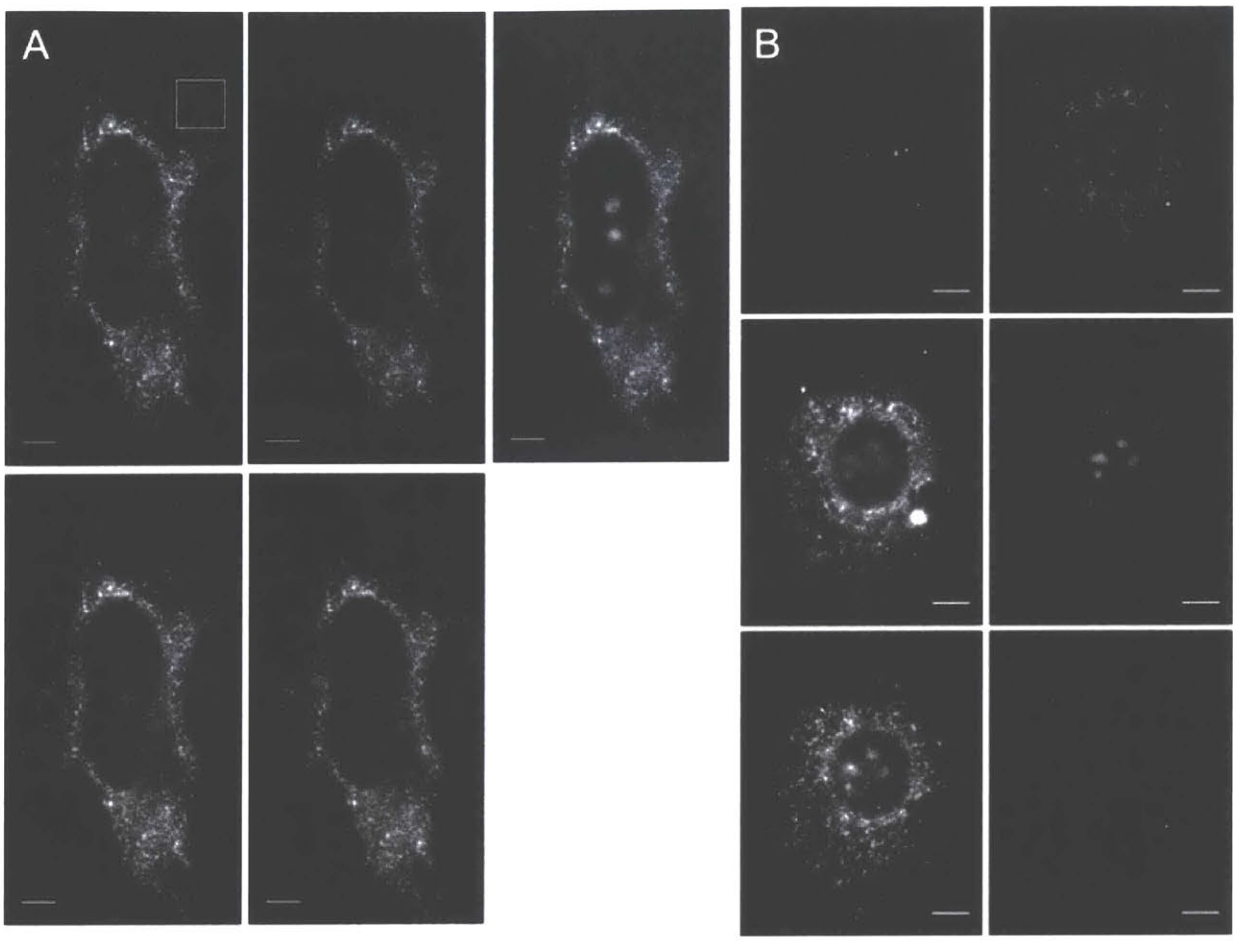

Figure 4.2. Multiplexed ExFISH via Serial Hybridization. (**a**) Five consecutive widefield fluorescence images (top to bottom, then left to right) of *GAPDH*, applied to the cell of **Figure 4.1a**. (**b**) Widefield fluorescence images showing ExFISH with serially delivered probes against six RNA targets (right to left, then top to bottom: *NEAT1*, *EEF2*, *ACTB*, *UBC*, *GAPDH*, and *USF2*) in a cultured HeLa cell (raw images of composite shown in **Figure 4.1e**). Scale bars: 20 μm in expanded units.

Multiplexed RNA FISH can be further facilitated in an ExM context with incorporation of toe-hold mediated strand displacement[5,6]. In this approach, FISH or amplification probes will possess a toe-hold regions for the binding of a displacement strand. Upon binding of this strand, the FISH probes or amplification strands will be displaced off, resetting the target for another round of RNA FISH probes. To facilitate multiplexed HCR readout, we developed modified HCR hairpins that can be disassembled using toe-hold mediated strand displacement[6] (**Figure 4.3**). These modified HCR amplifiers enable multiple cycles of HCR by disassembling the HCR polymer between subsequent cycles.

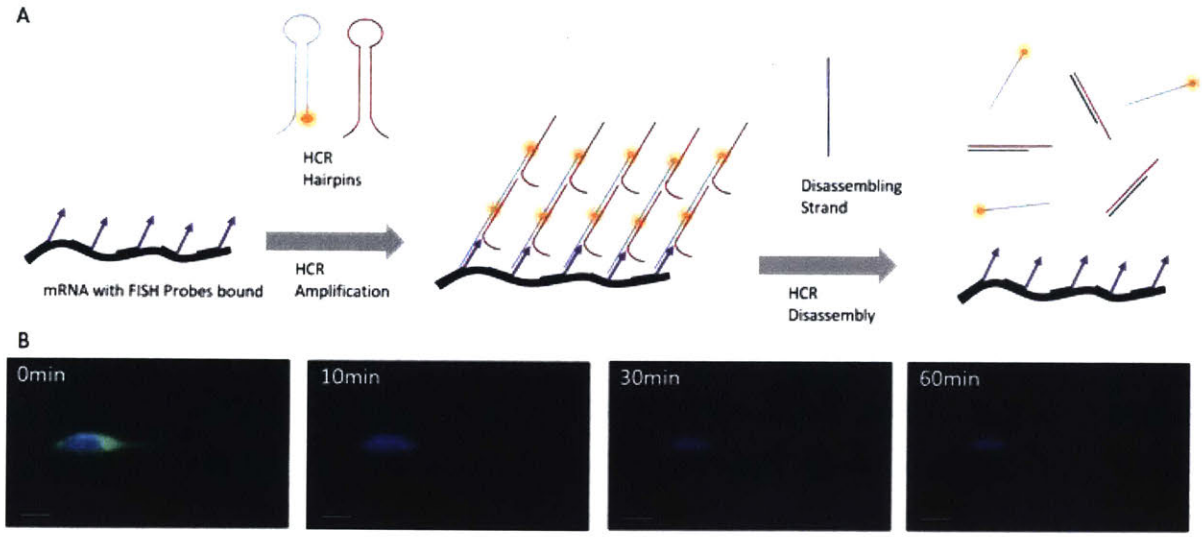

Figure 4.3. HCR reversal via toe-hold mediated strand displacement. (**a**) Schematic for HCR amplification and reversal. HCR amplification is initiated with custom-made HCR hairpins bearing toe-holds for toe-hold mediated strand displacement. After amplification, the addition of a disassembling strand initiates the disassembly of the HCR polymers via strand displacement. (**b**) ExFISH-treated Thy1-YFP brain slice (YFP in blue) is shown stained with YFP FISH probes bearing HCR initiators and amplified with custom made HCR hairpins bearing toe-holds for strand displacement (green dots). The different panels show the state of HCR reversal at different times after the addition of strands to initiate the disassembly of the HCR polymers. Scale bars: 20 μm (in post-expansion units).

Strategy for highly multiplexed detection of RNA with In Situ Sequencing

In addition to multiplexed smFISH, ExFISH presents the exciting possibility of implementing *in situ* sequencing. Recent years have seen the development of approaches that enable the sequencing of RNA targets and DNA probes in an *in situ* context using Next Generation Sequencing (NGS) chemistries[7–9]. By preserving the spatial context of the specimen, nucleic acid targets can be sequenced while at the same time maintaining their spatial relationship with respect to each other or other morphological markers. These chemistries involve a series of enzymatic steps such as reverse transcription, circularization, and rolling circle amplification (RCA). The specific sequencing steps also involve enzymatics, such as Sequencing by Ligation (SOLID) and Sequencing by Synthesis (Illumina). Consequently, *in situ* sequencing in intact tissue can be hampered by a series of factors. Firstly, enzymatic amplification steps increase the physical size of RNA/DNA targets. For instance, RCA produces amplified products that are 500 nm-800 nm in diameter[8]. With the limited resolution of light

microscopy, the increased size of amplicons limits the number of targets that can be resolved and sequenced. In addition, intact tissues can be prone to the buildup of fluorescent background over several rounds of sequencing, which can impeded sequencing.

We here propose a strategy for the highly multiplexed detection of RNA with ExFISH using *in situ* sequencing. In this approach (**Figure 4.4**), we plan to deliver RNA FISH padlock probes bearing sequencable barcodes to RNA targets after expansion. After delivery, these barcodes can then be sequenced revealing the identity of each RNA target in an *in situ* context. For the first part, we can deliver padlock probes that can be enzymatically ligated upon binding to their RNA target, thereby ensuring specificity. These circularized probes can then be amplified with RCA. After amplification, we can implement NGS chemistries such as SOLID[7,10] and Illumina[9] sequencing to read out the barcodes. As described in the previous section, the expanded gel can be immobilized on a glass surface so that there are minimal distortions during multiple sequencing rounds.

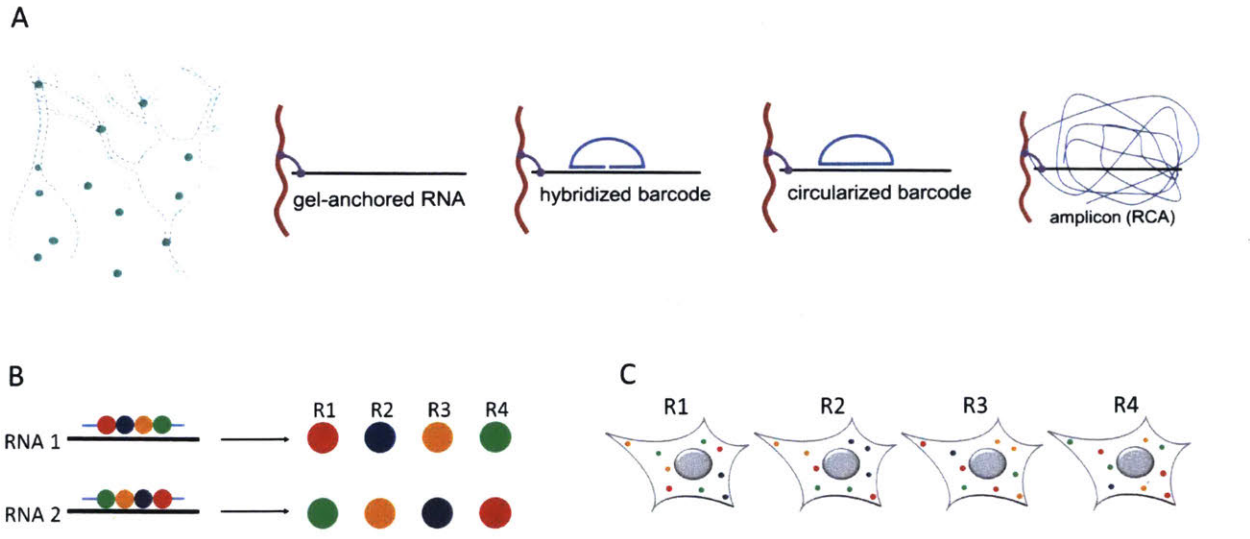

Figure 4.4. Strategy for the Highly Multiplexed Detection of RNA with ExFISH and *in situ* Sequencing. (**a**) Diagram showing the set of chemical and enzymatic steps leading to the generation of sequencing libraries. (left) After ExFISH, endogenous RNA molecules are retained in the expanded gel. (right) RNA targets are tagged with padlock probes bearing unique barcodes, followed by the circularization and amplification of these probes. (**b**) The unique barcode of each probe can be read-out via NGS *in situ* sequencing. (**c**) NGS *in situ* sequencing over several rounds results in a set of images of the sample with each RNA target displaying a sequence of colors representing its unique barcode.

We think that ExFISH provides an excellent context for the implementation of such NGS based *in situ* sequencing. The decrowding of RNA targets with ExFISH will allow for the resolvability of RCA amplicons, despite their large size. Since the enzymatics are performed after expansion, the effective size of the amplicons is divided by the expansion factor. Furthermore, ExFISH will minimize the accumulation of fluorescent background since during the digestion and expansion process, proteinaceous structures that result in non-specific binding will have been removed. The chemical homogeneity of the expanded gel as well as the efficient diffusion of reagents might also permit such sequencing-based schemes in thick tissue sections. Finally, the expanded gel, unlike biological tissues, is chemically inert, being primarily composed of polyacrylamide and polyacrylate. As a result, we think it can stably withstand repeated enzymatic and chemical interrogation of biological targets without loss of quality or integrity.

Simultaneous Imaging of RNA and Proteins with ExM

In terms of multiplexing, another exciting potential of ExFISH is for the simultaneous imaging of proteins and RNA. In chapter 3, I discussed how the combination of protein anchoring with ProExM[11] along with ExFISH can allow for the visualization of fluorescent proteins and RNA targets. In the future, the combination of fluorescent protein based neuron tracing and segmentation[12] along with ExFISH-based multiplexing may enable the accurate attribution of transcripts to their respective cells. It is also possible to apply an antibody staining with ExFISH for the visualization of protein targets. Antibodies can be applied before expansion and retained with Acryloyl-X[11], while endogenous RNA molecules can be retained with LabelX[13]. After expansion, while the antibody can be visualized with associated fluorophores, RNA molecules can be interrogated with ExFISH (**Figure 4.5**). Such an approach can open the door for addressing questions about the nanoscale organization of proteins and RNA.

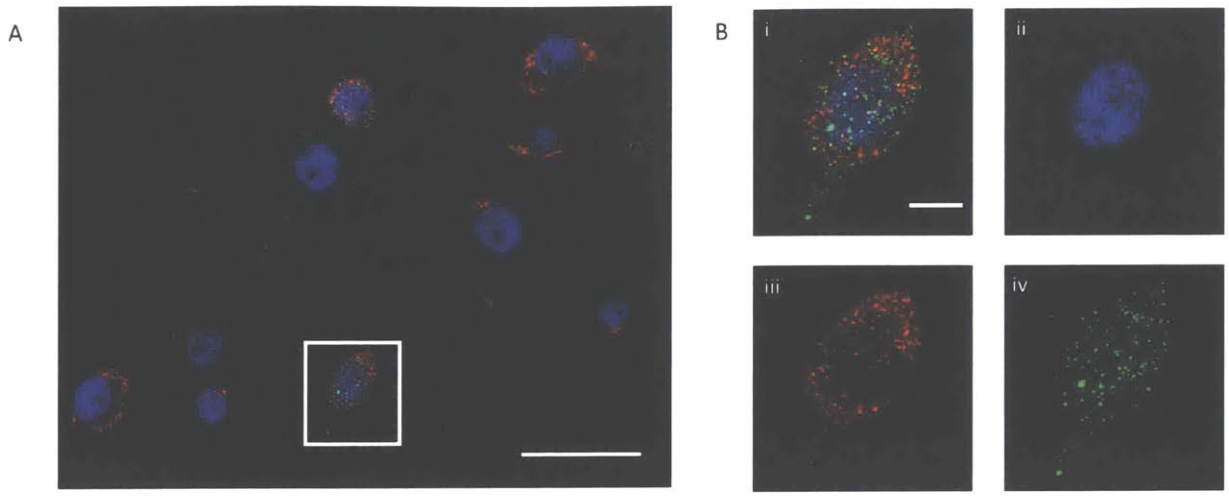

Figure 4.5. Simultaneous measurement of proteins and RNAs with ExFISH in combination with proExM. (**a**). Confocal image showing cultured primary hippocampal mouse neurons processed with a combination of ExFISH and proExM, with antibodies against RNA Polymerase II (blue) applied before expansion and staining for *ActB* RNA (red) and *Arc* RNA (green) with HCR amplification performed after expansion. (**b**). Images showing inset in A, with (i) showing overlay, and (ii), (iii), (iv) showing individual color channels. Scale bars, (a) 25 μm (50 μm, post expansion); (c) 5μm (10μm, post expansion).

Even more, a powerful direction for ExFISH would be the highly multiplexed detection of both proteins and RNA. As discussed in the previous section, there are multiple approaches for the multiplexed imaging of RNA. It might also be possible to implement multiplexing approaches for protein detection. For instance, it has been shown that multiple protein targets can be imaged with the serial application of antibodies[14,15]. Such an approach would require the retention of endogenous epitopes, which is not permitted with the current version of ExFISH due to the requirement for proteinase digestion. However, recent advances to ExM methods have shown that the proteinase digestion step can instead be replaced with heat-based denaturation that enables expansion while preserving epitopes[11,16,17]. A combination of such heat denaturation with RNA retention may enable the multiplexed detection of both proteins and RNA.

Finally, the ability to image proteins and RNA with even higher levels of expansion would widen the scope of biological problems that can be addressed. A recent ExM method, Iterative Expansion Microscopy (iExM), has extended the achievable expansion factor to 20x, reaching a lateral resolution of 25 nm[18]. This level of resolution would be useful in visualizing nanoscale interactions between proteins and RNA as well as the localization of RNA in

nanoscale compartments, such as synapses. iExM requires the application of oligonucleotide-tagged antibodies before expansion for the post-expansion visualization of targets. Furthermore, the high pH treatment step required to enable 20x expansion would most likely degrade RNA. We think it is possible to devise an iExM-like approach that can preserve both RNA and epitopes. In this approach, RNA molecules and proteins can be interrogated with labels after 20x expansion. The post expansion application of tags may also enable efficient binding of bulky tags such as antibodies to their respective targets.

Methods and Materials

Re-embedding of Expanded Gels in Acrylamide Matrix:

For serial staining in cells, expanded gels were re-embeded in acrylamide to stabilize the gels in the expanded state. Briefly: gels were expanded in water and cut manually to ~1 mm thickness with a stainless steel blade. Cut gels were incubated in 3% acrylamide, 0.15% N,N'-Methylenebisacrylamide with 0.05% APS, 0.05% TEMED and 5 mM Tris ph 10.5 for 20 minutes on a shaker. There is a ~30% reduction in gel size during this step. Excess solution is removed from the gels and the gels are dried with light wicking from a laboratory wipe. Gels are placed on top of a bind-silane treated (see below) coverslip or glass bottom plate with a coverslip placed on top of the gels before moving into a container and purged with nitrogen. The container is moved to a 37 °C incubator for gelation for 1.5 hours.

Staining of Re-embedded Gels:

Re-embeded staining of gels were performed with exact conditions as described above for expanded gels, except post-hybridization washes were changed to twice with wash buffer (10% formamide), 60 minutes per wash.

Probes were removed for multiple rounds of hybridization via treatment with DNAse I or 100% formamide. For DNAse I, samples were treated with DNAse I at 0.5 U/μL for 6 hours at RT. For formamide stripping, samples were treated with 100% formamide at 6 hours at 37C.

Bind-silane Treatment of Coverslips:

Coverslips and glass bottom 24 well plates were treated with Bind-Silane, a silanization reagent which incorporates acryloyl groups onto the surface of glass to perform in free radical polymerization. Briefly, 5 μL of Bind-Silane reagent was diluted into 8 mL of ethanol, 1.8 mL of

ddH_2O and 200 µL of acetic acid. Coverslips and glass bottom 24 well plates were washed with ddH_2O followed by 100% ethanol, followed by the diluted Bind-Silane reagent. After a brief wash with the diluted Bind-Silane reagent, the cover-slip was dried, then washed with 100% ethanol, and then dried again. Coverslips were prepared immediately before use.

Preparation, Expansion, and HCR-FISH of Brain Slice:

Brain slices from a Thy1-YFP mouse were treated with LabelX, expanded, and labeled with RNA-FISH probes as described in Chapter 3.

HCR Reversal via Toe-Hold Mediated Strand Displacement:

HCR amplification commences upon the addition of two HCR metastable amplifier hairpins. We designed a pair of HCR amplifiers, B2H1T and B2H2 (see below for sequence), where B2H1T bears a 6bp toe-hold for strand displacement. To initiate HCR amplification, aliquots of these amplifiers at 3 µM were snap-cooled by heating to 95 °C for 90 seconds, and leaving to cool at room temperature for 30 mins. Gelled samples were then incubated with HCR hairpins diluted to 60 nM in amplification buffer for 3hrs at room temperature. After amplification, gels were washed with 5× SSCT (5× SSC, 0.1% Tween 20) twice with one hour per wash. Subsequently, HCR reversal was initiated by the addition of a displacement strand (see below for sequence) at 200 nM in 5× SSCT.

B2H1T:

*ggCggTTTACTg*gATgATTgATgAggATTTACgAggAgCTCAgTCCATCCTCgTAAATCCTCA TCAATCATCAAATAG

B2H2:

/5'-Alexa546-C12/

CCTCgTAAATCCTCATCAATCATCCAgTAAACCgCCgATgATTgATgAggATTTACgAggA TggACTgAgCT

Displacement Strand:

CTATTTGATGATTGATGAGGATTTAcGAGGATGGAcTGAGcT

Primary Hippocampal Neuron Culture:

Hippocampal neurons were prepared from postnatal day 0 or 1 Swiss Webster (Taconic) mice (both male and female mice were used) as previously described[19,20] with the following modifications: dissected hippocampal tissue was digested with 50 units of papain (Worthington Biochem) for 6-8 min, and the digestion was stopped with ovomucoid trypsin inhibitor (Worthington Biochem). Cells were plated at a density of 20,000–30,000 per glass coverslip coated with Matrigel (BD Biosciences). Neurons were seeded in 100 µl plating medium containing MEM (Life Technologies), glucose (33 mM, Sigma), transferrin (0.01%, Sigma), Hepes (10 mM, Sigma), Glutagro (2 mM, Corning), Insulin (0.13%, Millipore), B27 supplement (2%, Gibco), and heat inactivated FBS (7.5%, Corning). After cell adhesion, additional plating medium was added. AraC (0.002 mM, Sigma) was added when glia density was 50–70% of confluence. Neurons were grown at 37 °C and 5% CO2 in a humidified atmosphere

Simultaneous Imaging of Proteins and RNA:

Cultured Hippocampal neurons were fixed with formaldehyde as described previously[18]. After fixation a primary antibody against RNA Polymerase II, pSer5 (abcam, ab5131) was applied at 10 µg/ml in antibody staining buffer (1.25% Ultrapure BSA, 1x PBS, 0.1% Triton-X) overnight at 4 °C. Secondary antibody (10 µg/ml) was applied in antibody staining buffer for 4 hours at room temperature. Subsequently, immunostained cultured neurons were treated with 0.1mg/ml AcX and 0.01mg/ml LabelX in MOPS buffer (20 mM MOPS, pH 7.7) overnight at room temperature. After performing two brief washes with PBS, samples were expanded as described previously[13]. HCR3.0 probes were purchased from Molecular Instruments. HCR3.0 labeling of RNA targets and amplification was performed as described previously[21].

References:

1. Lubeck, E. & Cai, L. Single-cell systems biology by super-resolution imaging and combinatorial labeling. *Nat. Methods* **9,** 743–8 (2012).
2. Lubeck, E., Coskun, A. F., Zhiyentayev, T., Ahmad, M. & Cai, L. Single-cell in situ RNA profiling by sequential hybridization. *Nat. Methods* **11,** 360–1 (2014).
3. Chen, K. H., Boettiger, A. N., Moffitt, J. R., Wang, S. & Zhuang, X. Spatially resolved,

highly multiplexed RNA profiling in single cells. *Science (80-.).* **348,** aaa6090-aaa6090 (2015).

4. Beliveau, B. J. *et al.* Versatile design and synthesis platform for visualizing genomes with Oligopaint FISH probes. *Proc. Natl. Acad. Sci. U. S. A.* **109,** 21301–6 (2012).
5. Zhang, D. Y. & Winfree, E. Control of DNA strand displacement kinetics using toehold exchange. *J. Am. Chem. Soc.* **131,** 17303–14 (2009).
6. Zhang, D. Y. & Seelig, G. Dynamic DNA nanotechnology using strand-displacement reactions. *Nat. Chem.* **3,** 103–113 (2011).
7. Lee, J. H. *et al.* Highly Multiplexed Subcellular RNA Sequencing in Situ. *Science (80-.).* **343,** 1360–1363 (2014).
8. Ke, R. *et al.* In situ sequencing for RNA analysis in preserved tissue and cells. *Nat. Methods* **10,** 857–60 (2013).
9. Chen, X., Sun, Y.-C., Church, G. M., Lee, J. H. & Zador, A. M. Efficient in situ barcode sequencing using padlock probe-based BaristaSeq. *Nucleic Acids Res.* **46,** e22–e22 (2018).
10. Nilsson, M. *et al.* Padlock Probes: Circularizing Oligonucleotides for Localized DNA Detection. *Science* **265,** 2085–2088
11. Tillberg, P. W. *et al.* Protein-retention expansion microscopy of cells and tissues labeled using standard fluorescent proteins and antibodies. *Nat. Biotechnol.* **34,** 987–992 (2016).
12. Cai, D., Cohen, K. B., Luo, T., Lichtman, J. W. & Sanes, J. R. Improved tools for the Brainbow toolbox. *Nat. Methods* **10,** 540–547 (2013).
13. Chen, F. *et al.* Nanoscale imaging of RNA with expansion microscopy. *Nat. Methods* **13,** 679–684 (2016).
14. Gut, G., Herrmann, M. D. & Pelkmans, L. Multiplexed protein maps link subcellular organization to cellular states. *Science* **361,** eaar7042 (2018).
15. Murray, E. *et al.* Simple, Scalable Proteomic Imaging for High-Dimensional Profiling of Intact Systems. *Cell* **163,** 1500–14 (2015).
16. Ku, T. *et al.* Multiplexed and scalable super-resolution imaging of three-dimensional protein localization in size-adjustable tissues. *Nat. Biotechnol.* 1–11 (2016). doi:10.1038/nbt.3641
17. Gambarotto, D. *et al.* Imaging cellular ultrastructures using expansion microscopy (U-ExM). *Nat. Methods* **16,** 71–74 (2019).

18. Chang, J.-B. *et al.* Iterative expansion microscopy. *Nat. Methods* **14,** (2017).
19. Klapoetke, N. C. *et al.* Independent optical excitation of distinct neural populations. *Nat. Methods* **11,** 338–46 (2014).
20. Chuong, A. S. *et al.* Noninvasive optical inhibition with a red-shifted microbial rhodopsin. *Nat. Neurosci.* **17,** 1123–1129 (2014).
21. Choi, H. M. T. *et al.* Third-generation in situ hybridization chain reaction: multiplexed, quantitative, sensitive, versatile, robust. *Development* **145,** (2018).

Chapter 5: Outlook on ExM Methods, Tool Development, and Applications

In the preceding chapters, I described the development of a technology for mapping RNA with nanoscale precision, known as ExFISH, as well as strategies for the multiplexed detection of transcripts. I also discussed an approach for the simultaneous imaging of RNA and proteins using this method. Here, I will provide an outlook for these techniques, discuss their applications, and highlight opportunities for further tool development.

Outlook on ExFISH and Nanoscale Imaging of RNA with ExM

One powerful attribute of ExM is that it is compatible with the visualization of new molecule classes and the incorporation of new amplification and analysis chemistries. RNA molecules can be anchored to the swellable polymer by applying the molecule LabelX, a reagent formed from the reaction of two commercially available reagents[1]. LabelX possesses an alkylating group which reacts primarily to guanine bases in RNA as well as DNA, as well as a carbon-carbon bond that can be incorporated into the gel. Thus, specimens treated with LabelX can be expanded in an even way. The ability to stain RNA after expansion opens the door to the use of various fluorescent *in situ* hybridization (FISH) strategies to interrogate RNA location and identity; we call this suite of technologies expansion FISH (ExFISH). We have shown that standard single-molecule FISH (smFISH) can be performed in cultured cells after expansion, allowing for the imaging of the nanoscale organization of RNA molecules such as long non-coding RNAs. The ability of expansion to decrowd RNA molecules improves quantification of RNA abundance. Furthermore, expansion supports multiplexed smFISH by allowing for the efficient delivery and removal of probes, making it possible to read out the identity and location of multiple RNA molecules over time. Another group developed a simple method for visualizing RNAs by applying gel-anchorable fluorescent FISH probes before expansion, which are then anchored to the polymer and expanded away from each other[2], and also obtained improved signal-to-noise ratio and more accurate RNA accounts than in the unexpanded state. This method does not directly retain RNAs themselves, but instead only retains the probes applied, so it should only be used when specific transcripts are desired to be imaged post-expansion, since washing in and out probes post-expansion will not be possible.

We anticipate ExFISH being used with a diversity of signal amplification strategies to enable better imaging of single RNA molecules in large, intact tissues. Signal amplification techniques such as hybridization chain reaction (HCR)[3–5] and rolling circle amplification (RCA)[6,7] produce bright signals by forming large assemblies of fluorophores which can be easily detected. ExM invites the use of such techniques by creating room around them for such large assemblies of fluorophores. For instance, we used HCR with ExFISH, which allowed for single molecule-resolution visualization of RNA with nanoscale precision in thick brain tissues. HCR-ExFISH enables the super-resolved localization of RNA molecules in small compartments, such as neural synapses, while allowing for them to be imaged over large regions of tissue. HCR has also been used to amplify the fluorescence connected to an antibody, enabling protein visualization with a 3-order-of-magnitude boost in brightness over conventional antibody staining[5]. Future investigations of how ExFISH protocols could be used for visualization of the 3-D configuration of the genome will be of great interest in the probing of epigenetic states, chromatin conformation, and other important determinants of cell fate, function, and health.

Outlook on ExM Methods for Biomolecular Mapping

Compared to conventional Super-Resolution Microscopy (SRM) methods, ExM offers numerous technical advantages, such as the ability to perform 3D nanoscale imaging of thick fixed specimens, as well as speed and ease of use **(Supplementary Table 5, Supplementary Note 1)**. In addition, ExM yields transparent samples as a byproduct of its physical mechanism. In comparison to current clearing techniques, ExM clears samples due to the expansion process, which results in a hydrogel mostly composed of water **(Supplementary Table 6, Supplementary Note 2)**. The clearest disadvantage of ExM is its incompatibility with live samples. In contrast to SRM methods, ExM poses unique considerations owing to its physical mechanism. The expansion achieved is designed to be isotropic, and measurements of isotropy with different ExM methods have shown that distortions arising from the expansion process are minimal, but not zero **(Supplementary Table 5, Supplementary Note 1)**.

While iExM offers 3D nanoscale imaging in tissues with resolution comparable to the best performing SRM techniques, it may be possible to achieve even higher levels of expansion and resolution by improving polymer composition and processing protocols. Already a proof-of-concept triple expansion has been demonstrated, resulting in ~53x linear expansion, although the

resolution was not validated[8]. This might actually exceed the resolution of existing SRM technologies, especially if antibodies or other labels are delivered post-expansion, thus reducing the resolution error introduced by the nonzero size of the tags that comes into play when the tags are delivered to a nonexpanded tissue.

Another area of future interest is the combination of multiple protocols. A unified protocol that enabled the visualization of DNA, RNA, proteins, and lipids could reveal the organization of complexes of multiple kinds of biomolecules. Already the combined use of protein-anchoring AcX and RNA-labeling LabelX has been used to visualize fluorescent proteins and FISH-labeled RNAs in the same sample[1], and the ExPath protocol has been used to perform DNA FISH in concert with antibody labeling of proteins in the same sample[9]. Combining multimodal anchoring and labeling strategies with iExM is also an exciting future direction, potentially enabling many biomolecules to be visualized within a single sample with extremely high resolution.

The aqueous nature of expanded specimens and the decrowding of biomolecules may open the door for highly multiplexed readout of molecular information with nanoscale precision. ExFISH has already been used for serial-staining with multiple FISH probes for multiplexed imaging of different transcripts after RNA anchoring and expansion[1]. It may be possible to implement in intact tissues the use of barcoded, combinatorial RNA-FISH multiplexing approaches[10,11], such as MERFISH[12–14] and seqFISH[15], in which coded FISH probes are administered serially to yield the location of exponentially increasing numbers of transcripts over many cycles of hybridization. The ability to follow individual transcripts over many rounds of hybridization would be facilitated by the decrowding of transcipts. Indeed expansion microscopy has been used with MERFISH to visualize, with 10x higher density, members of a ~130-RNA library with near-100% detection efficiency in cultured cells[14]. The covalent anchoring of RNA to the polymer may also help support controlled enzymatic reactions such as fluorescent *in situ* sequencing (FISSEQ) of RNA[6,7]. Such approaches would yield transcriptome data in conjunction with cell morphology, protein locations, and other biomolecular information, with nanoscale precision.

Such techniques could also be used to identify any biomolecular labels that are conjugated to oligonucleotide barcodes that are retained within the gel (e.g., by using DNA PAINT style probes[16]). For instance, it may be possible to deliver antibodies for various targets,

each bearing a unique oligonucleotide tag that can be read-out after expansion via multiplexed FISH or *in situ* sequencing, thus providing location and identity information for very large numbers of proteins. This scheme could be extended to label any biomolecule with an oligonucleotide barcode that can be identified after expansion, thereby enabling the nanoscale mapping of biomolecules throughout specimens in a highly multiplexed fashion.

Multiplexed Mapping of RNA, and Nanoscale Imaging of Transcripts and Proteins

We have recently achieved the ability to map RNA in tissues post-expansion in a scalable way using a combination of in situ hybridization and sequencing. Following ExFISH, once RNA molecules are covalently retained in the ExM hydrogel, we deliver barcode-bearing FISH probes against a set of RNA targets. These barcodes uniquely identify each RNA target. After enzymatic ligation and rolling-circle amplification (RCA), the barcodes are read-out using in situ sequencing chemistries, such as sequencing-by-ligation or sequencing-by-synthesis (see Chapter 4 for details). Each round of sequencing reveals the identity of a given "base" of each barcode, which appears as one of four colors (**Figure 5.1A, B**). Over many sequencing rounds, the sequence of the barcode can be reconstructed. Consequently, each round of sequencing is followed by 3D, volumetric imaging of the expanded tissues to image RNA targets in a given region. To enable multiple rounds of imaging of the same region with minimal distortion, the expanded gel is immobilized in a charge-neutral gel.

With this approach, it is possible to map transcripts in a scalable way and with nanoscale precision in tissues. Each round of imaging reveals an exponentially increasing information about the identity of transcripts. When applied to thick brain tissue sections, it is possible to map the localization and abundance of a set of transcripts, such as canonical cell-type markers (**Figure 5.1 A-C**). We anticipate that this ability will be especially crucial in mapping the various cell types of the brain and their interactions. Furthermore, we can simultaneously image proteins, such as fluorescent proteins in transgenic organisms, allowing for the morphology of cells to be visualize accurately. In brain tissues section of Thy1-YFP mice, we can image RNA in a multiplexed way while visualization the morphology of neurons (**Figure 5.1 D, E**), enabling us to visualize and localize transcripts in the dendrites and cell bodies of hippocampal neurons. While this ability is important for studying the local regulation of gene

expression, we also think it is crucial for accurately classifying the cell types of the brain based on their transcriptomic profile as well as morphology.

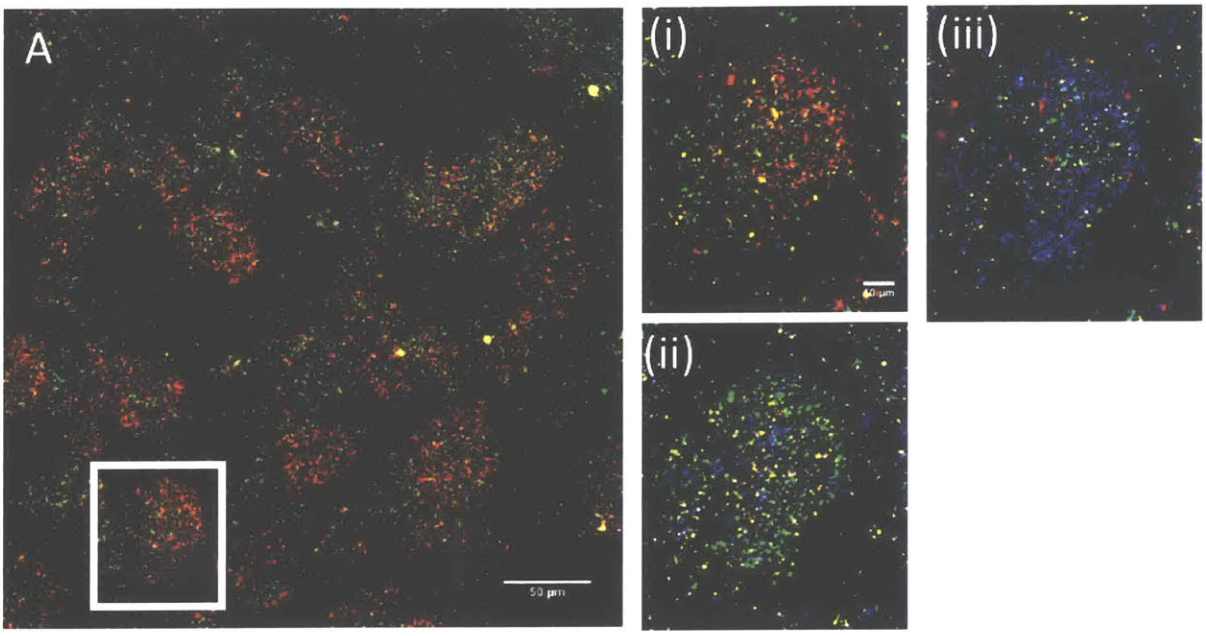

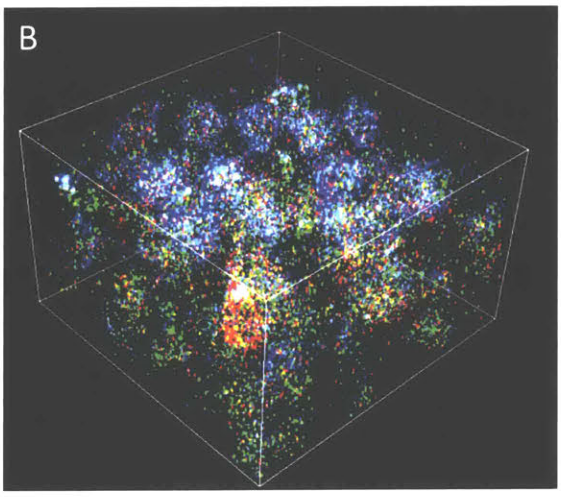

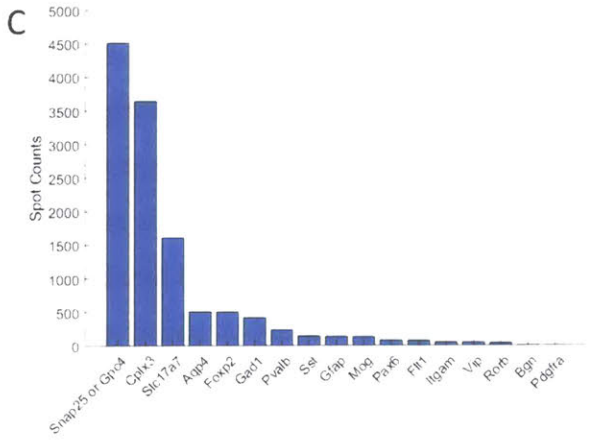

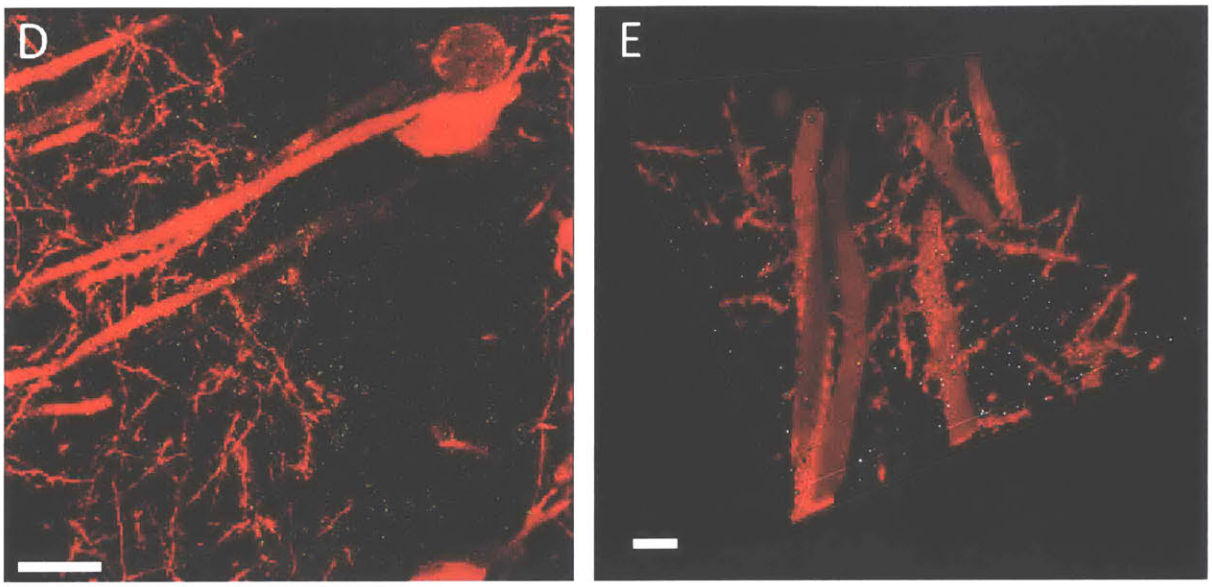

Figure 5.1: Nanoscale, multiplexed RNA mapping in the mouse brain. (**A**) Confocal images showing a single round of in situ sequencing of barcodes corresponding to 18 genes in a 50 μm thick cortical mouse brain tissue, insets shows an individual cell over three rounds of sequencing (i-iii). The four colors, blue, green, red, and orange, correspond to the 4 bases of sequencing read-out. (**B**) 3D-rendered image of the first round of in situ barcode read-out in the cortical brain sample. (**C**) Abundance of transcripts detected in the volume shown in (B). (**D**) Post-Expansion Confocal image showing Thy1-YFP hippocampal neurons (red), and transcripts (green) identified and localized from a set of 36-genes via a multiplexing experiment. The morphology of YFP expressing neurons was visualized by the application of antibodies before expansion. Transcripts were identified by the targeted-sequencing of barcode-bearing probes using Illumina sequencing chemistry. (**E**) 3D volume render showing six dendritically enriched transcripts: Dlg4 (green), Hpca (blue), Ddn (gray), Gria1 (cyan), CaMKIIa (magenta), Arc (yellow). Scale bars: (A), 15 μm; (A, insets), 3 μm; (D) 15 μm; (E) 5 μm

We are also currently developing a method that we call iterative-direct expansion microscopy (idExM) which enables the visualization of proteins and RNA with up to 20-fold expansion (~ 25nm lateral resolution). In this approach, proteins, RNA molecules, and antibody labels are directly retained in a hydrogel that undergoes iterative rounds of expansion, thereby allowing the use of conventional tags post-expansion to visualize proteins and RNA in thick tissues with resolution comparable to the best-performing super-resolution methods. We are using idExM to study the regulation of synaptic plasticity in the hippocampus. Owing to its high resolution, idExM enables to mapping of RNA molecules involved in synaptic plasticity (such as

Arc RNA and ribosomes) within dendrites and synapses (**Figure 5.2 A-D**). We expect that this ability will be useful in understanding the relationship between gene-regulation, and structural and functional changes of synapses that accompany synaptic plasticity. In addition, idExM is useful in deciphering molecular processes involving the interactions between proteins and RNA. With idExM, we are investigating the nanoscale regulation of transcription in the nucleus. For instance, we are able to associate sites of active transcription in the genome (visualized by labeling RNA Polymerase II) and nascent transcripts (**Figure 5.2 E-G**). Combined with the simultaneous imaging of the genome, idExM may reveal the relations between the 3D architecture of the genome and the regulation of transcription.

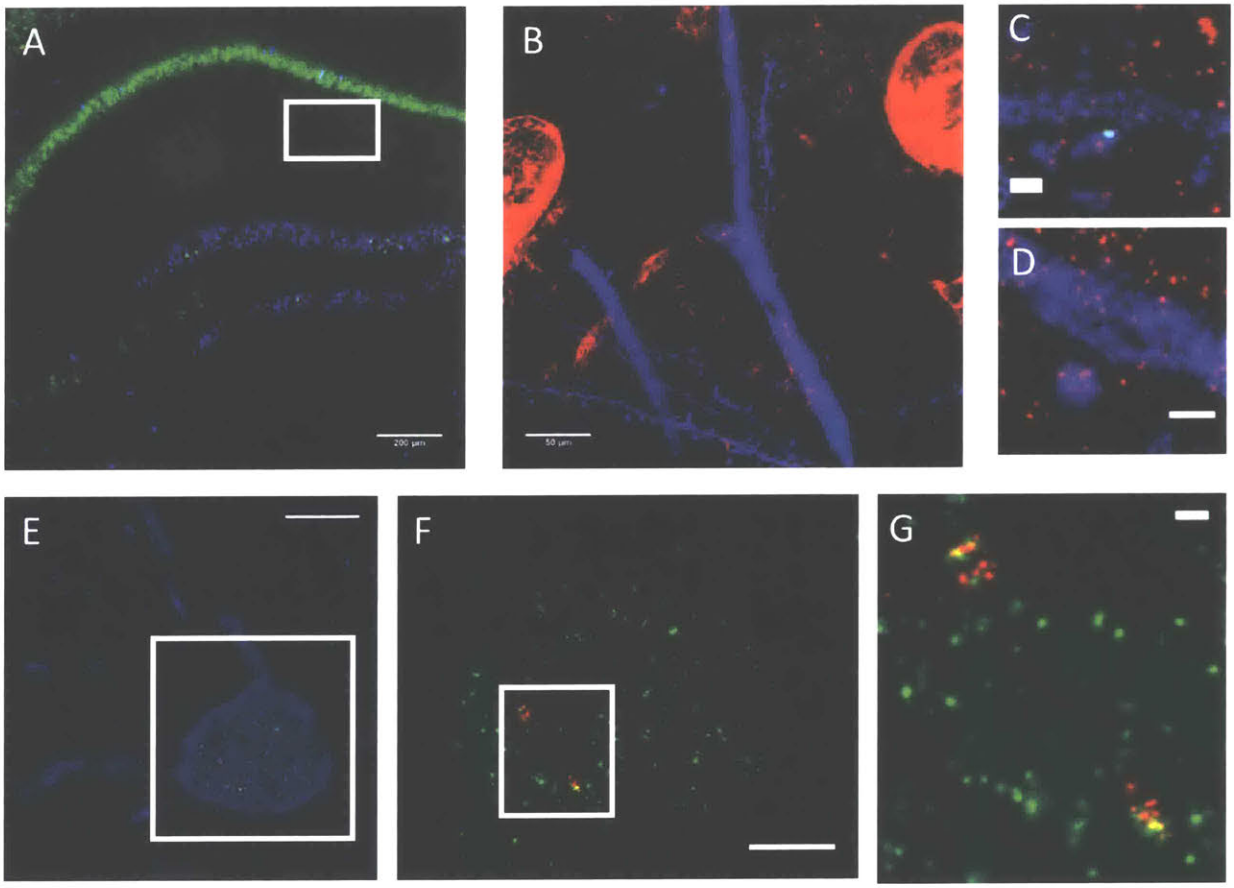

Figure 5.2: Nanoscale Imaging of RNA and Proteins with idExM in the mouse brain. (**A**) Pre-expansion confocal image of a Thy1-YFP mouse brain slice showing YFP expressing neurons (blue) and HCR V3.0 staining against Arc RNA (green). (**B**) idExM confocal image of neuronal dendrites in the hippocampus of a Thy1-YFP mouse brain tissue showing immunostaining against YFP (blue) and HCR V3.0 staining against 28s rrna (red) and Arc RNA (green). (**C**) A close up of a region in (B) showing an Arc RNA molecule inside a dendritic spine. (**D**) Another close up of a region in (B) showing 28s rrna particles inside a dendritic

shaft and an associated dendritic spine. (**E**) idExM confocal image of a neuronal cell body in the dentate gyrus of a Thy1-YFP mouse brain tissue showing immunostaining against YFP (blue) and actively transcribing RNA Polymerase II (green), and HCR V3.0 staining against arc RNA (red). (**F**) Inset of cell body shown in (E). (**G**) (Top) Close up of a region shown in (E) showing overlay between arc RNA transcription sites and RNA polymerase II clusters. Scale bars (expansion factor in parentheses); (A) 500 μm; (B) 5.8 μm (8.6x); (C) 350 nm (8.6x); (D) 500 nm (8.6x); (E) 5.3 μm (9x); (F) 2.5 μm (9x); (G) 280nm (9x);

Future Directions for Applications of ExFISH and ExM-Based Molecular Profiling

The ability of ExM to visualize new classes of biomolecules using appropriate chemistries opens the door for investigating many aspects of *in situ* RNA biology. Recent advances in the study of the chemistry of RNA bases in various conformations have enabled the development of chemical and enzymatic approaches to probe RNA secondary structure[17–20]. Such approaches can be combined with ExM to investigate the secondary structure of RNA molecules in an *in situ* context. Furthermore, it is becoming clearer that RNA modifications play crucial roles in regulating RNA processing[21]. These epitranscriptomic modifications are involved in regulating diverse cellular functions[22,23]. Research over the past decade has elucidated a set of chemistries and labeling strategies to study these RNA modifications[24]. It may be possible to applying these sequencing and antibody based approaches with ExFISH to study the spatial context of epitranscriptomic modifications. Given that these RNA modifications are quite pervasive, appearing on abundant RNA molecules such as rRNA and tRNAs, the resolution that can be achieved with ExM will be useful in associating RNA modifications to individual transcripts with single molecule precision.

Another exciting direction for ExM based molecular imaging is the *in situ* mapping of RNA translation. While vital regulation of cellular functions occurs via the spatiotemporal control of translation[25,26], the ability to observe the translated-fraction of transcripts may be more representative of protein production and distribution than the transcriptome. The past decade has seen the development of approaches that rely on the interaction of ribosomes and transcripts to measure translation in a high-throughput fashion[27,28]. None of these approaches has been extended to the *in situ* space or single cell level. The unique ability of ExM to retain biomolecules of interest can be leveraged for the mapping of translation. For instance, it may be possible to specifically retain endogenous RNA molecules undergoing translation, followed by interrogation with RNA FISH or *in situ* sequencing after expansion. Alternatively, it may be

possible to chemically mark translated transcripts such that they can be identified and visualized after expansion[29]. In combination with protein imaging with ExM, the mapping of translation will lead to better understanding of how regulatory processes unfold in different cell types and tissues.

The clearest weakness of ExM is the loss of dynamical information. Since specimens require fixation in preparation for ExM, information on cellular activity and molecular dynamics is mostly lost. However, ExM more than makes up for this deficit by enabling the nanoscale, multiplexed imaging of biomolecules in a single time frame. It is therefore conceivable to design schemes where live-cell imaging can be combined with ExM to gain information on dynamics. For instance, improved protein-engineering approaches have led to the development of sensors of neural activity with the desired properties for single-cell imaging[30,31]. It is in principle possible to perform ExM on specimens after live-cell imaging, where cells whose activity has been recorded during live-imaging can be identified after expansion. This would require the ability to register live-cell imaging data with images taken post-expansion, which is feasible. The addition of live-cell activity information to ExM nanoscale imaging would enable the study of cellular activity in relation to cellular biomolecular organization. Even more, this principle can be extended to the single molecule level. Advances in single-molecule imaging and protein-engineering have enabled live-cell imaging of RNA at the single molecule level[32,33], providing information on the molecular interaction and dynamics of individual target molecules. However, the number of colors that can be simultaneously imaged limits such schemes. Here, the multiplexing capability of ExM may useful. It may be possible to label a range of molecules with the same fluorophore, track their dynamics and activity, and after expansion, perform multiplexed imaging to identify each molecule. While this requires tracking individual molecules in the live-cell stage and throughout the expansion process, approaches developed for multiplexed RNA imaging[1,12,34] can be applied to achieve this goal.

One of the most fruitful scientific directions for ExM imaging of biomolecules is the classification and mapping of cell types in tissues. Especially in neuroscience, the task of understanding and classifying cell types can be daunting owing to the large variety of cells that are found in the brain[35]. Beyond molecular content, cells in the brain, ranging from neurons to various types of glia cells, are morphologically diverse, further compounding the task of studying cell types. RNA-seq and single cell RNA Seq (scRNA-Seq) have been the primary tools

for studying cell types[36–38]. However, the critical information of spatial context is lost. Particularly when studying brain cells, the process of isolating cells required by scRNA-Seq can lead to artifacts, such as the loss of neuronal processes. Multiplexed imaging of RNA with ExM may enable the study of cell types in tissues based on transcriptomic context while preserving the spatial context of cells. Even more, the subcellular, single-molecule precision of ExM may enable the fine-grain classification of similar cell types. The enhanced resolution of ExM may also allow for accurate tracing and segmentation of cellular morphologies, which is an important attribute of cells to consider when studying cell types. Combined with mapping of proteins using antibodies, the multiplexed imaging of RNA with ExM may open the door for classifying and studying cell types in tissues.

References:

1. Chen, F. *et al.* Nanoscale imaging of RNA with expansion microscopy. *Nat. Methods* **13,** 679–684 (2016).
2. Tsanov, N. *et al.* SmiFISH and FISH-quant - A flexible single RNA detection approach with super-resolution capability. *Nucleic Acids Res.* **44,** (2016).
3. Choi, H. M. T. *et al.* Programmable in situ amplification for multiplexed imaging of mRNA expression. *Nat. Biotechnol.* **28,** 1208–12 (2010).
4. Choi, H. M. T., Beck, V. A. & Pierce, N. A. Next-Generation in Situ Hybridization Chain Reaction: Higher Gain, Lower Cost, Greater Durability. *ACS Nano* **8,** 4284–4294 (2014).
5. Lin, R. *et al.* A hybridization-chain-reaction-based method for amplifying immunosignals. *Nat. Methods* **15,** 275–278 (2018).
6. Lee, J. H. *et al.* Highly Multiplexed Subcellular RNA Sequencing in Situ. *Science (80-.).* **343,** 1360–1363 (2014).
7. Ke, R. *et al.* In situ sequencing for RNA analysis in preserved tissue and cells. *Nat. Methods* **10,** 857–60 (2013).
8. Chang, J.-B. *et al.* Iterative expansion microscopy. *Nat. Methods* **14,** (2017).
9. Zhao, Y. *et al.* Nanoscale imaging of clinical specimens using pathology-optimized expansion microscopy. *Nat Biotech* **35,** 757–764 (2017).
10. Lubeck, E. & Cai, L. Single-cell systems biology by super-resolution imaging and combinatorial labeling. *Nat. Methods* **9,** 743–8 (2012).

11. Lubeck, E., Coskun, A. F., Zhiyentayev, T., Ahmad, M. & Cai, L. Single-cell in situ RNA profiling by sequential hybridization. *Nat. Methods* **11,** 360–1 (2014).
12. Chen, K. H., Boettiger, A. N., Moffitt, J. R., Wang, S. & Zhuang, X. Spatially resolved, highly multiplexed RNA profiling in single cells. *Sci.* **348,** (2015).
13. Moffitt, J. R. *et al.* High-throughput single-cell gene-expression profiling with multiplexed error-robust fluorescence in situ hybridization. *Proc. Natl. Acad. Sci.* **113,** 201612826 (2016).
14. Wang, G., Moffitt, J. R. & Zhuang, X. Multiplexed imaging of high-density libraries of RNAs with MERFISH and expansion microscopy. *Sci. Rep.* **8,** 4847 (2018).
15. Shah, S. *et al.* In Situ Transcription Profiling of Single Cells Reveals Spatial Organization of Cells in the Mouse Hippocampus. *Neuron* **92,** 342–357 (2016).
16. Wang, Y. *et al.* Rapid sequential in situ multiplexing with DNA-Exchange-Imaging in Neuronal Cells and Tissues. *Nano Lett.* acs.nanolett.7b02716 (2017). doi:10.1021/acs.nanolett.7b02716
17. Caprara, M. RNA structure determination using chemical methods. *Cold Spring Harb. Protoc.* **2013,** pdb.prot078485 (2013).
18. Kertesz, M. *et al.* Genome-wide measurement of RNA secondary structure in yeast. *Nature* **467,** 103–107 (2010).
19. Low, J. T. & Weeks, K. M. SHAPE-directed RNA secondary structure prediction. *Methods* **52,** 150–158 (2010).
20. Lucks, J. B. *et al.* Multiplexed RNA structure characterization with selective 2'-hydroxyl acylation analyzed by primer extension sequencing (SHAPE-Seq). *Proc. Natl. Acad. Sci. U. S. A.* **108,** 11063–8 (2011).
21. Roundtree, I. A., Evans, M. E., Pan, T. & He, C. Dynamic RNA Modifications in Gene Expression Regulation. *Cell* **169,** 1187–1200 (2017).
22. Ki-Jun Yoon, A. *et al.* Temporal Control of Mammalian Cortical Neurogenesis by m 6 A Methylation. *Cell* **171,** 1–13 (2017).
23. Zhao, B. S. *et al.* m6A-dependent maternal mRNA clearance facilitates zebrafish maternal-to-zygotic transition. *Nature* **542,** 475–478 (2017).
24. Li, X., Xiong, X. & Yi, C. Epitranscriptome sequencing technologies: decoding RNA modifications. *Nat. Methods* **14,** 23 (2017).

25. Holt, C. E. & Schuman, E. M. The central dogma decentralized: new perspectives on RNA function and local translation in neurons. *Neuron* **80,** 648–57 (2013).
26. Glock, C., Heumüller, M. & Schuman, E. M. mRNA transport and local translation in neurons. *Curr. Opin. Neurobiol.* **45,** 169–177 (2017).
27. Heiman, M. *et al.* A translational profiling approach for the molecular characterization of CNS cell types. *Cell* **135,** 738–48 (2008).
28. Ingolia, N. T., Ghaemmaghami, S., Newman, J. R. S. & Weissman, J. S. Genome-wide analysis in vivo of translation with nucleotide resolution using ribosome profiling. *Science* **324,** 218–23 (2009).
29. David, A. *et al.* Nuclear translation visualized by ribosome-bound nascent chain puromycylation. *J. Cell Biol.* **197,** 45–57 (2012).
30. Chen, T.-W. *et al.* Ultrasensitive fluorescent proteins for imaging neuronal activity. *Nature* **499,** 295–300 (2013).
31. Piatkevich, K. D. *et al.* A robotic multidimensional directed evolution approach applied to fluorescent voltage reporters. *Nat. Chem. Biol.* **14,** 352–360 (2018).
32. Wu, B., Eliscovich, C., Yoon, Y. J. & Singer, R. H. Translation dynamics of single mRNAs in live cells and neurons. *Science* **352,** 1430–5 (2016).
33. Buxbaum, A. R., Wu, B. & Singer, R. H. Single -Actin mRNA Detection in Neurons Reveals a Mechanism for Regulating Its Translatability. *Science (80-.).* **343,** 419–422 (2014).
34. Lee, J. H. *et al.* Highly Multiplexed Subcellular RNA Sequencing in Situ. *Science (80-.).* **343,** 1360–1363 (2014).
35. Zeng, H. & Sanes, J. R. Neuronal cell-type classification: challenges, opportunities and the path forward. *Nat. Rev. Neurosci.* **18,** 530–546 (2017).
36. Tasic, B. *et al.* Adult mouse cortical cell taxonomy revealed by single cell transcriptomics. *Nat. Neurosci.* **advance on,** 1–37 (2016).
37. Zeisel, A. *et al.* Cell types in the mouse cortex and hippocampus revealed by single-cell RNA-seq. *Science (80-.).* **347,** 1138–42 (2015).
38. Halpern, K. B. *et al.* Single-cell spatial reconstruction reveals global division of labour in the mammalian liver. *Nature* (2017). doi:10.1038/nature21065

6. Appendix

Appendix 6.1: Supplementary Tables

Supplemental Table 1. List of reagents and suppliers			
Chemical Supplies	Chemical Name	Supplier	Part Number
ExM Gel or Preparation	Sodium Acrylate (purity note:*)	Sigma	408220
	Acrylamide	Sigma	A9099
	N,N'-Methylenebisacrylamide	Sigma	M7279
	Ammonium Persulfate	Sigma	A3678
	N,N,N',N'-Tetramethylethylenediamine	Sigma	T7024
	VA-044	Wako	27776-21-2
	4-Hydroxy-TEMPO	Sigma	176141
Hybridization Buffer	Dextran Sulfate	Sigma	D8906-50g
	SSC	Thermo Fisher	AM9765
	Formamide	Thermo Fisher	AM9342
Fixation and Permeabilization	Paraformaldehyde	Electron Microscopy Sciences	15710
	Tissue-prep Buffered 10% Formalin	Electron Microscopy Sciences	15742-10
	Triton X-100	Sigma	93426
	Glycine	Sigma	50046
	10x PBS	Thermo Fisher	AM9624
Protein Digestion	Proteinase K	New England Biolabs	P8107S
	Ethylenediaminetetraacetic acid	Sigma	EDS
	Sodium Chloride	Sigma	
	Tris-HCl	Life Technologies	AM9855
HCR Amplification	Amplification Buffer	Molecular Instruments	N/A
	Tween 20		
LabelX Preparation	Label-IT ® Amine	Mirus Bio	MIR 3900
	Acryloyl-X, SE	Thermo Fisher	A20770
LabelX Treatment	MOPS	Sigma	M9381-25G
Reembeded Gels Staining	DNAse I	Sigma	4716728001
Bind-silane Treatment	Bind-Silane	Sigma	GE17-1330-01
	* check for yellow color upon resuspension: that indicates poor quality; solution should be clear (see http://expansionmicroscopy.org)		

Decades (Transcript Abundance)	Mean (Ratio of # spots detected in individual cells after ExM, to # spots detected before ExM)	Standard Deviation	P-Value
10s	1.082	0.177	0.107
100s	1.105	0.138	$3.24*10^{-4}$
1000s	1.596	0.562	$7.09*10^{-4}$

Supplementary Table 2. Statistical Analysis of RNA FISH spots detected in individual cells before and after ExFISH. For RNA molecules detected before vs after expansion, spots were counted by an automated algorithm. The ratio of the number of spots after ExM to spots counted before ExM was determined in each cell. Spot counts were grouped into decades based on the pre-expansion spot count. The table shows the results of a one-sample T-test performed on the ratio of spots counts for each decade to determine significant deviation from the expected mean ratio value of one.

Target	Total Spot Count (Averaged Across Both Red and Blue Channels)	Co-localized Spots	Co-localization %	Hybridization Efficiency	Volume analyzed (μm^3 in unexpanded coordinates)	Density (Co-localized Puncta per μm^3)
ActB	27504	15866	0.577	0.76	236749	0.067
Dlg4	9795	5174	0.528	0.727	236749	0.022
Camk2a	14440	8799	0.609	0.781	147968	0.059
Dlg4 Missense	1540	4	0.003	0.051	147968	0
mCherry	1209	0	0	0	147968	0

Supplementary Table 3. Analysis of two-color colocalization of FISH probes with HCR amplification in expanded slices.

Supplementary Table 4

Accession YFP	Accession Probe Sequence	Initiator Type
YFP B1 1	gAggAgggCAgCAAACgggAAgAgTCTTCCTTTACgTAATctcgcccttgctcaccat	B1
YFP B1 2	gAggAgggCAgCAAACgggAAgAgTCTTCCTTTACgTAATcaccaccccggtgaacag	B1
YFP B1 3	gAggAgggCAgCAAACgggAAgAgTCTTCCTTTACgTAATtccagctcgaccaggatg	B1
YFP B1 4	gAggAgggCAgCAAACgggAAgAgTCTTCCTTTACgTAATtgtggccgtttacgtcgc	B1
YFP B1 5	gAggAgggCAgCAAACgggAAgAgTCTTCCTTTACgTAATctcgccggacacgctgaa	B1
YFP B1 6	gAggAgggCAgCAAACgggAAgAgTCTTCCTTTACgTAATtaggtggcatcgccctcg	B1
YFP B1 7	gAggAgggCAgCAAACgggAAgAgTCTTCCTTTACgTAATacttcagggtcagcttgc	B1
YFP B1 8	gAggAgggCAgCAAACgggAAgAgTCTTCCTTTACgTAATcttgccggtggtgcagat	B1
YFP B1 9	gAggAgggCAgCAAACgggAAgAgTCTTCCTTTACgTAATgtgggccagggcacgggc	B1
YFP B1 10	gAggAgggCAgCAAACgggAAgAgTCTTCCTTTACgTAATagccgaaggtggtcacga	B1
YFP B1 11	gAggAgggCAgCAAACgggAAgAgTCTTCCTTTACgTAATggcgaagcactgcaggcc	B1
YFP B1 12	gAggAgggCAgCAAACgggAAgAgTCTTCCTTTACgTAATttcatgtggtcggggtag	B1
YFP B1 13	gAggAgggCAgCAAACgggAAgAgTCTTCCTTTACgTAATacttgaagaagtcgtgct	B1
YFP B1 14	gAggAgggCAgCAAACgggAAgAgTCTTCCTTTACgTAATgtagccttcgggcatggc	B1
YFP B1 15	gAggAgggCAgCAAACgggAAgAgTCTTCCTTTACgTAATaagatggtgcgctcctgg	B1
YFP B1 16	gAggAgggCAgCAAACgggAAgAgTCTTCCTTTACgTAATagttgccgtcgtccttga	B1
YFP B1 17	gAggAgggCAgCAAACgggAAgAgTCTTCCTTTACgTAATcacctcggcgcgggtctt	B1
YFP B1 18	gAggAgggCAgCAAACgggAAgAgTCTTCCTTTACgTAATagggtgtcgccctcgaac	B1
YFP B1 19	gAggAgggCAgCAAACgggAAgAgTCTTCCTTTACgTAATtcagctcgatgcggttca	B1
YFP B1 20	gAggAgggCAgCAAACgggAAgAgTCTTCCTTTACgTAATctccttgaagtcgatgcc	B1
YFP B1 21	gAggAgggCAgCAAACgggAAgAgTCTTCCTTTACgTAATtgccccaggatgttgccg	B1
YFP B1 22	gAggAgggCAgCAAACgggAAgAgTCTTCCTTTACgTAATtgtagttgtactccagct	B1
YFP B1 23	gAggAgggCAgCAAACgggAAgAgTCTTCCTTTACgTAATgatatagacgttgtggct	B1
YFP B1 24	gAggAgggCAgCAAACgggAAgAgTCTTCCTTTACgTAATttcttctgcttgtcggcc	B1
YFP B1 25	gAggAgggCAgCAAACgggAAgAgTCTTCCTTTACgTAATtgaagttcaccttgatgc	B1
YFP B1 26	gAggAgggCAgCAAACgggAAgAgTCTTCCTTTACgTAATctcgatgttgtggcggat	B1
YFP B1 27	gAggAgggCAgCAAACgggAAgAgTCTTCCTTTACgTAATgcgagctgcacgctgccg	B1
YFP B1 28	gAggAgggCAgCAAACgggAAgAgTCTTCCTTTACgTAATtgttctgctggtagtggt	B1
YFP B1 29	gAggAgggCAgCAAACgggAAgAgTCTTCCTTTACgTAATggggccgtcgccgatggg	B1
YFP B1 30	gAggAgggCAgCAAACgggAAgAgTCTTCCTTTACgTAATtggttgtcgggcagcagc	B1
YFP B1 31	gAggAgggCAgCAAACgggAAgAgTCTTCCTTTACgTAATcggactggtagctcaggt	B1
YFP B1 32	gAggAgggCAgCAAACgggAAgAgTCTTCCTTTACgTAATgttggggtctttgctcag	B1
YFP B1 33	gAggAgggCAgCAAACgggAAgAgTCTTCCTTTACgTAATaccatgtgatcgcgcttc	B1
YFP B1 34	gAggAgggCAgCAAACgggAAgAgTCTTCCTTTACgTAATcggtcacgaactccagca	B1
YFP B1 35	gAggAgggCAgCAAACgggAAgAgTCTTCCTTTACgTAATgccgagagtgatcccggc	B1
YFP B1 36	gAggAgggCAgCAAACgggAAgAgTCTTCCTTTACgTAATtacttgtacagctcgtcc	B1

Gad1 Accession: NM_008077.3

	Probe Sequence	Initiator
Gad1 1	GGCGAAGGAGTGGAAGATGCCAAAAgCTCAgTCCATCCTCgTAAATCCTCATCAATCATC	B2
Gad1 2	GGATCCGCTCCCGCGTTCGAGGAAgCATTCTTTCTTgAggAgggCAgCAAACgggAAgAg	B1
Gad1 3	GTAGGGCGCAGGTTGGTAGTATAAAgCTCAgTCCATCCTCgTAAATCCTCATCAATCATC	B2
Gad1 4	TGGGCTACGCCACACCAAGTATAAgCATTCTTTCTTgAggAgggCAgCAAACgggAAgAg	B1
Gad1 5	AGGCCCAGTTTTCTGGTGCATCAAAgCTCAgTCCATCCTCgTAAATCCTCATCAATCATC	B2
Gad1 6	TTGGTCCTTTGTAAGAAGCCACAAgCATTCTTTCTTgAggAgggCAgCAAACgggAAgAg	B1
Gad1 7	AGACGACTCTTCTCTTCCAGGCAAAgCTCAgTCCATCCTCgTAAATCCTCATCAATCATC	B2
Gad1 8	GAGGACTGCCTCTCCCTGAAGGAAgCATTCTTTCTTgAggAgggCAgCAAACgggAAgAg	B1
Gad1 9	TTTTCACAGGAAAGCAGGTTCTAAAgCTCAgTCCATCCTCgTAAATCCTCATCAATCATC	B2
Gad1 10	GTGCGCCGGAAGCGGGCACCCTAAgCATTCTTTCTTgAggAgggCAgCAAACgggAAgAg	B1
Gad1 11	AACAGGTTGGAGAAGTCGGTCTAAAgCTCAgTCCATCCTCgTAAATCCTCATCAATCATC	B2
Gad1 12	CCGTTCTTAGCTGGAAGCAGATAAgCATTCTTTCTTgAggAgggCAgCAAACgggAAgAg	B1
Gad1 13	AAGAACTGCGCAGTTTGCTCCTAAAgCTCAgTCCATCCTCgTAAATCCTCATCAATCATC	B2
Gad1 14	TAGTTGAGGAGTATGTCTACCAAAgCATTCTTTCTTgAggAgggCAgCAAACgggAAgAg	B1
Gad1 15	GAGCGATCAAATGTCTTGCGGAAAAgCTCAgTCCATCCTCgTAAATCCTCATCAATCATC	B2
Gad1 16	TGTGGGTGGTGGAAATCCAGAAAAgCATTCTTTCTTgAggAgggCAgCAAACgggAAgAg	B1
Gad1 17	CCTTCCATGCCTTCCAGCAACTAAAgCTCAgTCCATCCTCgTAAATCCTCATCAATCATC	B2
Gad1 18	TCGGGGTGGTCAGACAGCTCCAAAgCATTCTTTCTTgAggAgggCAgCAAACgggAAgAg	B1
Gad1 19	TCAACCAGGATCTGCTCCAGAGAAAgCTCAgTCCATCCTCgTAAATCCTCATCAATCATC	B2
Gad1 20	CGAACCCCGTACTTCAGGGTGTAAgCATTCTTTCTTgAggAgggCAgCAAACgggAAgAg	B1
Gad1 21	TTGAAAAATCGAGGGTGACCTGAAAgCTCAgTCCATCCTCgTAAATCCTCATCAATCATC	B2
Gad1 22	CCAATGATATCCAAACCAGTAGAAgCATTCTTTCTTgAggAgggCAgCAAACgggAAgAg	B1
Gad1 23	GATGTCAGCCATTCACCAGCTAAAAgCTCAgTCCATCCTCgTAAATCCTCATCAATCATC	B2
Gad1 24	TCATATGTGAACATATTGGTATAAgCATTCTTTCTTgAggAgggCAgCAAACgggAAgAg	B1
Gad1 25	ATGAGAACAAACACGGGTGCAAAAAgCTCAgTCCATCCTCgTAAATCCTCATCAATCATC	B2
Gad1 26	TCTCTCATCTTCTTAAGAGTAAAAgCATTCTTTCTTgAggAgggCAgCAAACgggAAgAg	B1
Gad1 27	TCTTTATTTGACCATCCAACGAAAAgCTCAgTCCATCCTCgTAAATCCTCATCAATCATC	B2
Gad1 28	GCTCCCCCAGGAGAAAATATCCAAgCATTCTTTCTTgAggAgggCAgCAAACgggAAgAg	B1
Gad1 29	ATGATGCTGTACATATTGGATAAAAgCTCAgTCCATCCTCgTAAATCCTCATCAATCATC	B2
Gad1 30	ACTTCTGGGAAGTACTTGTAACAAgCATTCTTTCTTgAggAgggCAgCAAACgggAAgAg	B1
Gad1 31	ACAGCCGCCATGCCTTTTGTCTAAAgCTCAgTCCATCCTCgTAAATCCTCATCAATCATC	B2
Gad1 32	TGTTCTGAGGTGAAGAGGACCAAAgCATTCTTTCTTgAggAgggCAgCAAACgggAAgAg	B1
Gad1 33	GCTTTCTTTATGGAATAGTGACAAAgCTCAgTCCATCCTCgTAAATCCTCATCAATCATC	B2
Gad1 34	TTGTCGGTTCCAAAGCCAAGCGAAgCATTCTTTCTTgAggAgggCAgCAAACgggAAgAg	B1
Gad1 35	TCATTGCACTTTATCAAAATCAAAAgCTCAgTCCATCCTCgTAAATCCTCATCAATCATC	B2
Gad1 36	TCTAAATCAGCCGGAATTATCTAAgCATTCTTTCTTgAggAgggCAgCAAACgggAAgAg	B1
Gad1 37	TGTTTGGCATCAAGAATTTTTGAAAgCTCAgTCCATCCTCgTAAATCCTCATCAATCATC	B2
Gad1 38	GCATTGACATAAAGGGGAACATAAgCATTCTTTCTTgAggAgggCAgCAAACgggAAgAg	B1
Gad1 39	CCGTAAACAGTCGTGCCTGCGGAAAgCTCAgTCCATCCTCgTAAATCCTCATCAATCATC	B2
Gad1 40	TCCGCAATTTCCTGGATTGGATAAgCATTCTTTCTTgAggAgggCAgCAAACgggAAgAg	B1
Gad1 41	CAAAGGTTGTATTTCTCACATAAAAgCTCAgTCCATCCTCgTAAATCCTCATCAATCATC	B2
Gad1 42	CCACCACCCCAGGCAGCATCCAAAgCATTCTTTCTTgAggAgggCAgCAAACgggAAgAg	B1
Gad1 43	CGGTGCTTCCGGGACATGAGCAAAAgCTCAgTCCATCCTCgTAAATCCTCATCAATCATC	B2
Gad1 44	TTGGCCCTTTCTATGCCGCTGAAAgCATTCTTTCTTgAggAgggCAgCAAACgggAAgAg	B1

Gad1 45	TTGTGAGGGTTCCAGGTGACTGAAAgCTCAgTCCATCCTCgTAAATCCTCATCAATCATC	B2
Gad1 46	GCAGAGCACTGGAGCAGCACGCAAgCATTCTTTCTTgAggAgggCAgCAAACgggAAgAg	B1
Gad1 47	ATACCCTTTTCCTTGACCAGAAAAAgCTCAgTCCATCCTCgTAAATCCTCATCAATCATC	B2
Gad1 48	CCTGCACACATCTGGTTGCATCAAgCATTCTTTCTTgAggAgggCAgCAAACgggAAgAg	B1

Accession:
NM_007393.3
ActB

	Probe Sequence	Initiator
ActB B2 2	CCTCgTAAATCCTCATCAATCATCCAgTAAACCgCCAAggaatacagcccggggagcatc	B2
ActB B2 4	CCTCgTAAATCCTCATCAATCATCCAgTAAACCgCCAAcacccacataggagtccttctg	B2
ActB B2 6	CCTCgTAAATCCTCATCAATCATCCAgTAAACCgCCAAcaatggggtacttcagggtcag	B2
ActB B2 8	CCTCgTAAATCCTCATCAATCATCCAgTAAACCgCCAAggtgccagatcttctccatgtc	B2
ActB B2 10	CCTCgTAAATCCTCATCAATCATCCAgTAAACCgCCAAtcatcttttcacggttggcctt	B2
ActB B2 12	CCTCgTAAATCCTCATCAATCATCCAgTAAACCgCCAAtggctacgtacatggctggggt	B2
ActB B2 14	CCTCgTAAATCCTCATCAATCATCCAgTAAACCgCCAAcaatgcctgtggtacgaccaga	B2
ActB B2 16	CCTCgTAAATCCTCATCAATCATCCAgTAAACCgCCAAcctcgtagatgggcacagtgtg	B2
ActB B2 18	CCTCgTAAATCCTCATCAATCATCCAgTAAACCgCCAAatcttcatgaggtagtctgtca	B2
ActB B2 20	CCTCgTAAATCCTCATCAATCATCCAgTAAACCgCCAAatttccctctcagctgtggtgg	B2
ActB B2 22	CCTCgTAAATCCTCATCAATCATCCAgTAAACCgCCAAtcgaagtctagagcaacatagc	B2
ActB B2 24	CCTCgTAAATCCTCATCAATCATCCAgTAAACCgCCAAtagctcttctccagggaggaag	B2
ActB B2 26	CCTCgTAAATCCTCATCAATCATCCAgTAAACCgCCAAcggaaccgctcgttgccaatag	B2
ActB B2 28	CCTCgTAAATCCTCATCAATCATCCAgTAAACCgCCAAcaggattccatacccaagaagg	B2
ActB B2 30	CCTCgTAAATCCTCATCAATCATCCAgTAAACCgCCAAtcaacgtcacacttcatgatgg	B2
ActB B2 32	CCTCgTAAATCCTCATCAATCATCCAgTAAACCgCCAAgtggtaccaccagacagcactg	B2
ActB B2 34	CCTCgTAAATCCTCATCAATCATCCAgTAAACCgCCAAagagcagtaatctccttctgca	B2
ActB B2 36	CCTCgTAAATCCTCATCAATCATCCAgTAAACCgCCAAttgcgctcaggaggagcaatga	B2
ActB B2 38	CCTCgTAAATCCTCATCAATCATCCAgTAAACCgCCAAaaggtggacagtgaggccagga	B2
ActB B2 40	CCTCgTAAATCCTCATCAATCATCCAgTAAACCgCCAAgaggggccggactcatcgtact	B2
Act Short HCR 1	gAggAgggCAgCAAACgggAAgAgTCTTCCTTTACgTTgcgcagcgatatcgtcatccat	B1
Act Short HCR 3	gAggAgggCAgCAAACgggAAgAgTCTTCCTTTACgTTccattcccaccatcacaccctg	B1
Act Short HCR 5	gAggAgggCAgCAAACgggAAgAgTCTTCCTTTACgTTtacctctcttgctctgggcctc	B1
Act Short HCR 7	gAggAgggCAgCAAACgggAAgAgTCTTCCTTTACgTTcccagttggtaacaatgccatg	B1
Act Short HCR 9	gAggAgggCAgCAAACgggAAgAgTCTTCCTTTACgTTcacgcagctcattgtagaaggt	B1
Act Short HCR 11	gAggAgggCAgCAAACgggAAgAgTCTTCCTTTACgTTtgaaggtctcaaacatgatctg	B1
Act Short HCR 13	gAggAgggCAgCAAACgggAAgAgTCTTCCTTTACgTTcatacagggacagcacagcctg	B1
Act Short HCR 15	gAggAgggCAgCAAACgggAAgAgTCTTCCTTTACgTTtgaccccgtctccggagtccat	B1
Act Short HCR 17	gAggAgggCAgCAAACgggAAgAgTCTTCCTTTACgTTggatggcgtgagggagagcata	B1
Act Short HCR 19	gAggAgggCAgCAAACgggAAgAgTCTTCCTTTACgTTaagctgtagccacgctcggtca	B1
Act Short HCR 21	gAggAgggCAgCAAACgggAAgAgTCTTCCTTTACgTTagcttctctttgatgtcacgca	B1
Act Short HCR 23	gAggAgggCAgCAAACgggAAgAgTCTTCCTTTACgTTgatgcggcagtggccatctcct	B1
Act Short HCR 25	gAggAgggCAgCAAACgggAAgAgTCTTCCTTTACgTTatgacctggccgtcaggcagct	B1
Act Short HCR 27	gAggAgggCAgCAAACgggAAgAgTCTTCCTTTACgTTggctggaaaagagcctcagggc	B1
Act Short HCR 29	gAggAgggCAgCAAACgggAAgAgTCTTCCTTTACgTTttgaatgtagtttcatggatgc	B1
Act Short HCR 31	gAggAgggCAgCAAACgggAAgAgTCTTCCTTTACgTTttggcatagaggtctttacgga	B1
Act Short HCR 33	gAggAgggCAgCAAACgggAAgAgTCTTCCTTTACgTTctgtcagcaatgcctgggtaca	B1

Act Short HCR 35	gAggAgggCAgCAAACgggAAgAgTCTTCCTTTACgTTttgatcttcatggtgctaggag	B1
Act Short HCR 37	gAggAgggCAgCAAACgggAAgAgTCTTCCTTTACgTTgagccaccgatccacacagagt	B1
Act Short HCR 39	gAggAgggCAgCAAACgggAAgAgTCTTCCTTTACgTTtgcttgctgatccacatctgct	B1
Act Short HCR 41	gAggAgggCAgCAAACgggAAgAgTCTTCCTTTACgTTtagaagcacttgcggtgcacga	B1
Act Short HCR 41	gAggAgggCAgCAAACgggAAgAgTCTTCCTTTACgTTtagaagcacttgcggtgcacga	B1

Accession:
NM_00110975
2.1
Dlg4

	Probe Sequence	Initiator
DLG4 B1 2	GGGCTGTGTTCCAGAGGGGGCGAAgCATTCTTTCTTgAggAgggCAgCAAACgggAAgAg	B1
DLG4 B1 4	GTGTCCGTGTTGACAATCACAGAAgCATTCTTTCTTgAggAgggCAgCAAACgggAAgAg	B1
DLG4 B1 6	TCCTCATACTCCATCTCCCCCTAAgCATTCTTTCTTgAggAgggCAgCAAACgggAAgAg	B1
DLG4 B1 8	GTGCCACCTGCGATGCTGAAGCAAgCATTCTTTCTTgAggAgggCAgCAAACgggAAgAg	B1
DLG4 B1 10	GGAATGATCTTGGTGATAAAGAAAgCATTCTTTCTTgAggAgggCAgCAAACgggAAgAg	B1
DLG4 B1 12	AACAGGATGCTGTCGTTGACCCAAgCATTCTTTCTTgAggAgggCAgCAAACgggAAgAg	B1
DLG4 B1 14	AGGGCCTCCACTGCAGCTGAATAAgCATTCTTTCTTgAggAgggCAgCAAACgggAAgAg	B1
DLG4 B1 16	GCTGGGGGTTTCCGGCGCATGAAAgCATTCTTTCTTgAggAgggCAgCAAACgggAAgAg	B1
DLG4 B1 18	CTGAAGCCAAGTCCTTTAGGCCAAgCATTCTTTCTTgAggAgggCAgCAAACgggAAgAg	B1
DLG4 B1 20	ACGTAGATGCTATTATCTCCAGAAgCATTCTTTCTTgAggAgggCAgCAAACgggAAgAg	B1
DLG4 B1 22	CCGATCTGCAACCTGCCATCCTAAgCATTCTTTCTTgAggAgggCAgCAAACgggAAgAg	B1
DLG4 B1 24	TCCTCATGCATGACATCCTCTAAAgCATTCTTTCTTgAggAgggCAgCAAACgggAAgAg	B1
DLG4 B1 26	TTGGCCACCTTTAGGTACACAAAAgCATTCTTTCTTgAggAgggCAgCAAACgggAAgAg	B1
DLG4 B1 28	GAGGTTGTGATGTCTGGGGGAGAAgCATTCTTTCTTgAggAgggCAgCAAACgggAAgAg	B1
DLG4 B1 30	TCGGTGCCCAAGTAGCTGCTATAAgCATTCTTTCTTgAggAgggCAgCAAACgggAAgAg	B1
DLG4 B2 1	TCTTCATCTTGGTAGCGGTATTAAAgCTCAgTCCATCCTCgTAAATCCTCATCAATCATC	B2
DLG4 B2 3	GGAGAATTGGCCTGGTTGGGGAAAAgCTCAgTCCATCCTCgTAAATCCTCATCAATCATC	B2
DLG4 B2 5	GTTCCGTTCACATATCCTGGGGAAAgCTCAgTCCATCCTCgTAAATCCTCATCAATCATC	B2
DLG4 B2 7	AGACCTGAGTTACCCCTTTCCAAAAgCTCAgTCCATCCTCgTAAATCCTCATCAATCATC	B2
DLG4 B2 9	GATGGGTCGTCACCGATGTGTGAAAgCTCAgTCCATCCTCgTAAATCCTCATCAATCATC	B2
DLG4 B2 11	AGGCGGCCATCCTGGGCTGCAGAAAgCTCAgTCCATCCTCgTAAATCCTCATCAATCATC	B2
DLG4 B2 13	GTCACCTCCCGGACATCCACTTAAAgCTCAgTCCATCCTCgTAAATCCTCATCAATCATC	B2
DLG4 B2 15	TAGAGGCGAACGATGGAACCCGAAAgCTCAgTCCATCCTCgTAAATCCTCATCAATCATC	B2
DLG4 B2 17	TTGATAAGCTTGATCTCTATGAAAAgCTCAgTCCATCCTCgTAAATCCTCATCAATCATC	B2
DLG4 B2 19	ATGTGCTGGTTCCCAACGCCCCAAAgCTCAgTCCATCCTCgTAAATCCTCATCAATCATC	B2
DLG4 B2 21	TGGGCAGCGCCTCCTTCGATGAAAAgCTCAgTCCATCCTCgTAAATCCTCATCAATCATC	B2
DLG4 B2 23	CCCACACTGTTGACCGCCAGGAAAAgCTCAgTCCATCCTCgTAAATCCTCATCAATCATC	B2
DLG4 B2 25	TCATATGTGTTCTTCAGGGCTGAAAgCTCAgTCCATCCTCgTAAATCCTCATCAATCATC	B2
DLG4 B2 27	TAGCTGTCACTCAGGTAGGCATAAAgCTCAgTCCATCCTCgTAAATCCTCATCAATCATC	B2
DLG4 B2 29	CTGATCTCATTGTCCAGGTGCTAAAgCTCAgTCCATCCTCgTAAATCCTCATCAATCATC	B2

Accession:
NM_177407.4
Camk2a

	Probe Sequence	Initiator
Camk2a iso2 1	gAggAgggCAgCAAACgggAAgAgTCTTCCTTTACgAACGGGTGCAGGTGATGGTAGCCA	B1
Camk2a iso2 2	CCTCgTAAATCCTCATCAATCATCCAgTAAACCgCCAATCCTCAAAGAGCTGGTACTCTT	B2
Camk2a iso2 3	gAggAgggCAgCAAACgggAAgAgTCTTCCTTTACgAAACAGAGAAGGCTCCCTTTCCCA	B1
Camk2a iso2 4	CCTCgTAAATCCTCATCAATCATCCAgTAAACCgCCAACCAGCCAGCACCTTCACACACC	B2
Camk2a iso2 5	gAggAgggCAgCAAACgggAAgAgTCTTCCTTTACgAAATAATCTTGGCAGCATACTCCT	B1
Camk2a iso2 6	CCTCgTAAATCCTCATCAATCATCCAgTAAACCgCCAATGATCTCTGGCTGAAAGCTTCT	B2
Camk2a iso2 7	gAggAgggCAgCAAACgggAAgAgTCTTCCTTTACgAACGGGCCTCACGCTCCAGCTTCT	B1
Camk2a iso2 8	CCTCgTAAATCCTCATCAATCATCCAgTAAACCgCCAAATATTGGGGTGCTTCAACAAGC	B2
Camk2a iso2 9	gAggAgggCAgCAAACgggAAgAgTCTTCCTTTACgAAGAGATGCTGTCATGGAGTCGGA	B1
Camk2a iso2 10	CCTCgTAAATCCTCATCAATCATCCAgTAAACCgCCAATCGAAGATAAGGTAGTGGTGCC	B2
Camk2a iso2 11	gAggAgggCAgCAAACgggAAgAgTCTTCCTTTACgAAAACAGTTCCCCACCAGTAACCA	B1
Camk2a iso2 12	CCTCgTAAATCCTCATCAATCATCCAgTAAACCgCCAACTGTAATACTCCCGGGCCACAA	B2
Camk2a iso2 13	gAggAgggCAgCAAACgggAAgAgTCTTCCTTTACgAAATACAGTGGCTGGCATCAGCTT	B1
Camk2a iso2 14	CCTCgTAAATCCTCATCAATCATCCAgTAAACCgCCAACAGTGTAGCACAGCCTCCAAGA	B2
Camk2a iso2 15	gAggAgggCAgCAAACgggAAgAgTCTTCCTTTACgAACGATGCACCACCCCCATCTGGT	B1
Camk2a iso2 16	CCTCgTAAATCCTCATCAATCATCCAgTAAACCgCCAAGCCAGCAACAGATTCTCAGGCT	B2
Camk2a iso2 17	gAggAgggCAgCAAACgggAAgAgTCTTCCTTTACgAAACAGCAGCGCCCTTGAGCTTCG	B1
Camk2a iso2 18	CCTCgTAAATCCTCATCAATCATCCAgTAAACCgCCAATCTATGGCCAGGCCAAAGTCTG	B2
Camk2a iso2 19	gAggAgggCAgCAAACgggAAgAgTCTTCCTTTACgAACATGCCTGCTGCTCCCCCTCCA	B1
Camk2a iso2 20	CCTCgTAAATCCTCATCAATCATCCAgTAAACCgCCAAAGGTATCCAGGTGTCCCTGCGA	B2
Camk2a iso2 21	gAggAgggCAgCAAACgggAAgAgTCTTCCTTTACgAATCCTTCCTCAGCACTTCTGGGG	B1
Camk2a iso2 22	CCTCgTAAATCCTCATCAATCATCCAgTAAACCgCCAAGCCCACAGGTCCACGGGCTTCC	B2
Camk2a iso2 23	gAggAgggCAgCAAACgggAAgAgTCTTCCTTTACgAAAAGATATACAGGATGACGCCAC	B1
Camk2a iso2 24	CCTCgTAAATCCTCATCAATCATCCAgTAAACCgCCAATCATCCCAGAACGGGGGATACC	B2
Camk2a iso2 25	gAggAgggCAgCAAACgggAAgAgTCTTCCTTTACgAATGCTGGTACAGGCGATGCTGGT	B1
Camk2a iso2 26	CCTCgTAAATCCTCATCAATCATCCAgTAAACCgCCAAGATGGGAAATCATAGGCACCAG	B2
Camk2a iso2 27	gAggAgggCAgCAAACgggAAgAgTCTTCCTTTACgAAGGGGTGACGGTGTCCCATTCTG	B1
Camk2a iso2 28	CCTCgTAAATCCTCATCAATCATCCAgTAAACCgCCAAAGCATCTTATTGATCAGATCCT	B2
Camk2a iso2 29	gAggAgggCAgCAAACgggAAgAgTCTTCCTTTACgAAATGCGTTTGGACGGGTTGATGG	B1
Camk2a iso2 30	CCTCgTAAATCCTCATCAATCATCCAgTAAACCgCCAACATGGGTGCTTGAGAGCCTCAG	B2
Camk2a iso2 31	gAggAgggCAgCAAACgggAAgAgTCTTCCTTTACgAAGCCACGGTGGAGCGGTGCGAGA	B1
Camk2a iso2 32	CCTCgTAAATCCTCATCAATCATCCAgTAAACCgCCAATCCACGGTCTCCTGTCTGTGCA	B2
Camk2a iso2 33	gAggAgggCAgCAAACgggAAgAgTCTTCCTTTACgAACTGGCATTGAACTTCTTCAGGC	B1
Camk2a iso2 34	CCTCgTAAATCCTCATCAATCATCCAgTAAACCgCCAAGTGGTGAGGATGGCTCCCTTCA	B2
Camk2a iso2 35	gAggAgggCAgCAAACgggAAgAgTCTTCCTTTACgAAGAGAAGTTCCTGGTGGCCAGCA	B1
Camk2a iso2 36	CCTCgTAAATCCTCATCAATCATCCAgTAAACCgCCAATTCTTCTTGTTTCCTCCGCTCT	B2
Camk2a iso2 37	gAggAgggCAgCAAACgggAAgAgTCTTCCTTTACgAATCAGAAGATTCCTTCACACCAT	B1
Camk2a iso2 38	CCTCgTAAATCCTCATCAATCATCCAgTAAACCgCCAATCTTCGTCCTCAATGGTGGTGT	B2
Camk2a iso2 39	gAggAgggCAgCAAACgggAAgAgTCTTCCTTTACgAAATTTCCTGTTTGCGCACTTTGG	B1
Camk2a iso2 40	CCTCgTAAATCCTCATCAATCATCCAgTAAACCgCCAAGCTTCGATCAGCTGCTCTGTCA	B2
Camk2a iso2 41	gAggAgggCAgCAAACgggAAgAgTCTTCCTTTACgAAGACTCAAAGTCTCCATTGCTTA	B1
Camk2a iso2 42	CCTCgTAAATCCTCATCAATCATCCAgTAAACCgCCAAGTCATTCCAGGGTCGCACATCT	B2
Camk2a iso2 43	gAggAgggCAgCAAACgggAAgAgTCTTCCTTTACgAACCCAGGGCCTCTGGTTCAAAGG	B1
Camk2a iso2 44	CCTCgTAAATCCTCATCAATCATCCAgTAAACCgCCAACGATGAAAGTCCAGGCCCTCCA	B2
Camk2a iso2 45	gAggAgggCAgCAAACgggAAgAgTCTTCCTTTACgAAGACCACAGGTTTTCAAAATAGA	B1
Camk2a iso2 46	CCTCgTAAATCCTCATCAATCATCCAgTAAACCgCCAAATGGTGGTGTGCACGGGCTTGC	B2

Camk2a iso2 47	gAggAgggCAgCAAACgggAAgAgTCTTCCTTTACgAAATCAGGTGGATGTGAGGGTTCA	B1
Camk2a iso2 48	CCTCgTAAATCCTCATCAATCATCCAgTAAACCgCCAAATATAGGCGATGCAGGCTGACT	B2

Accession
Number

	Probe Sequence	Initiator
mCherry 2C 1	cttcttcacctttgaaaccatAAgCATTCTTTCTTgAggAgggCAgCAAACgggAAgAg	B1
mCherry 2C 3	ccatatgaactttaaatctcatAAgCATTCTTTCTTgAggAgggCAgCAAACgggAAgAg	B1
mCherry 2C 5	cttcaccttcaccttcaatttcAAgCATTCTTTCTTgAggAgggCAgCAAACgggAAgAg	B1
mCherry 2C 7	caccttttagtaactttcaatttAAgCATTCTTTCTTgAggAgggCAgCAAACgggAAgAg	B1
mCherry 2C 9	catacataaattgtggtgacaaAAgCATTCTTTCTTgAggAgggCAgCAAACgggAAgAg	B1
mCherry 2C 11	ttaaataatctggaatatcagcAAgCATTCTTTCTTgAggAgggCAgCAAACgggAAgAg	B1
mCherry 2C 13	tcaaaattcataactctttcccAAgCATTCTTTCTTgAggAgggCAgCAAACgggAAgAg	B1
mCherry 2C 15	ctctcaatttaactttataaatAAgCATTCTTTCTTgAggAgggCAgCAAACgggAAgAg	B1
mCherry 2C 17	ccatagtttttttttgcataacAAgCATTCTTTCTTgAggAgggCAgCAAACgggAAgAg	B1
mCherry 2C 19	tcaatctttgtttaatttcaccAAgCATTCTTTCTTgAggAgggCAgCAAACgggAAgAg	B1
mCherry 2C 21	taatattaacattataagcaccAAgCATTCTTTCTTgAggAgggCAgCAAACgggAAgAg	B1
mCherry 2C 23	tttcatattgttcaacaatagtAAgCATTCTTTCTTgAggAgggCAgCAAACgggAAgAg	B1
mCherry 2C 2	attctttaataatagccatattAAAgCTCAgTCCATCCTCgTAAATCCTCATCAATCATC	B2
mCherry 2C 4	attcatgaccattaactgaaccAAAgCTCAgTCCATCCTCgTAAATCCTCATCAATCATC	B2
mCherry 2C 6	cagtttgagtaccttcatatggAAAgCTCAgTCCATCCTCgTAAATCCTCATCAATCATC	B2
mCherry 2C 8	tatcccaagcaaatggtaatggAAAgCTCAgTCCATCCTCgTAAATCCTCATCAATCATC	B2
mCherry 2C 10	gatgtttaacataagcttttgaAAAgCTCAgTCCATCCTCgTAAATCCTCATCAATCATC	B2
mCherry 2C 12	ttaaaaccttctggaaatgacaAAAgCTCAgTCCATCCTCgTAAATCCTCATCAATCATC	B2
mCherry 2C 14	gagtaacagtaacaacaccaccAAAgCTCAgTCCATCCTCgTAAATCCTCATCAATCATC	B2
mCherry 2C 16	gaccatctgatggaaaattagtAAAgCTCAgTCCATCCTCgTAAATCCTCATCAATCATC	B2
mCherry 2C 18	ttctttctgatgaagcttcccaAAAgCTCAgTCCATCCTCgTAAATCCTCATCAATCATC	B2
mCherry 2C 20	gtaattgaactggttttttagcAAAgCTCAgTCCATCCTCgTAAATCCTCATCAATCATC	B2
mCherry 2C 22	tcattatgtgaagtaatatccaAAAgCTCAgTCCATCCTCgTAAATCCTCATCAATCATC	B2
mCherry 2C 24	atttatataattcatccataccAAAgCTCAgTCCATCCTCgTAAATCCTCATCAATCATC	B2

Accession

	Probe Sequence	Initiator
DLG4 ShHCR mis 1	AATACCGCTACCAAGATGAAGAAAAgCTCAgTCCATCCTCgTAAATCCTCATCAATCATC	B2
DLG4 ShHCR mis 3	TCCCCAACCAGGCCAATTCTCCAAAgCTCAgTCCATCCTCgTAAATCCTCATCAATCATC	B2
DLG4 ShHCR mis 5	CCCCAGGATATGTGAACGGAACAAAgCTCAgTCCATCCTCgTAAATCCTCATCAATCATC	B2
DLG4 ShHCR mis 7	TGGAAAGGGGTAACTCAGGTCTAAAgCTCAgTCCATCCTCgTAAATCCTCATCAATCATC	B2
DLG4 ShHCR mis 9	CACACATCGGTGACGACCCATCAAAgCTCAgTCCATCCTCgTAAATCCTCATCAATCATC	B2
DLG4 ShHCR mis 11	CTGCAGCCCAGGATGGCCGCCTAAAgCTCAgTCCATCCTCgTAAATCCTCATCAATCATC	B2
DLG4 ShHCR mis 13	AAGTGGATGTCCGGGAGGTGACAAAgCTCAgTCCATCCTCgTAAATCCTCATCAATCATC	B2
DLG4 ShHCR mis 15	CGGGTTCCATCGTTCGCCTCTAAAAgCTCAgTCCATCCTCgTAAATCCTCATCAATCATC	B2
DLG4 ShHCR mis 17	TCATAGAGATCAAGCTTATCAAAAAgCTCAgTCCATCCTCgTAAATCCTCATCAATCATC	B2
DLG4 ShHCR mis 19	GGGGCGTTGGGAACCAGCACATAAAgCTCAgTCCATCCTCgTAAATCCTCATCAATCATC	B2

DLG4 ShHCR mis 21	TCATCGAAGGAGGCGCTGCCCAAAAgCTCAgTCCATCCTCgTAAATCCTCATCAATCATC	B2
DLG4 ShHCR mis 23	TCCTGGCGGTCAACAGTGTGGGAAAgCTCAgTCCATCCTCgTAAATCCTCATCAATCATC	B2
DLG4 ShHCR mis 25	CAGCCCTGAAGAACACATATGAAAAgCTCAgTCCATCCTCgTAAATCCTCATCAATCATC	B2
DLG4 ShHCR mis 27	ATGCCTACCTGAGTGACAGCTAAAAgCTCAgTCCATCCTCgTAAATCCTCATCAATCATC	B2
DLG4 ShHCR mis 29	AGCACCTGGACAATGAGATCAGAAAgCTCAgTCCATCCTCgTAAATCCTCATCAATCATC	B2
DLG4 ShHCR mis 2	CGCCCCCTCTGGAACACAGCCCAAgCATTCTTTCTTgAggAgggCAgCAAACgggAAgAg	B1
DLG4 ShHCR mis 4	CTGTGATTGTCAACACGGACACAAgCATTCTTTCTTgAggAgggCAgCAAACgggAAgAg	B1
DLG4 ShHCR mis 6	AGGGGGAGATGGAGTATGAGGAAAgCATTCTTTCTTgAggAgggCAgCAAACgggAAgAg	B1
DLG4 ShHCR mis 8	GCTTCAGCATCGCAGGTGGCACAAgCATTCTTTCTTgAggAgggCAgCAAACgggAAgAg	B1
DLG4 ShHCR mis 10	TCTTTATCACCAAGATCATTCCAAgCATTCTTTCTTgAggAgggCAgCAAACgggAAgAg	B1
DLG4 ShHCR mis 12	GGGTCAACGACAGCATCCTGTTAAgCATTCTTTCTTgAggAgggCAgCAAACgggAAgAg	B1
DLG4 ShHCR mis 14	ATTCAGCTGCAGTGGAGGCCCTAAgCATTCTTTCTTgAggAgggCAgCAAACgggAAgAg	B1
DLG4 ShHCR mis 16	TCATGCGCCGGAAACCCCCAGCAAgCATTCTTTCTTgAggAgggCAgCAAACgggAAgAg	B1
DLG4 ShHCR mis 18	GGCCTAAAGGACTTGGCTTCAGAAgCATTCTTTCTTgAggAgggCAgCAAACgggAAgAg	B1
DLG4 ShHCR mis 20	CTGGAGATAATAGCATCTACGTAAgCATTCTTTCTTgAggAgggCAgCAAACgggAAgAg	B1
DLG4 ShHCR mis 22	AGGATGGCAGGTTGCAGATCGGAAgCATTCTTTCTTgAggAgggCAgCAAACgggAAgAg	B1
DLG4 ShHCR mis 24	TAGAGGATGTCATGCATGAGGAAAgCATTCTTTCTTgAggAgggCAgCAAACgggAAgAg	B1
DLG4 ShHCR mis 26	TTGTGTACCTAAAGGTGGCCAAAAgCATTCTTTCTTgAggAgggCAgCAAACgggAAgAg	B1
DLG4 ShHCR mis 28	CTCCCCCAGACATCACAACCTCAAgCATTCTTTCTTgAggAgggCAgCAAACgggAAgAg	B1
DLG4 ShHCR mis 30	ATAGCAGCTACTTGGGCACCGAAAgCATTCTTTCTTgAggAgggCAgCAAACgggAAgAg	B1

Probe Name	Oligonucleotide Sequence	Sequence Name
UBC	atggtcttaccagtcagagt	hUBC_1
	gacattctcgatggtgtcac	hUBC_2
	gggatgccttccttatcttg	hUBC_3
	atcttccagctgttttccag	hUBC_4
	cagtgagtgtcttcacgaag	hUBC_5
	tcctggatctttgctttgac	hUBC_6
	cagggtagactctttctgga	hUBC_7
	cttcacgaagatctgcatcc	hUBC_8
	tcttggatctttgccttgac	hUBC_9
	cagtgagtgtcttcacgaag	hUBC_10
	tgacgttctcgatagtgtca	hUBC_11
	tccttgtcttggatctttgc	hUBC_12
	cagggtagactctttctgga	hUBC_13
	cttcacgaagatctgcatcc	hUBC_14
	agagtgatggtcttaccagt	hUBC_15
	tcttggatctttgccttgac	hUBC_16
	cttcacgaagatctgcatcc	hUBC_17
	agagtgatggtcttaccagt	hUBC_18
	tcttggatctttgccttgac	hUBC_19
	tgtttcccagcaaagatcaa	hUBC_20
	cttcacgaagatctgcatcc	hUBC_21
	agagtgatggtcttaccagt	hUBC_22
	tcttggatctttgccttgac	hUBC_23

	tgtttcccagcaaagatcaa	hUBC_24
	cttcacgaagatctgcatcc	hUBC_25
	agagtgatggtcttaccagt	hUBC_26
	tcttggatctttgccttgac	hUBC_27
	tgtttcccagcaaagatcaa	hUBC_28
	gacattctcgatggtgtcac	hUBC_29
	gggatgccttccttatcttg	hUBC_30
	tgtttcccagcaaagatcaa	hUBC_31
	agagtggactctttctggat	hUBC_32
EEF2	atctggtctaccgtgaagtt	hEEF2_1
	ttggccttcttgtccatgat	hEEF2_2
	gtatcagtgaagcgtgtctc	hEEF2_3
	ttgacttgatggtgatgcaa	hEEF2_4
	ctcgtagaagagggagatgg	hEEF2_5
	tccttgctctgcttgatgaa	hEEF2_6
	gggagtcaatgaggttgatg	hEEF2_7
	cggtccatcttgttcatcat	hEEF2_8
	gtggagatgatgacgttcac	hEEF2_9
	gtaccgaggacaggatcgat	hEEF2_10
	caaactgcttcagggtgaag	hEEF2_11
	aacttggccacatacatctc	hEEF2_12
	atgtcctctactttcttggc	hEEF2_13
	ttcatgatcgcatcaaacac	hEEF2_14
	gtccagtttgatgtccagtt	hEEF2_15
	gatggtgatcatctgcaaca	hEEF2_16
	tttggggtcacagcttttaa	hEEF2_17
	gtagaaccgacctttgtcgg	hEEF2_18
	ccatgatcctgaccttcagg	hEEF2_19
	ttcttcccaggggtatagtt	hEEF2_20
	tctggattggcttcaggtag	hEEF2_21
	ggcccatcatcaagattgtt	hEEF2_22
	gtcttcaccaggaactggtc	hEEF2_23
	ctgacgctgaacttcatcac	hEEF2_24
	atgatatgctctcccgactc	hEEF2_25
	gactcttcactgaccgtctc	hEEF2_26
	cttcatgtacagccggttgt	hEEF2_27
	tcgcctttatcgatgtcctc	hEEF2_28
	tgatgtcggtgaggatgttg	hEEF2_29
	cactgtccttgatctcgttg	hEEF2_30
	gtcagcacactggcatagag	hEEF2_31
	atctccacaaggtagatggg	hEEF2_32
USF2	ggatccagacccgggtccag	usf2_withUTR_1
	tactggatgttgtggtcgcc	usf2_withUTR_2
	catttgtctctgtgcggaac	usf2_withUTR_3
	attttggatcacagcctgtc	usf2_withUTR_4

	gactgccaccattgctgaag	usf2_withUTR_5
	ctgggaaataggcaaatcgt	usf2_withUTR_6
	gacacagccgtagtatctcc	usf2_withUTR_7
	gtctgaagcacatcctgggg	usf2_withUTR_8
	ggcgatcgtcctctgtgttc	usf2_withUTR_9
	tggttccatcaatttttgga	usf2_withUTR_10
	ttctcctctcatctcggggt	usf2_withUTR_11
	ctccacttcgttgtgctggg	usf2_withUTR_12
	cagttgttgatcttgtccct	usf2_withUTR_13
	gattttcgaaagctggacga	usf2_withUTR_14
	gttgtctgcgttacagtctg	usf2_withUTR_15
	ggccttggacaggatccctc	usf2_withUTR_16
	cgcaactcccggatgtaatc	usf2_withUTR_17
	ctgcatgcgctggttggtct	usf2_withUTR_18
	gctcggcctctttgaaggtc	usf2_withUTR_19
	agctcgttgtccatctgcag	usf2_withUTR_20
	caccatctccaggttgtgct	usf2_withUTR_21
	tgtatccacagaaatgcatt	usf2_withUTR_22
	ggaggataccgtttccaagt	usf2_withUTR_23
	gtgagaccactagaagtgcc	usf2_withUTR_24
	cataggtccaggccccgggt	usf2_withUTR_25
	cagggacccagaaacaagag	usf2_withUTR_26
	gggccagtttattgcagtta	usf2_withUTR_27
TOP2A	ctgggcggagcaaaatatgt	hTOP2A_CDS_1
	tcttcatcgtaaacccacat	hTOP2A_CDS_2
	ccggatcaattgtgactcta	hTOP2A_CDS_3
	ccttttccattattccatat	hTOP2A_CDS_4
	agaagttaggagctgtccaa	hTOP2A_CDS_5
	ccagcaatatcatatgctct	hTOP2A_CDS_6
	ttactggcagtttatttcca	hTOP2A_CDS_7
	tgttgatccaaagctcttgg	hTOP2A_CDS_8
	aactggacttgggccttaaa	hTOP2A_CDS_9
	atcattggcatcatcgagtt	hTOP2A_CDS_10
	gtcaggataagcgtacactc	hTOP2A_CDS_11
	ggaaaaccccatatttgtct	hTOP2A_CDS_12
	tttcttgtactgaagaccca	hTOP2A_CDS_13
	ttggtcctgatctgtcataa	hTOP2A_CDS_14
	ctccagaaaacgatgtcgca	hTOP2A_CDS_15
	gttaaccattcctttcgatc	hTOP2A_CDS_16
	agctaattgggcaaccttta	hTOP2A_CDS_17
	atgtatcgtggactagcaga	hTOP2A_CDS_18
	acgctggttgtcatcatata	hTOP2A_CDS_19
	ttcttctccatccatcaaac	hTOP2A_CDS_20
	cccttgaagttcttgtaact	hTOP2A_CDS_21
	tatgagaggaggtgtcttct	hTOP2A_CDS_22

	tgtatggtattccctatagt	hTOP2A_CDS_23
	tcagtttagcagattcagca	hTOP2A_CDS_24
	cttcacaggatccgaatcat	hTOP2A_CDS_25
	gtggaatgactctttgacca	hTOP2A_CDS_26
	tgctcctatctgattctgaa	hTOP2A_CDS_27
	agtggaggtggaagactgac	hTOP2A_CDS_28
	aattcaaagctggatccctt	hTOP2A_CDS_29
	caggatcaggcttttgagag	hTOP2A_CDS_30
	cttggatttcttgcttgtga	hTOP2A_CDS_31
	tatggaagtcatcactctcc	hTOP2A_CDS_32
NEAT1	gacctagtctccttgccaag	NEAT1_1
	ggatattttccatgcagcct	NEAT1_2
	acaagttgaagattagccct	NEAT1_3
	ccttggtctggaaaaaaagg	NEAT1_4
	cgagctaagttcagttccac	NEAT1_5
	ggccgagcgaaaattacata	NEAT1_6
	cctgtcaaacatgctaggtg	NEAT1_7
	actgccacctggaaaataaa	NEAT1_8
	gtgagctcacaagaagagtt	NEAT1_9
	accagatgaccaggtaatgt	NEAT1_10
	cggtccatgaagcatttttg	NEAT1_11
	tcgccatgaggaacactata	NEAT1_12
	aatctgcaggcatcaattga	NEAT1_13
	cctggaaacagaacattgga	NEAT1_14
	gcatctgctgtggacttttt	NEAT1_15
	ggctctggaacaagcattta	NEAT1_16
	tgcagcatctgaaaaccttt	NEAT1_17
	accggaggctcaatttagaa	NEAT1_18
	caaggttccaagcacaaaac	NEAT1_19
	acagcttagggatcttcttg	NEAT1_20
	tggcatcaacgttaaaatgt	NEAT1_21
	tctacaaggcatcaatctgc	NEAT1_22
	aagaacttctccgagaaacg	NEAT1_23
	gccccaagttatttcatcag	NEAT1_24
	gcgtttagcacaacacaatg	NEAT1_25
	ggaatgaccaacttgtaccc	NEAT1_26
	caatgcccaaactagacctg	NEAT1_27
	tcctagtaatctgcaatgca	NEAT1_28
	agcaagaacaaaagagcact	NEAT1_29
	ggtcctcttactagaatgcc	NEAT1_30
	ctgtgtcacctgttttcagt	NEAT1_31
	cctttggttctcggaaaact	NEAT1_32
	agctggtaaagacatttccc	NEAT1_33
	ctctgaaacaggctgtcttg	NEAT1_34
	gcccatctttcaagtgacta	NEAT1_35

aaccacctaagttgctaagg	NEAT1_36
tcgtcttaagtggtccctta	NEAT1_37
atccagaagagcccatctaa	NEAT1_38
acctgtgacaaatgaggaac	NEAT1_39
agatgtgtttctaaggcacg	NEAT1_40
acagtgaccacaaaaggtta	NEAT1_41
agcaaaggtacatggattct	NEAT1_42
cagggttttcagatcacaca	NEAT1_43
ccccaagtcattggttaaga	NEAT1_44
tcccaacgacagtaattgtt	NEAT1_45
cccatacatgcgtgactaat	NEAT1_46
caacagcatacccgagacta	NEAT1_47
acagagcaacataccagtac	NEAT1_48

Supplementary Table 5 Comparison of ExM and its variants with various super-resolution optical microscopy techniques

Principle	Patterned Illumination		Single Molecule Localization		Physical Magnification		
SRM Technique	STED	SIM	STORM/ PALM[a]	DNA PAINT	Pre-Expansion labeling ExM1.0/proExM/ExPath/	Post-expansion labeling proExM/MAP/ExFISH	iExM
Lateral Resolution[a]	20-60nm[1–4]	~ 100nm[5–7]	20-30nm[8–11]	10-50nm[12–14]	65-75nm[15–17]	65-75nm[15,18], 100nm (ExFISH)[19]	25nm[20]
Axial Resolution[a]	500-700nm[21], 30-50nm (isoSTED)[22,23]	~ 300nm (3D-SIM)[5,6]	50-70nm (3D STORM)[9,10] ~100nm (2D STORM, TIRF)[21] 75nm (BP-FPALM)[24] 15-25nm (iPALM)[11] 20nm (dual objective)[25]	80nm[12]	~ 200nm[15–17]	200nm[15,18], 300nm (ExFISH)[19]	50nm[20]
Depth of Imaging	10-80μm[26,27]	10-20μm[21]	< 10μm[9,21]	10μm[12]	~ 250μm-1mm (limited by working distance and numerical aperture of objective)[15–17]	~250μm-1mm (limited by working distance and numerical aperture of objective)[15,18,19]	~100μm - 500μm (limited by working distance and numerical aperture of objective)[20]
Speed[b]	2D Speed ~ 10^2μm^2/s-10^3μm^2/s [28–30]	2D Speed ~ 10^3μm^2/s (TIRF-SIM)[7]	2D Speed ~ 10^3μm^2/s (2D-STORM)[34,35]	2D Speed ~1μm^2/s-10μm^2/s [12–14]	2D Speed ~ 10^4μm^2/s-10^5μm^2/s (Spinning Disk Confocal)[15–17]	2D Speed ~ 10^4μm^2/s-10^5μm^2/s (Spinning Disk Confocal)[15,18,19]	2D Speed ~ 10^3μm^2/s-10^4μm^2/s (Spinning Disk Confocal)[20]

	3D Speed ~ $10\mu m^3/s$ (estimated)[31]	3D Speed ~ $10^2\mu m^3/s$ - $10^3\mu m^3/s$[32,33]	3D Speed ~ $10^2\mu m^3/s$ (estimated)[34]	3D Speed ~ $1\mu m^3/s$ (estimated)[12]	3D Speed ~ $10^4\mu m^3/s$ (light sheet, estimated)[19]	3D Speed ~ $10^4\mu m^3/s$ (light sheet)[19]	3D Speed ~ $10^3\mu m^3/s$ (light sheet, estimated)[19]
Maximum number of colors imaged simultaneously in biological samples	2-3[2,36–38]	4[6]	2-3[39–41]	3[12]	3-4[15–17]	3-4[15,18,19]	3-4[20]
Live Imaging	Yes[28,42]	Yes[7,32,33]	Yes[34,43]	No[12,44]	No[15–17]	No[15,18,19]	No[20]
Probe requirements	Photostable dyes and FPs[4,36,42]	Conventional dyes[6,7]	Photoswitchable dyes and FPs[8,34,45]	Oligonucleotide coupled labels and dyes[12,44,46]	Conventional dyes and fluorescent proteins (except for cyanine family dyes)[15–17]	Conventional dyes[15,18,19]	Conventional dyes (except for cyanine family dyes)[20]
Root Mean Square (RMS) measurement length error due to distortion (as a function of measurement length)	-	-	-	-	1-4% (over 0-2500μm) (ExM 1.0) 1-5% (over 0-100μm) (proExM) 1-3% (over 0-1500μm) (ExPATH)	3-4% (over 0-2000μm) (MAP) <1% (over 0-160μm) (ExFISH)	2.5% (over 0-40μm)

[a] Resolutions demonstrated in an *in situ* biological context

[b] Given speeds are for single color.

Supplementary Table 6 Comparison of ExM and its variants with various tissue clearing methods

Mechanism of clearing	Clearing method	Final RI	Time for processing (after fixation)	FP preservation	Demonstrated compatibility with immunostaining
Solvent-based dehydration and RI matching	3DISCO [47]	1.56[47]	Hours-days[47]	Limited, 1-2 days[47]	Yes[47]
	iDISCO [48]	1.56[48]	Days-weeks[48]	Limited, 1-2 days[48]	Yes[48]
Immersion and RI matching in aqueous solution	SeeDB [49]	1.49[49]	Days[49]	Yes[49]	Yes[49]
	TDE [50,51]	1.42-1.45[50,51]	Hours-Days[50,51]	Yes[50,51]	Yes[51]
Hyperhydration	Sca*l*e [52]	1.38[52]	Days-months[52]	Yes[52]	No[52]
	Sca*l*eS[53]	1.44[53]	Days[53]	Yes[53]	Yes[53]
	CUBIC [54]	1.49[54]	Days-weeks[54]	Yes[54]	Yes[54]
	CUBIC-X[55]	1.467[55]	Days-weeks[55]	Yes[55]	No[55]
Hydrogel Embedding, Lipid removal, and RI matching	CLARITY [56]	1.45[56]	Days-weeks[56,57]	Yes[56]	Yes[56]
	PACT, PARS [58,59]	1.38-1.48[58,59]	Days-weeks[58,59]	Yes[58,59]	Yes[58,59]
Dilution caused by expansion, removal of non-anchored biomolecules, RI matching with water immersion lens	ExM: ExM 1.0, proExM, ExFISH, ExPATH, MAP, iExM [15–20,60] ExPath	1.33	Days	Yes	Yes

Supplementary Note 1. Comparison between expansion microscopy and other super-resolution imaging techniques

Classical super-resolution microscopy (SRM) techniques achieve high levels of resolution by overcoming Abbe's diffraction limit (on the order of half the wavelength of light) via two general classes of strategy. The first class of strategy uses patterned illumination to manipulate the fluorescence behavior of molecules in a region smaller than the diffraction limit. This way, nearby fluorophores within a diffraction-limited distance can be uniquely identified, thereby achieving subdiffraction-limit resolution. For example, stimulated emission depletion (STED) microscopy[61,62], REversible Saturable Optical Linear Fluorescence Transitions (RESOLFT) technology[63], and super-resolution structured illumination microscopy (SIM)[64,65] belong to this group. The second class of strategy utilizes the photoswitching properties of genetically encoded or small-molecule fluorophores to stochastically enable individual molecules to be visualized at different times, so that each frame contains sparsely distributed, rarely overlapping bright spots representing individual fluorophores, for which the localization can be determined with nanoscale precision by calculation of the centroid of each spot. Assembling these points over time enables reconstruction of the entire image, but now with nanoscale resolution. This second group includes photoactivated localization microscopy (PALM)[45] , fluorescence photoactivation localization microscopy (FPALM)[66] , stochastic optical reconstruction microscopy (STORM)[67], and DNA points accumulation for imaging in nanoscale topography (DNA PAINT)[44,68]. The first class of strategy presents specialized hardware requirements (e.g., special laser or optical configurations), and while the second class of strategy can take advantage of conventional widefield or TIRF microscopes, one challenge is in achieving high efficacy contrast and switching of single molecules. In addition, these tools can be complex to use, and exhibit shallow depth of imaging capability, and/or slow imaging speed in comparison to standard microscopes. ExM, of course, is a relatively new technology and thus early adopters may need to be adaptable when trying it out for the first time, but protocols are freely available[69] and tutorials explaining how to overcome standard debugging problems (e.g., sample drift during handling, delicacy of expanded samples) have been published[70,71].

In comparison to standard SRM approaches, ExM offers numerous technical advantages – and some disadvantages **(Supplementary Table 5)**. ExM does not require any additional hardware beyond what typical labs already have access to. ExM also enables 3D-nanoscale imaging in thick specimens, and over large volumes. Especially with the advent of microscope objectives with long working distances and high numerical aperture (NA), which can support imaging over long axial distances, potentially very large depths (e.g., millimeter to centimeter depth) could be accessed with nanoscale resolution using ExM. In particular, the transparency and refractive index homogeneity of ExM-processed samples enables fast 3D imaging microscopy techniques, such as light-sheet microscopy, to be used with ExM to enable fast, 3D, super-resolution imaging. ExM is compatible with a wide range of fluorophores and fluorescent proteins. In terms of lateral and axial resolutions, ExM variants such as ExM1.0, proExM, ExFISH, and ExPath perform better than SIM, while allowing imaging of thick specimens and/or large volumes. iExM achieves resolutions comparable to STED, PALM, and STORM while maintaining the many advantages of ExM described above. A common question is whether

expanding a specimen slows down imaging, because a greater volume must be imaged; all super-resolution methods are slower than their diffraction limited counterparts, but ExM has a "best of both worlds" attribute – it has the voxel sizes of super-resolution microscopy, but the voxel acquisition speeds of fast diffraction limited microscopy. Of course, a clear limitation of ExM is that it is not compatible with live-cell imaging and is unlikely ever to be fully adapted to a general live imaging context.

There are considerations and caveats that are unique to ExM, because of its reliance on physical magnification as opposed to optical magnification. Of course, the expansion of the sample must be isotropic and even, to a level acceptable for the biological or medical question under investigation. Isotropy is typically quantified, when ExM is first applied to a given tissue type, by measuring the distortions incurred during expansion, by aligning and comparing pre- and post-expansion images of the same specimen via a non-rigid registration process. Pre-expansion images are typically taken with a classical super-resolution method, and post-expansion images by a confocal microscope. For the published ExM methods, and across a wide variety of samples, the distortions are ~1-5% of measurement length, over length scales from tens of microns to hundreds of microns (**Supplementary Table 5**). While non-zero, such distortions are acceptable for a wide variety of biological and medical investigations; nevertheless, in the future, new polymer chemistries might reduce the error still further. In addition, some specimens like *C. elegans*, with its tough cuticle, or bone, may pose special challenges in terms of insuring even expansion, requiring additional technology development and validation beyond existing protocols.

In addition to distortion errors across extended distances, there are nanoscale resolution errors that arise from the gelation and expansion process. We estimated that for iExM, the ExM method with the greatest degree of physical magnification described to date, the resolution error added by gelation and expansion is between 5-10 nm; we estimated this by studying the broadening of the point spread function (PSF), as modeled by the side wall of a microtubule, caused by sample expansion[20]. This level of error is beginning to approach the expected mesh size (i.e., polymer spacing) for polyacrylamide gels (1-2 nm)[72], and it implies an upper limit on the resolution that can be potentially be achieved with the current free radical-synthesized ExM gel chemistry. Of course, higher expansion factors would be required to get the resolution down to this level. And while this value points to a potential error on the length scale of an individual biomolecule, the actual precision in localizing a given biological target would depend on the type of label used. For instance, antibodies applied before expansion could add ~20 nm to the imprecision of localizing individual protein targets, while oligonucleotide tags (as used in iExM) would add another ~ 4-5 nm[20].

In addition, labeling density is an important consideration-- insufficient labeling density causes misrepresentation of the biological structure in question. Though label size and density are issues shared with conventional SRM methods, they could, in principle, be overcome by a unique feature of ExM: the application of tags after expansion, when biomolecular targets have been moved apart from each other. In such a case, positional errors due to the size of labels would be reduced, because the effective tag size would be divided by the expansion factor (e.g.,

post-20x expansion applied antibodies would, in principle, introduce an error of ~20/20 ~ 1 nm). This kind of logic explains why ExM is amenable to signal amplification post-expansion since the effective size of an amplified tag is much lower than its actual size (e.g. with HCR amplification, a 500 nm HCR amplicon created after a 3x ExFISH expansion would have an effective size, in biological terms, of 500 / 3 ~ 150 nm)[19,20]. Of course, the amplification step itself should be as isotropic as possible. But any error in the isotropy of the amplification process will, if performed post-expansion, be divided by the expansion factor. In summary, postponing amplification and other post-labeling analysis steps until after expansion is complete may enhance image quality.

Finally, the resolution of ExM methods have been validated, to date, by studying known biological structures such as microtubules. While this approach works well in contexts where such known structures are present, going forward, ExM would benefit from versatile approaches that allow the measurement of its resolution in any given biological context. Such approaches might include engineered, nanoscale structures like DNA-origami nanorulers[73,74] or artificial protein-complexes[75] that can be added to samples pre-expansion, and imaged after expansion, so that the final structure can be compared to the known ground truth.

Supplementary Note 2. Expansion Microscopy and tissue clearing

ExM achieves tissue clearing as a byproduct of its physical mechanism. This raises the question of how ExM compares to other methods that result in tissue clearing. Biological specimens appear opaque due to an inhomogeneous refractive index (RI) arising from the distribution of the various molecular components of tissues. This inhomogeneity results in non-uniform scattering, which renders the specimen opaque. Furthermore, absorption of light by molecules reduces imaging depth. Tissue clearing techniques work by homogenizing the RI within a specimen so that non-uniform light scattering is minimized[76]. Various techniques clear tissues using various chemical approaches to homogenize RI within specimens (**Supplementary Table 6**). Some of these approaches include solvent-based dehydration and RI matching (3DISCO, BABB, iDISCO)[47,48,77], hyper-hydration based clearing (Sca*l*e, CUBIC)[52,54], RI matching in aqueous solutions (SeeDB)[49], and hydrogel-supported lipid-removal and RI matching (CLARITY, PACT/PARS)[56,59]. The last set of protocols also use hydrogel embedding chemistries related to the Hausen and Dreyer protocol[78], but follow the embedding with removal of the lipids and immersion in compounds that even out refractive index. In comparison, the physical magnification of specimens via ExM homogenizes RI within specimens via dilution of all the polymer-anchored components in water. After expansion, >99% of the volume of the gel is composed of water, which homogenizes the RI of the expanded specimen and matches the RI to that of water (1.33), rendering it transparent. In addition, the loss of non-anchored biomolecules during the expansion process also contributes to the clearing of the specimens by rendering the non-aqueous component more uniform. However, most ExM variants have only been applied to relatively small specimens to date, with the exception of MAP and CUBIC-X, which have been applied to an entire mouse brain[18,55].

References

1. Donnert, G. *et al.* Macromolecular-scale resolution in biological fluorescence microscopy. *Proc. Natl. Acad. Sci. U. S. A.* **103,** 11440–5 (2006).

2. Meyer, L. *et al.* Dual-Color STED Microscopy at 30-nm Focal-Plane Resolution. *Small* **4,** 1095–1100 (2008).

3. WILDANGER, D., MEDDA, R., KASTRUP, L. & HELL, S. W. A compact STED microscope providing 3D nanoscale resolution. *J. Microsc.* **236,** 35–43 (2009).

4. Willig, K. I., Harke, B., Medda, R. & Hell, S. W. STED microscopy with continuous wave beams. *Nat. Methods* **4,** 915–918 (2007).

5. Gustafsson, M. G. L. *et al.* Three-dimensional resolution doubling in wide-field fluorescence microscopy by structured illumination. *Biophys. J.* **94,** 4957–70 (2008).

6. Schermelleh, L. *et al.* Subdiffraction multicolor imaging of the nuclear periphery with 3D structured illumination microscopy. *Science* **320,** 1332–6 (2008).

7. Kner, P., Chhun, B. B., Griffis, E. R., Winoto, L. & Gustafsson, M. G. L. Super-resolution video microscopy of live cells by structured illumination. *Nat. Methods* **6,** 339–342 (2009).

8. Heilemann, M. *et al.* Subdiffraction-Resolution Fluorescence Imaging with Conventional Fluorescent Probes. *Angew. Chemie Int. Ed.* **47,** 6172–6176 (2008).

9. Huang, B., Jones, S. A., Brandenburg, B. & Zhuang, X. Whole-cell 3D STORM reveals interactions between cellular structures with nanometer-scale resolution. *Nat. Methods* **5,** 1047–1052 (2008).

10. Huang, B., Wang, W., Bates, M. & Zhuang, X. Three-Dimensional Super-Resolution Reconstruction Microscopy. *Science (80-.).* **319,** 810–813 (2008).

11. Shtengel, G. *et al.* Interferometric fluorescent super-resolution microscopy resolves 3D cellular ultrastructure. *Proc. Natl. Acad. Sci. U. S. A.* **106,** 3125–30 (2009).

12. Schueder, F. *et al.* Multiplexed 3D super-resolution imaging of whole cells using spinning disk confocal microscopy and DNA-PAINT. *Nat. Commun.* **8,** (2017).

13. Auer, A., Strauss, M. T., Schlichthaerle, T. & Jungmann, R. Fast, Background-Free DNA-PAINT Imaging Using FRET-Based Probes. *Nano Lett.* **17,** 6428–6434 (2017).

14. Lee, J., Park, S., Kang, W. & Hohng, S. Accelerated super-resolution imaging with FRET-PAINT. *Mol. Brain* **10,** 63 (2017).

15. Chen, F., Tillberg, P. W. & Boyden, E. S. Expansion microscopy. *Science (80-.).* **347,** 543–548 (2015).

16. Zhao, Y. *et al.* Nanoscale imaging of clinical specimens using pathology-optimized expansion microscopy. *Nat Biotech* **35,** 757–764 (2017).

17. Tillberg, P. W. *et al.* Protein-retention expansion microscopy of cells and tissues labeled using standard fluorescent proteins and antibodies. *Nat. Biotechnol.* **34,** 987–992 (2016).

18. Ku, T. *et al.* Multiplexed and scalable super-resolution imaging of three-dimensional protein localization in size-adjustable tissues. *Nat Biotech* **34,** 973–981 (2016).

19. Chen, F. *et al.* Nanoscale imaging of RNA with expansion microscopy. *Nat. Methods* **13,** 679–684 (2016).

20. Chang, J.-B. *et al.* Iterative expansion microscopy. *Nat. Methods* **14,** (2017).

21. Schermelleh, L., Heintzmann, R. & Leonhardt, H. A guide to super-resolution fluorescence microscopy. *J. Cell Biol.* **190,** 165–175 (2010).

22. Schmidt, R. *et al.* Spherical nanosized focal spot unravels the interior of cells. *Nat. Methods* **5,** 539–544 (2008).

23. Schmidt, R. *et al.* Mitochondrial Cristae Revealed with Focused Light. *Nano Lett.* **9,** 2508–2510 (2009).

24. Juette, M. F. *et al.* Three-dimensional sub–100 nm resolution fluorescence microscopy of thick samples. *Nat. Methods* **5,** 527–529 (2008).

25. Xu, K., Babcock, H. P. & Zhuang, X. Dual-objective STORM reveals three-dimensional filament organization in the actin cytoskeleton. *Nat. Methods* **9,** 185–188 (2012).

26. Urban, N. T., Willig, K. I., Hell, S. W. & Nägerl, U. V. STED Nanoscopy of Actin Dynamics in Synapses Deep Inside Living Brain Slices. *Biophys. J.* **101,** 1277–1284 (2011).

27. Willig, K. I. *et al.* Nanoscopy of Filamentous Actin in Cortical Dendrites of a Living Mouse. *Biophys. J.* **106,** L01–L03 (2014).

28. Westphal, V. *et al.* Video-Rate Far-Field Optical Nanoscopy Dissects Synaptic Vesicle Movement. *Science (80-.).* **320,** 246–249 (2008).

29. Moneron, G. *et al.* Fast STED microscopy with continuous wave fiber lasers. *Opt. Express* **18,** 1302 (2010).

30. Schneider, J. *et al.* Ultrafast, temporally stochastic STED nanoscopy of millisecond dynamics. *Nat. Methods* **12,** 827–830 (2015).

31. Nägerl, U. V., Willig, K. I., Hein, B., Hell, S. W. & Bonhoeffer, T. Live-cell imaging of dendritic spines by STED microscopy. *Proc. Natl. Acad. Sci. U. S. A.* **105,** 18982–7 (2008).

32. Fiolka, R., Shao, L., Rego, E. H., Davidson, M. W. & Gustafsson, M. G. L. Time-lapse two-color 3D imaging of live cells with doubled resolution using structured illumination. *Proc. Natl. Acad. Sci. U. S. A.* **109,** 5311–5 (2012).

33. Shao, L., Kner, P., Rego, E. H. & Gustafsson, M. G. L. Super-resolution 3D microscopy of live whole cells using structured illumination. *Nat. Methods* **8,** 1044–1046 (2011).

34. Jones, S. A., Shim, S.-H., He, J. & Zhuang, X. Fast, three-dimensional super-resolution

imaging of live cells. *Nat. Methods* **8,** 499–505 (2011).

35. Huang, F. *et al.* Video-rate nanoscopy using sCMOS camera–specific single-molecule localization algorithms. *Nat. Methods* **10,** 653–658 (2013).

36. Donnert, G. *et al.* Two-Color Far-Field Fluorescence Nanoscopy. *Biophys. J.* **92,** L67–L69 (2007).

37. Bossi, M. *et al.* Multicolor Far-Field Fluorescence Nanoscopy through Isolated Detection of Distinct Molecular Species. *Nano Lett.* **8,** 2463–2468 (2008).

38. Bückers, J., Wildanger, D., Vicidomini, G., Kastrup, L. & Hell, S. W. Simultaneous multi-lifetime multi-color STED imaging for colocalization analyses. *Opt. Express* **19,** 3130 (2011).

39. Bates, M., Huang, B., Dempsey, G. T. & Zhuang, X. Multicolor super-resolution imaging with photo-switchable fluorescent probes. *Science* **317,** 1749–53 (2007).

40. Shroff, H. *et al.* Dual-color superresolution imaging of genetically expressed probes within individual adhesion complexes. *Proc. Natl. Acad. Sci. U. S. A.* **104,** 20308–13 (2007).

41. Wilmes, S. *et al.* Triple-Color Super-Resolution Imaging of Live Cells: Resolving Submicroscopic Receptor Organization in the Plasma Membrane. *Angew. Chemie Int. Ed.* **51,** 4868–4871 (2012).

42. Hein, B., Willig, K. I. & Hell, S. W. Stimulated emission depletion (STED) nanoscopy of a fluorescent protein-labeled organelle inside a living cell. *Proc. Natl. Acad. Sci. U. S. A.* **105,** 14271–6 (2008).

43. Hess, S. T. *et al.* Dynamic clustered distribution of hemagglutinin resolved at 40 nm in living cell membranes discriminates between raft theories. *Proc. Natl. Acad. Sci. U. S. A.* **104,** 17370–5 (2007).

44. Jungmann, R. *et al.* Multiplexed 3D cellular super-resolution imaging with DNA-PAINT and Exchange-PAINT. *Nat. Methods* **11,** 313–8 (2014).

45. Betzig, E. *et al.* Imaging Intracellular Fluorescent Proteins at Nanometer Resolution. *Science (80-.).* **313,** 1642–1645 (2006).

46. Wang, Y. *et al.* Rapid sequential in situ multiplexing with DNA-Exchange-Imaging in Neuronal Cells and Tissues. *Nano Lett.* acs.nanolett.7b02716 (2017). doi:10.1021/acs.nanolett.7b02716

47. Ertürk, A. *et al.* Three-dimensional imaging of solvent-cleared organs using 3DISCO. *Nat Protoc* **7,** 1983–1995 (2012).

48. Renier, N. *et al.* iDISCO: A Simple, Rapid Method to Immunolabel Large Tissue Samples for Volume Imaging - suppl original. *Cell* **159,** (2014).

49. Ke, M.-T., Fujimoto, S. & Imai, T. SeeDB : a simple and morphology-preserving optical clearing agent for neuronal circuit reconstruction. *Nat. Publ. Gr.* **16,** 1154–1161 (2013).

50. Aoyagi, Y., Kawakami, R., Osanai, H., Hibi, T. & Nemoto, T. A rapid optical clearing protocol using 2,2'-thiodiethanol for microscopic observation of fixed mouse brain. *PLoS One* **10,** 1–13 (2015).

51. Costantini, I. *et al.* A versatile clearing agent for multi-modal brain imaging. *Sci. Rep.* **5,** 9808 (2015).

52. Hama, H. *et al.* Scale: a chemical approach for fluorescence imaging and reconstruction of transparent mouse brain. *Nat. Neurosci.* **14,** 1481–8 (2011).

53. Hama, H. *et al.* ScaleS: an optical clearing palette for biological imaging. *Nat. Neurosci.* **18,** 1518–1529 (2015).

54. Susaki, E. A. *et al.* Whole-brain imaging with single-cell resolution using chemical cocktails and computational analysis. *Cell* **157,** 726–739 (2014).

55. Murakami, T. C. *et al.* A three-dimensional single-cell-resolution whole-brain atlas using CUBIC-X expansion microscopy and tissue clearing. *Nat. Neurosci.* **21,** 625 (2018).

56. Chung, K. *et al.* Structural and molecular interrogation of intact biological systems. *Nature* **497,** 332–7 (2013).

57. Tomer, R., Ye, L., Hsueh, B. & Deisseroth, K. Advanced CLARITY for rapid and high-resolution imaging of intact tissues. *Nat. Protoc.* **9,** 1682–97 (2014).

58. Treweek, J. B. *et al.* Whole-body tissue stabilization and selective extractions via tissue-hydrogel hybrids for high-resolution intact circuit mapping and phenotyping. *Nat. Protoc.* **10,** 1860–1896 (2015).

59. Yang, B. *et al.* Single-cell phenotyping within transparent intact tissue through whole-body clearing. *Cell* **158,** 945–958 (2014).

60. Chozinski, T. J. *et al.* Expansion microscopy with conventional antibodies and fluorescent proteins. *Nat. Methods* (2016). doi:10.1038/nmeth.3833

61. Hell, S. W. & Wichmann, J. Breaking the diffraction resolution limit by stimulated emission: stimulated-emission-depletion fluorescence microscopy. *Opt. Lett.* **19,** 780–2 (1994).

62. Klar, T. A., Jakobs, S., Dyba, M., Egner, A. & Hell, S. W. Fluorescence microscopy with diffraction resolution barrier broken by stimulated emission. *Proc. Natl. Acad. Sci. U. S. A.* **97,** 8206–10 (2000).

63. Hofmann, M., Eggeling, C., Jakobs, S. & Hell, S. W. Breaking the diffraction barrier in fluorescence microscopy at low light intensities by using reversibly photoswitchable proteins. *Proc. Natl. Acad. Sci.* **102,** 17565–17569 (2005).

64. Gustafsson, M. G. Surpassing the lateral resolution limit by a factor of two using structured illumination microscopy. *J. Microsc.* **198,** 82–7 (2000).

65. Heintzmann, R. & Cremer, C. G. Laterally modulated excitation microscopy: improvement of resolution by using a diffraction grating. in *Proc. SPIE* (eds. Bigio, I. J., Schneckenburger, H., Slavik, J., Svanberg, K. & Viallet, P. M.) **3568,** 185–196

(International Society for Optics and Photonics, 1999).

66. Hess, S. T., Girirajan, T. P. K. & Mason, M. D. Ultra-high resolution imaging by fluorescence photoactivation localization microscopy. *Biophys. J.* **91,** 4258–72 (2006).

67. Rust, M. J., Bates, M. & Zhuang, X. Sub-diffraction-limit imaging by stochastic optical reconstruction microscopy (STORM). *Nat. Methods* **3,** 793–796 (2006).

68. Jungmann, R. *et al.* Single-molecule kinetics and super-resolution microscopy by fluorescence imaging of transient binding on DNA origami. *Nano Lett.* **10,** 4756–61 (2010).

69. ExpansionMicroscopy.org: Physical Specimen Expansion Enabling 3-D Large Volume, Nanoscale Imaging.

70. Gao, R., Asano, S. M. & Boyden, E. S. Q&A Expansion Microscopy. *BMC Biol.* (2017). doi:10.1073/pnas.1617699113

71. Karagiannis, E. & Boyden, E. Expansion microscopy: development and neuroscience applications. *Curr Opin Neurobiol* **50,** 56–63 (2018).

72. Cohen, Y., Ramon, O., Kopelman, I. J. & Mizrahi, S. Characterization of inhomogeneous polyacrylamide hydrogels. *J. Polym. Sci. Part B Polym. Phys.* **30,** 1055–1067 (1992).

73. Raab, M. *et al.* Using DNA origami nanorulers as traceable distance measurement standards and nanoscopic benchmark structures. *Sci. Rep.* **8,** 1780 (2018).

74. Scheible, M. B. & Tinnefeld, P. Quantifying Expansion Microscopy with DNA Origami Expansion Nanorulers. *Biorxiv* (2018). doi:10.1101/265405

75. Bale, J. B. *et al.* Accurate design of megadalton-scale two-component icosahedral protein complexes. *Science* **353,** 389–94 (2016).

76. Richardson, D. S. & Lichtman, J. W. Clarifying Tissue Clearing. *Cell* **162,** 246–257 (2015).

77. Dodt, H.-U. *et al.* Ultramicroscopy: three-dimensional visualization of neuronal networks in the whole mouse brain. *Nat. Methods* **4,** 331–336 (2007).

78. Hausen, P. & Dreyer, C. The Use of Polyacrylamide as an Embedding Medium for Immunohistochemical Studies of Embryonic Tissues. *Stain Technol.* **56,** 287–293 (1981).